Multifunctional Hydrogels Integrated with Reversible Noncovalent Interactions for Bioengineering and Sensing Applications

by

Xuwen Peng

A thesis submitted in partial fulfillment of the requirements for the degree of

Doctor of Philosophy

in

Chemical Engineering

Department of Chemical and Materials Engineering
University of Alberta

Abstract

Hydrogels bear a close resemblance to human tissues and thus have been extensively employed for a broad range of applications in recent years. Intelligent hydrogels that can respond to diverse stimuli, such as pH, temperature, ionic strength, strain and stress, hold great promise for a variety of biological engineering and sensing applications. Nevertheless, weak mechanical properties and narrow functionality have limited the application of traditional hydrogels generally based on permanent covalent bonds. Incorporating reversible noncovalent interactions within hydrogel networks is an effective approach that lifts those restrictions. In the context of the growing demand for bioengineering and sensing applications, it is of great significance yet remains a challenge to integrate multifunctionalities such as mechanical robustness, self-healing properties, stimuli-responsiveness and conductivity into one hydrogel through the introduction of reversible interactions, functional components and well-designed structures. In this thesis, a review of multifunctional hydrogels, non-covalent interactions and corresponding hydrogels, and bioengineering and sensing applications of hydrogels is presented first, followed by three original research projects investigating the integrated multifunctional hydrogels for different potential biomedical and electrical sensing applications.

Hydrogels with good stretchability, high adhesiveness, sensitive electrical responsiveness, biocompatible and antibacterial features are exceptionally desirable materials for various biomedical and sensing applications. In the first project, we fabricated a highly stretchable, moldable, self-healing and antibacterial hydrogel with electrical responsiveness by introducing dynamic noncovalent interactions, i.e., hydrogen-bonding

among hydroxyl groups of poly (vinyl alcohol) (PVA), carboxyl moieties of poly (methyl vinyl ether-alt-maleic acid) (PMVEMA), and the catechol groups in tannic acid (TA). The prepared PPTA hydrogel shows a wide spectrum of desirable properties, including fast gelation, excellent and adjustable mechanical properties (true stress at break and fracture strain up to ~7 MPa and ~2300%, respectively), self-healing and remolding abilities, robust adhesion to diverse substrates, antimicrobial activity to both *Escherichia coli* and *staphylococcus aureus* bacteria, and stability under a broad range of pH environments (pH 1−10). Moreover, this hydrogel demonstrates good sensitivity for monitoring strain, pressure and human motions. Therefore, this hydrogen-bonding-driven, multifunctional hydrogel with facile fabrication and flexible modification provides an exciting paradigm for biosensing and bioengineering applications.

Hydrogels combining both conductive capability and robust mechanical properties hold great promise in wearable soft electronics. In the second project, we fabricated a multifunctional hydrogel for strain sensing applications. By incorporating a conductive polymer network Poly(3,4-ethylenedioxythiophene)-poly(styrenesulfonate) (PEDOT: PSS) into the PVA/ poly (acrylic acid) (PAA) double network (DN) hydrogel, this PEDOT: PSS@PVA/PAA hydrogel system presents good stretchability, high toughness and fatigue resistance. Besides the improvement of mechanical properties, the multiple hydrogen bonding interactions also endow the hydrogel with self-healing properties and strong adhesion to various substrates. Moreover, the hydrogel shows high electrical sensitivity (Gauge Factor from 2.21 to 3.82) to strains, which enables it to sense different types of motions (e.g., stretching, compressing, bending, etc.). Precise detections of many subtle human motions including pulse and vocal cord vibration were achieved. This work

provides new insights into the development of multifunctional conductive hydrogels for wearable sensors, electronic skin, and other bioelectrical engineering applications.

Multifunctional hydrogels that respond to bio-related stimuli hold significant promise for smart drug delivery systems. In the third project, a pH-responsive microgel-embedded hydrogel with adhesiveness and robust mechanical properties was developed as a dual drug delivery system for wound-healing. The polyacrylamide (PAAm)/ chitosan (CS) semi-interpenetrating (semi-IPN) hydrogel exhibits excellent stretchability, compressibility and elasticity. Meanwhile, this hydrogel can tightly adhere to various surfaces of porcine tissues and subduct the mismatch between hydrogel and tissue interfaces. Moreover, by incorporating poly (N-isopropylacrylamide-co-acrylic acid) (PNIPAAm-AAc) based microgel particles, the hybrid hydrogel system can be used for dual drug delivery of both bovine serum albumin (BSA, model protein) and Sulfamethoxazole (SMZ) in a pH-responsive manner. Compared with traditional oral, injection and smear medications, this integrated microparticle-based drug delivery system shows advantages such as high drug loading efficiency (more than 80%), controllable drug releasing behaviors and sustained drug releasing duration (over 48h), which have the potential for applications of smart wound dressing materials in biomedical engineering.

This thesis work develops three multifunctional hydrogels based on various non-covalent interactions for applications in bioengineering and sensing. This work broadens the application of hydrogels in some bioengineering areas and provides new insights for developing novel, intelligent, wearable electronics for sensing applications.

Preface

This thesis is an original work by Xuwen Peng, which contains published contents from the peer-reviewed journals as described below.

Part of Chapter 2 of this thesis has been published as Gao, Y., Peng, X., Wu, Q., Yang, D., Wang, W., Peng, Q., Wang, T., Wang, J., Liu, J., Zhang, H., and Zeng, H., Hydrogen-Bonding-Driven Multifunctional Polymer Hydrogel Networks Based on Tannic Acid. *ACS Applied Polymer Materials*, **2022**, 4(3), pp.1836-1845. Some of the research conducted in this chapter belongs to an international collaboration, led by Prof. Hao Zhang and Prof. Hongbo Zeng at University of Alberta and Prof. Jifang Liu at Guangzhou Medical University. I was responsible for materials synthesis, data collection and analysis, as well as the manuscript composition. Dr. Yongfeng Gao helped with the microgel synthesis, manuscript composition and revision. Dr. Qiuqiu Wu helped with the antimicrobial experiment, Dr. Wenda Wang, Diling Yang, Dr. Qiongyao Peng, Tao Wang, and Dr. Jianmei Wang contributed to the manuscript revision. Dr. Jifang Liu, Dr. Hao Zhang and Dr. Hongbo Zeng were the corresponding authors.

Chapter 3 of this thesis has been published as Peng, X., Wang, W., Yang, W., Chen, J., Peng, Q., Wang, T., Yang, D., Wang, J., Zhang, H., and Zeng, H., Stretchable, compressible, and conductive hydrogel for sensitive wearable soft sensors. *Journal of Colloid and Interface Science*, **2022**, 618, pp.111-120. I was responsible for materials synthesis, data collection and analysis, as well as the manuscript composition. Dr. Wenda Wang, Dr. Jingsi Chen, Dr. Qiongyao Peng, Tao Wanga, Diling Yang, Dr. Jianmei Wang contributed to the manuscript revision. Dr. Wenshuai Yang helped conduct the material characterization. Dr. Hao Zhang and Dr. Hongbo Zeng were the corresponding authors and

were involved in the experimental design and manuscript composition.

Chapter 4 of this thesis has been submitted to *ACS Applied Materials & Interfaces* as Peng, X.; Peng, Q.; Wu, M.; Wang, W.; Gao, Y.; Yang. D.; Peng, Q.; Wang. T.; Zhang, H., Zeng, H. A pH and temperature dual-responsive microgel embedded adhesive tough hydrogel for drug delivery and wound healing. I was responsible for materials synthesis, data collection and analysis, as well as the manuscript composition. Dr. Wu Meng, Dr. Wenda Wang, Dr. Jingsi Chen, Dr. Qiongyao Peng, Tao Wanga, Diling Yang contributed to the manuscript revision. Dr. Yongfeng Gao synthesized the microgel. Dr. Hao Zhang and Dr. Hongbo Zeng were corresponding authors and were involved in the experimental design and manuscript composition.

Acknowledgements

I would like to thank many individuals; my Ph.D. study would not be possible without their generous help.

First and foremost, I would like to express my sincere gratitude to Prof. Hao Zhang, Prof. Hongbo Zeng and Prof. Xihua Wang, for guiding me to conduct research in the world of functional materials and interface science. I immensely appreciate their tremendous support, precious suggestions, and kind encouragement. Their enthusiasm for science, dedication to innovation, breadth of intellect and kindness to everyone have impacted me in developing my career and lift path.

Secondly, I would like to thank all the group members, for their selfless assistance, support and suggestions. The harmony in our groups encouraged me and I would convey the spirit to other group members. My special thanks to Dr. Jingsi Chen, Dr. Meng Wu, Dr. Qiongyao Peng, Dr. Wenda Wang and Dr. Yongfeng Gao for their valuable advice and help with manuscript revisions.

Thirdly, I would like to acknowledge the Natural Sciences and Engineering Research Council of Canada (NSERC) and Canada Foundation for Innovation (CFI) for the support of related research activities.

I also wish to thank all my friends for companying me during my dark days. In addition, I would like to thank Jiaxin Liu and her family for the past favour.

Finally, my deep thanks go to my parents, for their endless love, unconditional support, and generous encouragement throughout my whole life.

Table of Contents

List of Figures

Abbreviations and Symbols

PVA	poly(vinyl alcohol)
PMVEMA	poly (methyl vinyl ether-alt-maleic acid)
TA	tannic acid
PEDOT: PSS	poly(3,4-ethylenedioxythiophene)-poly(styrenesulfonate)
PAA	polyacrylic acid
DN	double network
GF	Gauge Factor
PAAm	polyacrylamide
CS	chitosan
semi-IPN	semi-interpenetrating
PNIPAAm-AAc	poly (N-isopropylacrylamide-co-acrylic acid)
BSA	bovine serum albumin
SMZ	sulfamethoxazole
3D	three-dimensional
PHEMA	polyhydroxyethylmethacrylate
PAMPS	poly(2-acrylamido-2-methyl-1-propanesulfonic acid
CNT	carbon nanotube
rGO	reduced graphene oxide
CPs	conducting polymers
PA	polyacetylene
PPy	polypyrrole
PPv	poly(phenylene) vinylene
PTh	polythiophene

PANi	polyaniline
CPHs	conducting polymer hydrogels
FT	freezing-thawing
UPy	2-ureido-4[1H]-pyrimidinone
PANI/PSS	polyaniline/poly(4-styrenesulfonate)
PEG	poly(ethylene glycol)
PMETAC	poly (2-(methacryloyloxy) ethyltrimethylammonium chloride)
PNaAMPS	poly (2-acrylamido-2-methyl- propane sulfonic acid sodium salt)
PAH	poly(allylamine hydrochloride)
eΦAM	N-4-Ethylphenylacrylamide
C18	stearyl methacrylate
C22	dococyl acrylate
CD	cyclodextrin
CB	cucurbituril
CE	crown ether
ECMs	extracellular matrices
SA	sulfosuccinic acid
DOPA	3,4-dihydroxy-L-phenylalanine
PDA	poly(dopamine)
H-bonding	hydrogen bonding
HA	hydroxyapatite
RGD	Arg-Gly-Asp
ATP	adenosine triphosphate
ADP	adenosine diphosphate

UTP	uridine triphosphate
PF127-CHO	benzaldehyde-terminated Pluronic®F127
Cip	ciprofloxacin hydrochloride
CHX	chlorhexidine
PLLA-PEG-PLLA	poly(L-lactide)-b-poly(ethylene glycol)-b-poly(L-lactide)
PMETA	poly[2(methacryloyloxy)-ethyl] trimethylammonium iodide
E. coil	*Escherichia coli*
PEI	polyethyleneimine
SGF	simulated gastric fluid
SIF	simulated intestinal fluid
SA	salicylic acid
LCST	low critical solution temperature ()
HEC	hydroxyethyl cellulose
HA	hyaluronic acid
ILTG	isoliquiritigenin
SC	stratum corneum
PPTA	PVA/PMVEMA/TA
PVP	poly(N-vinylpyrrolidone)
FDA	the United States Food and Drug Administration
ESCs	Embryonic stem cells
MRSA	*Methicillin-resistant Staphylococcus Aureus*
SEM	scanning electron microscope
FTIR	Fourier transform infrared spectroscopy
G′	storage modulus

G″	loss modulus
γ	oscillatory strain
ω	angular frequency
R	resistance
U	voltage
I-t	current-time
σ	conductivity
$\Delta R/R_0$	relative resistance change
D	diameter
APS	ammonium persulfate
MBAA	N, N′-Methylenebis(acrylamide)
TEMED	N, N, N′, N′-tetramethylethylenediamine
LED	light-emitting diode
λ	strain
S	sensitivity
P	pressure
AFM	atomic force microscopy
SFA	surface force apparatus
PBS	phosphate-buffered saline
UV-Vis	ultraviolet-visible
pKa	negative decadic logarithm of the acid dissociation constant

CHAPTER 1 General Introduction

1.1 Multifunctional Hydrogels

Hydrogels are three-dimensional (3D) networks of natural or synthetic polymers that are chemically or physically crosslinked with high water content. Because of their tunable properties and functionalities, hydrogels and their applications have received increasing attention since the first report of a biocompatible polyhydroxyethylmethacrylate (PHEMA) hydrogel and its application as contact lenses in the 1960s.[1-2] The advances in fabrication methodologies and functionalization strategies have enabled the development of multifunctional hydrogels with desired physical, chemical, and biological characteristics (e.g., tissue-mimicking, antibacterial, anti-fouling, self-healing, and stimuli-responsive).[3-6] Functional hydrogels have demonstrated outstanding potential in biomedical and bioengineering applications such as cell encapsulation, cell culture scaffolds, and wound adhesives.[7-10] Hydrogels with conductive and stretchable features have also attracted enormous attention. They are promising materials for bioengineering with applications ranging from wearable sensing devices, implantable electrodes, soft actuators and electronic skin to portable medical apparatus and instruments.[11-15]

Conventional hydrogels using permanent covalent bonds usually suffer from poor mechanical properties such as limited stretchability, low tensile strength and weak self-healing capability, which limit their applications as substitutes for soft tissues.[16] In more recent studies, dynamic and reversible molecular interactions, particularly noncovalent interactions such as hydrogen bonding, ionic, π–π, cation–π, anion–π and hydrophobic interactions, have been applied to fabricate advanced hydrogels, endowing the hydrogels

with functionalities such as self-healing, stimuli-responsive and shape-memory properties, to increase their lifespan and preserve their structural integrity and functionalities.

In addition, combining double network structures with non-covalent interactions involved hydrogel systems is a widely employed strategy for preparing strong, stretchable and tough hydrogels. The double-network hydrogel was first reported by Gong et al. and consisted of asymmetric structured networks where one was a ductile network of a homogeneous neutral polymer and the other was a rigid network of polyelectrolyte, the structure illustrated in **Figure 1.1**.[17] This hybrid hydrogel showed improved mechanical properties over the single-network hydrogels and the mechanical properties could be adjusted through the optimization of the structure. For instance, the poly(2-acrylamido-2-methyl-1-propanesulfonic acid)/polyacrylamide (PAMPS/PAAm) double-network hydrogel sustained a fracture tensile stress of 1 – 10 MPa with strain in the range of 1000 – 2000%, and the compression stress reached to 20 – 60 MPa with a strain of 90 – 95%.[18] These impressive mechanical behaviors were comparable to those of load-bearing bio-tissues and inspired future studies on mechanically robust hydrogels.[19]

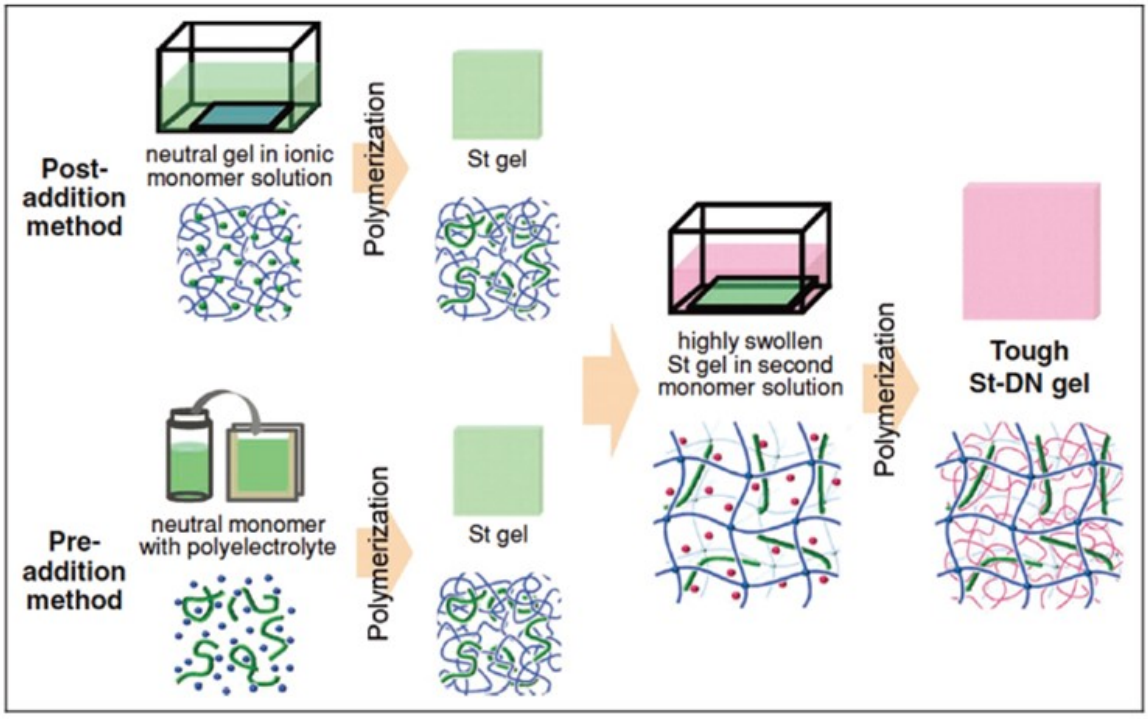

Figure 1.1. Schematic illustration for the fabricating process of typical double-network hydrogel. Reproduced with permission from the literature (Reprinted with permission from reference [17], © Wiley-VCH GmbH, Weinheim).

With the synergy of the flexible and biocompatible features of soft hydrogels and the electronic transportational property of conductors, conductive hydrogels have emerged and attracted enormous attention for the fabrication of bioelectronics in the past three decades. Many strategies—including using conductive polymers, conductive fillers, free ions and their mixtures—have been developed for preparing conductive hydrogels. As illustrated in **Figure 1.2**,[21] the most straightforward strategy is to distribute conductive nanomaterials such as carbon nanotubes (CNTs),[22] metal nanoparticles or nanowires,[12, 23-24] graphite,[25] and reduced graphene oxide (rGO)[26] as fillers within insulating or low-conductive hydrogel matrices. These fillers not only endow the hydrogels with good conductivity but also help them release stress upon stretching due to their self-organizing ability.[27] For example, Chen et al. presented a series of high-performance lithium

electrodes based on hydrogels consisting of super-long carbon nanotubes, conductive polymer poly (3,4-ethylenedioxythiophene): poly(4-styrenesulfonate) (PEDOT: PSS) and electrochemically active nanoparticles (TiO_2 or Si nanoparticle). The hybrid networked hydrogels possessed superior mechanical properties, stability and conductivity due to the formation of a 3D crosslinked carbon nanotube network.[22] Meanwhile, conducting polymers (CPs), such as polyacetylene (PA), polypyrrole (PPy), poly(phenylene) vinylene (PPv), polythiophene (PTh), polyaniline (PANi), poly (3,4-ethylenedioxythiophene) (PEDOT) and their derivatives have shown great potential in the development of conductive hydrogels. The unique π-conjugated structure of the conducting polymers allows for the transport of electrons, and their broad conductivity can be facilely modulated by the use of doping chains with suitable ions.[28] Conducting polymer hydrogels (CPHs), composed of mesh-like frameworks of conducting polymers, exhibit several advantages over other conductive materials. Compared to nanomaterials such as metallic particles and carbon nanotubes, conducting polymers show versatile processability and much better compatibility with other polymeric components in hydrogels, yielding materials with ultra-flexibility as well as high conductivity.[29] Due to the high water content maintained in the porous structure, CPHs provide a good interface between biological and synthetic systems, which have served as promising platforms for diverse bio-applications such as drug release,[30] soft tissue engineering,[31] and artificial muscle.[32] One prominent feature of CPHs is the combination of ionic and electronic conductive paths. Their conjugated backbones delocalize π-bonded electrons and their swollen, pore-rich structures allow ions to pass freely, a quality that endows CPHs with high volumetric capacitance within the high surface area of their porous structure.[33] CPHs with satisfying mechanical properties are primarily prepared based on the formation of interpenetrating networks by mixing or triggering the polymerization of conducting polymers within the network of non-

conductive hydrogels. Recently, hydrogels composed of interconnected networks of pure conducting polymers have been developed and explored as electrodes and biosensors to enhance electrical conductivity.[34]

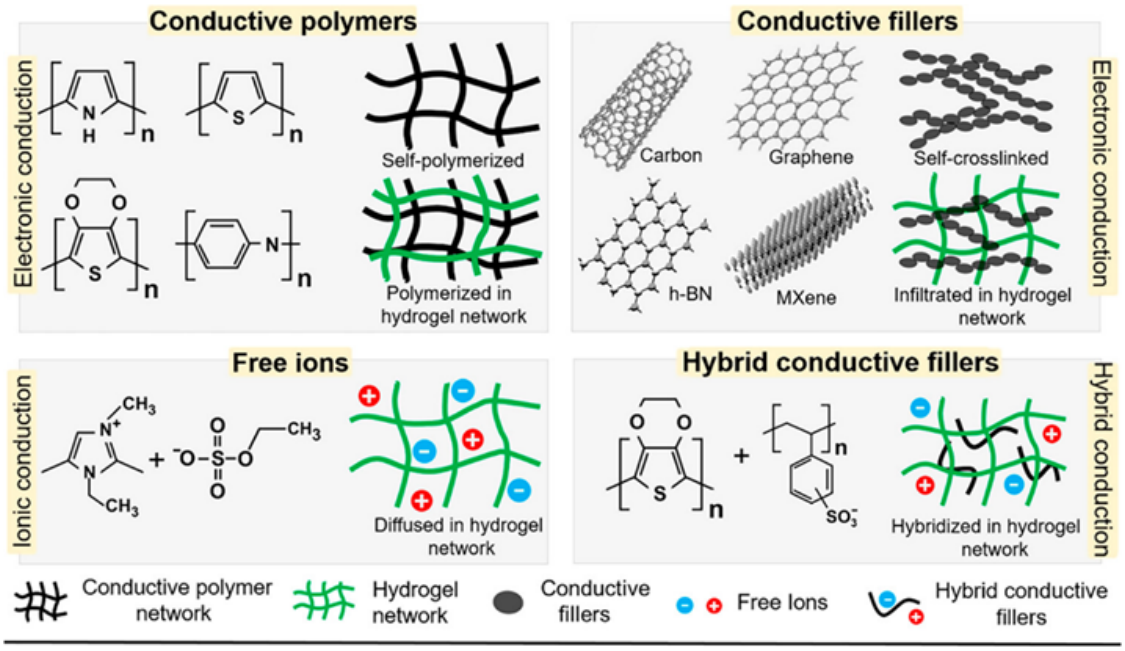

Figure 1.2. Different strategies for fabricating conductive hydrogels including using conductive polymers, conductive fillers, free ions and their mixtures. (Reprinted with permission from reference [20], © Wiley-VCH GmbH, Weinheim).

Synthetic hydrogels able to respond to different physical or chemical stimuli including temperature,[35] pH,[36] pressure,[37] light,[38] ionic strength,[39] and electric and magnetic fields[40-41] have been intensively studied, and these "smart" materials hold promise for a wide range of applications such as biosensors and bio-actuators in bioengineering.[42]

In conclusion, over the past two decades, multifunctional hydrogels have become some of the most promising materials, but they are also challenging as they require a balanced combination of materials, design and manufacture. Hydrogels hold several

advantages when applied in the field of bioelectronics, such as flexibility, functionality,[43] biocompatibility,[44] conductivity, and stimuli-responsiveness. Based on the above merits, hydrogels have attracted increasing research interest and have stimulated the development of bioelectronics.[12]

1.2 Noncovalent Interactions

Noncovalent interactions involve weak electromagnetic interactions rather than intra- or inter-molecular electron sharing. Even though noncovalent interactions are generally weaker than covalent interactions, they are ubiquitous in the universe and play a dominant role in the design, synthesis and catalysis of large molecules, especially for the self-assembly of organic molecules like proteins and amino acids. [45-46] Noncovalent interactions **(Figure 1.3)** are mainly divided into electrostatic interactions (e.g. ionic interactions, hydrogen bonding, halogen bonding), π-effects (e.g. π–π interactions, cation–π interactions, anion–π interactions), van der Waals forces and hydrophobic interactions.[47]

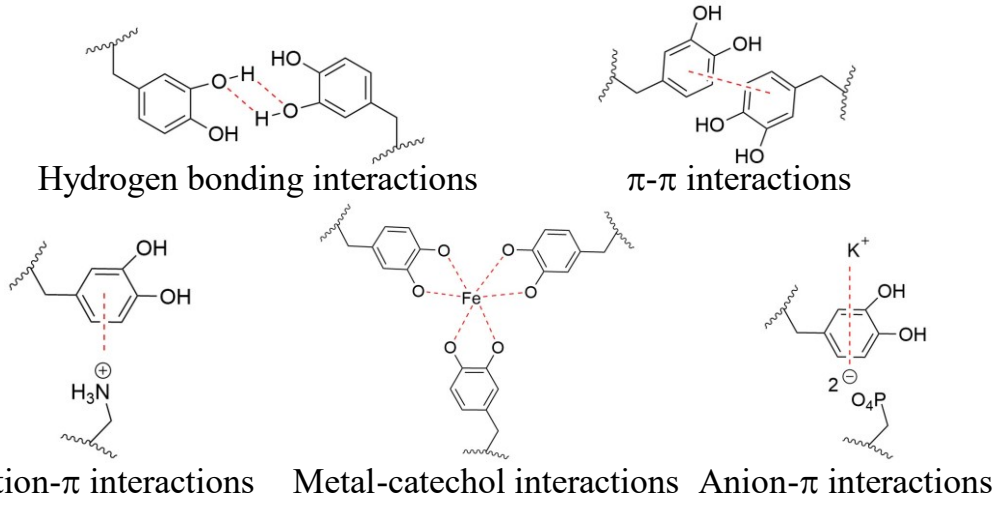

Figure 1.3. Illustration of some noncovalent interactions.

1.2.1 Hydrogen Bonding

A hydrogen bonding interaction is a dipole-dipole attractive force between a hydrogen atom and a very electronegative atom, specifically an N, O, or F, and another neighboring electronegative atom or a functional group with long-pair electrons. It plays an important role in determining structures of biomolecules and has been commonly used in hydrogel fabrications.[48-49] Polymers like polyacrylamide (PAAm) and poly (vinyl alcohol) (PVA) can crosslink independently due to the multiple hydrogen bonding between the polymer chains. However, those structures are unstable due to the formation of competitive hydrogen bonds with the surrounding water molecules. A robust mechanical PVA hydrogel could be produced by the hydrogen bond crosslinking with a polyphenol such as tannic acid (TA) to stabilize the network; it could also be prepared through a freezing-thawing (FT) process, which is physically crosslinked by hydrogen bonding between PVA crystallites formed in the freezing process and PVA chains.[50-52] Inspired by the biological system (e.g., protein structures like alpha helixes and beta pleated sheets), multiple hydrogen bonding interactions have been introduced for self-assembly supramolecular hydrogels.[53] As a benefit for the strong and reversible dimerization of ureidopyrimidinone (UPy) in a self-complementary array through quadruple hydrogen bonds, UPy moieties are excellent associating agents for self-assembling polymers and hydrogels to construct a crosslinked system without phase separation. Meijer's group represented a supramolecular UPy network (**Figure 1.4a**) with good mechanical properties and excellent reversibility.[54] Chen et al. developed a multifunctional polyaniline/poly(4-styrenesulfonate) (PANI/PSS) hydrogel by introducing UPy groups as crosslinking points into the interpenetrating PANI/PSS network (**Figure 1.4b**). The self-complementary quadruple hydrogen bonding endows the hydrogel with excellent mechanical strength,

good injectability and rapid self-healing performance within 30 s upon damage.[55] Based on those findings, multiple hydrogen bonding interactions have recently been widely employed for hydrogels.[51, 56]

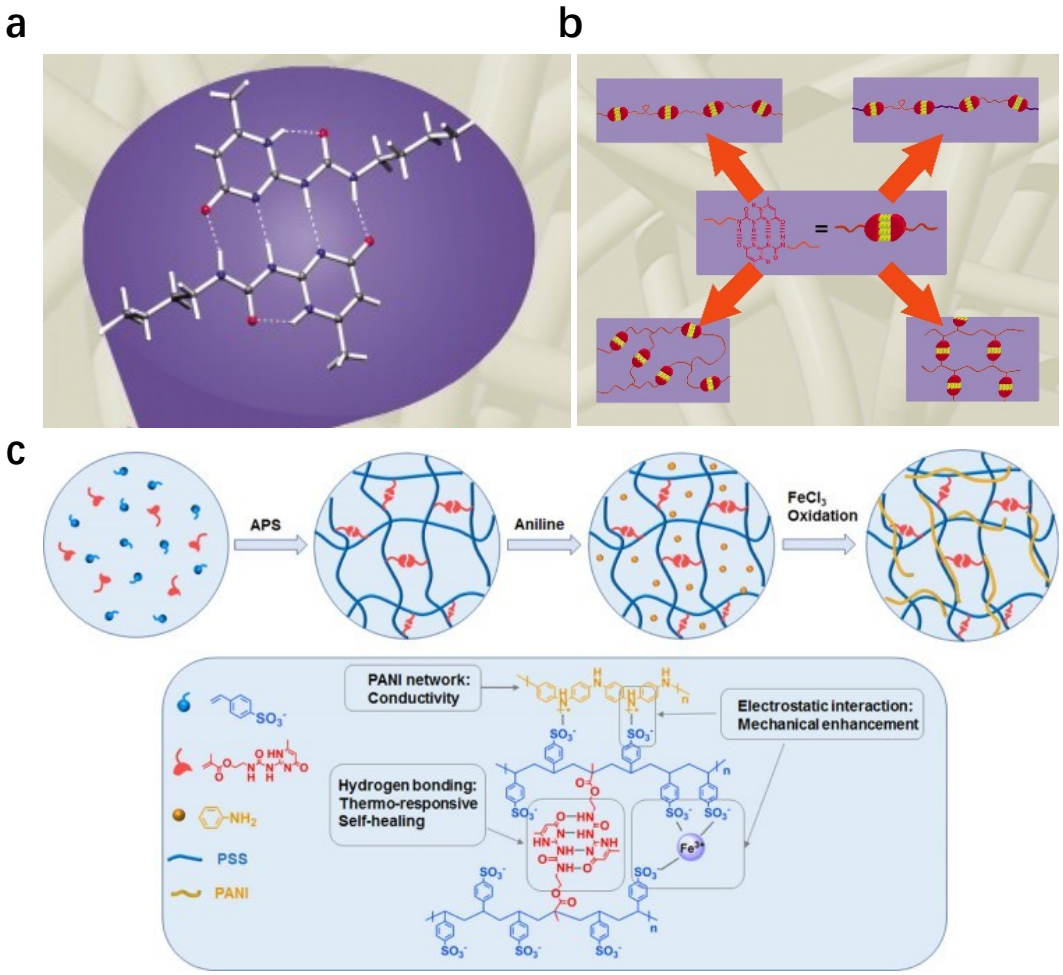

Figure 1.4 (a) Schematic representation of the H-bonded dimer of the UPy group. (b) Different possible architectures of supramolecular UPy group contained polymers (Reprinted with permission from reference [54], © Springer Nature Limited). (c) Schematic illustration of the synthesis process and the formation mechanism of the supramolecular PANI/PSS–UPy hydrogel (Reprinted with permission from reference [55], © American Chemical Society).[55]

1.2.2 Electrostatic Interactions

Electrostatic interactions are forces that occur between nearby atoms or molecules with partially opposite charges. They exist widely in biological molecules such as proteins, peptides and enzymes. Electrostatic interactions significantly affect molecular recognition and assembly by providing constant and strong interactions and have been applied to biocompatible hydrogels. Han et al. developed a bottom-up electrostatic self-assembly hydrogel for tissue engineering by immersing poly (ethylene glycol) (PEG)-based hydrogel into a solution with positive poly (2-(methacryloyloxy) ethyltrimethylammonium chloride) (PMETAC) or negative poly (2-acrylamido-2-methyl- propane sulfonic acid sodium salt) (PNaAMPS)-charged microgels. This multilayer hydrogel has shown a controlled 3D construction and great potential for applications in cell encapsulation, drug delivery and tissue regeneration.[57] A supramolecular hydrogel with the combination of peptides and polymers was reported by Criado-Gonzalez et al. The electrostatic interaction between the phosphate groups of Phosphorylated-Fmoc-Tripeptide and charged amino groups of Poly(allylamine hydrochloride) (PAH, a cationic polyelectrolyte) driven the formation of hydrogel, enhanced the mechanical properties of the hydrogel, endowed it with antimicrobial capacity and provided a new possibility for injectable biomaterials.[58]

1.2.3 Hydrophobic Interactions

"Hydrophobic interaction" is a term describing the spontaneous aggregating tendency of nonpolar functional groups or molecules between hydrophobes. This process is essential to biology because it is responsible for protein folding and stabilization, formation of phospholipid bilayer membranes and vesicles and so on. Hydrophobic interactions can be adopted into hydrogel systems by polymerizing hydrophilic monomer

chains with hydrophobic sequences. For example, the hydrophobically modified hydrogel of hydrophilic acrylamide (AAm) and hydrophobic N-4-Ethylphenylacrylamide (eΦAM) copolymer was synthesized by three different methods: homogeneous, micellar and heterogeneous polymerization. Hydrogels prepared by micellar polymerization (surfactant solubilized eΦAM micelles copolymerized with AM monomers and potassium persulfate initiator in an aqueous medium) showed thickening features because of the intermolecular hydrophobic associations.[59] A micellar polymerized hydrogel with a large amount of hydrophobic stearyl methacrylate (C18) or dococyl acrylate (C22) in the presence of AM was reported by Tuncaboylu et al. The incredible associated force between a hydrophobic fragment of C18 or C22 acts as a unique non-covalent crosslinker, maintains the structure in an aqueous solution and affords the hydrogel a self-healing ability and high toughness.[60]

1.2.4 Host-guest Interactions

Host-guest interactions refer to the complexation that involves two or more ions or molecules through unique molecularly recognized structures and noncovalent interactions. Guest units can be attracted into the cavity of the host units by hydrophobic interactions, hydrogen bonding, van der Waals force, etc. Host-guest interactions exist widely in biological systems, especially in the processes of biorecognition. Host-guest interaction-based hydrogels can be achieved by incorporating appropriate host molecules such as cyclodextrins (CDs), cucurbituril (CB), crown ether (CE) and paired guest molecules, while displaying diverse functionalities through the bonding of different guest molecules with various binding affinities. A self-standing supramolecular hydrogel was synthesized by the radical polymerization of a poly(acrylamide) modified CD host and a hydrophobic aliphatic guest, and the self-healing capacity was attributed to the reversible and sufficient host-guest interaction between CDs and the guest units of the cooperative complexation.[61]

The association and dissociation of host-guest complexes caused by external conditions imbue hydrogels with stimuli (e.g. pH,[62] temperature,[63] light[64] and redox[65-66]) responsivity and allow them to be applied in different areas such as artificial muscles, soft actuators and robots.[67]

1.2.5 Ionic Interactions

Ionic interactions involve the electrostatic attraction between two atoms or molecules with fully permanent opposite charges or strongly different electronegativities.[68] Alginate hydrogel is one of the most common kinds of hydrogel crosslinked by ionic interaction. Alginate is a natural polysaccharide that has been extensively used as synthetic extracellular matrices (ECMs). Cell adhesion ligand modified alginate hydrogel was used to culture mouse skeletal myoblasts [69] by employing ionic interactions and demonstrated the promise of alginate hydrogels in bioengineering in areas including interactive cell culture,[70-71] protein release[72] and cell encapsulation[73].

1.2.6 Multiple Non-covalent Interactions

Although non-covalent interactions are weaker than covalent interactions (which is proven by the typically far lower chemical energy release during bond formation), the various synergistic effects resulting from multiple non-covalent interactions play a role in the association and stabilization of hydrogels. By combining multiple non-covalent interactions within hydrogel systems, many attractive features emerge such as self-healing, high tensile/compressive strength, anti-fatigue, shape memory, stimuli-responsiveness, etc. Gao et al. prepared a multiple hydrogen-bonded and carboxyl-Ca^{2+} coordinating crosslinked supramolecular hydrogel by a directly photoinitiated polymerization and soaking strategy. Due to the multiple non-covalent interactions, the hydrogel exhibited an excellent stretchability (up to 2300%), high tensile (to a maximum of 1.3 MPa) and

compressive (to a maximum of 10.8 MPa) strength, self-healing capacity and reusability. Moreover, the tunable mechanical properties which were influenced by the changes in pH and Ca^{2+} concentration could be used for biosensors.[74] A tough, reusable and durable underwater adhesive hydrogel was reported by Fan et al. Benefiting from the π–π and cation–π interactions between the cationic and aromatic monomers contained in copolymer chains, the hydrogel not only showed a robust mechanical property (720% fracture strain with 1.0 MPa fracture stress and 0.35 MPa elastic modulus) but also exhibited instant and repeatable underwater adhesion with diverse surfaces via the interfacial electrostatic and hydrophobic interactions.[75] A straightforward sulfosuccinic acid (SA) soaked PVA hydrogel with enhanced mechanical and conductivity properties was achieved by employing hydrogen bonding interaction and electrostatic interaction, and the hydrogel showed promise in functional sensing applications.[76] Inspired by the adhesion mechanism in mussels, vital wet adhesive protein 3,4-dihydroxy-L-phenylalanine (DOPA) has been well investigated. DOPA, or molecules with catechol groups, could incorporate multiple non-covalent interactions such as hydrogen bonding interaction, metal-catechol coordination, cation-π interaction, anion-π interaction, π-π interaction, etc. into hydrogel networks, thereby having a wide application for functional hydrogels. By incorporating multiple non-covalent interactions, including electrostatic interactions, hydrogen bonding, hydrophobic interactions, and π–π interaction, hydrogels show enhanced adhesion to different surfaces. The positively charged PNIPAAm microgel (MR) and poly(dopamine) (PDA) contained hydrogel complex exhibited incredible adhesion to inorganic, organic and biological tissue surfaces due to the diverse non-covalent interactions, which also simultaneously endowed the hydrogel with excellent stretchability and self-healing capacity.[77] Feng et al. reported a multiple hydrogen bonding (H-bonding) interactions introduced hydrogel with two non-covalent crosslinked networks, and this mechanically

robust, self-healing, and shape memorizing hydrogel exhibited great promise for biomedical applications.[78]

1.3 Bioengineering and Sensing Applications of Multifunctional Hydrogels

Based on the increasing requirements of modern intelligent materials for human-machine platforms, tremendous efforts have been devoted to managing the functionality and performance of hydrogels and integrating them with novel biological features by enhanced processing techniques for biomedical applications. Multifunctional hydrogels with reversible noncovalent interactions possess many features, including self-healing properties, stimuli-responsiveness and biological tissue mimicking, rendering them perfect candidates to fulfill those requirements and have already been widely employed in related fields. A brief introduction to hydrogels utilized in relevant bioengineering and sensing applications is summarized in the following section.

1.3.1 Hydrogels for Bioengineering (Tissue Engineering, Wound Healing and Controlled Drug Delivery)

Tissue engineering has been proposed for the restoration, maintenance or improvement of biological tissues or organs and the generation of artificial tissues or organs by assembling functional constructs.[79] Materials used in tissue engineering should simulate the extracellular matrix of tissues, support cellular activities including cell adhesion, migration, differentiation and proliferation, and accelerate the repair and regeneration of tissues.[80] Taking advantage of tissue-mimicking, biocompatible and biodegradable multifunctional hydrogels are highly desired materials for tissue engineering applications, especially for tissue scaffolds because they can serve as platforms for cell growth and generation. Cell-laden hydrogel is a good example of tissue engineering applications.

Hydrogels have been employed as scaffolds for microencapsulation and have acted as immobilization media to support the growth of transplanted cells and protect them from attacks of the immune system.[81-82] Various cells (e.g., cardiomyocytes, hepatocytes, chondrocytes and stem cells) can be distributed homogeneously and encapsulated into hydrogel systems by adding them to the polymer solutions before gelation. Chondrocytes were encapsulated in degradable hydrophilic poly (vinyl alcohol)-co-poly (ethylene glycol) (PVA-co-PEG) hydrogels and secreted into the extracellular matrix. The elastic, porous and water abundant hydrogel not only provides structural scaffolding for the encapsulated cells but also allows nutrient transport between cells and extracellular matrices; this has been proposed as a new alternative treatment for the unspontaneous recovering process of damaged cartilage.[83] It has been proven that the pre-osteoblast cell-laden chitosan-HA hydrogel with bone-like nanostructured hydroxyapatite (HA) scaffolds accelerated bone regeneration.[84] Synthetic hydrogels incorporated with naturally derived proteins such as cell-adhesive, enzyme-sensitive and growth factor-binding peptides are emerging in tissue engineering. Bioactive sequences including collagen, gelatin, elastin, and fibrin peptides have been successfully combined with hydrogel networks via reactive groups such as the amine, thiol and maleimide groups and endowed the resulting natural ECM-mimicking hydrogels with one or more biofunctions. [85] For example, a self-assembling peptide-based hydrogel scaffold has been used to support the neuronal differentiation of encapsulated neural stem cells while enhancing the reconstruction of damaged brain tissue.[86] Arg-Gly-Asp (RGD) peptide sequences modified alginate or Poly (ethylene glycol) (PEG) hydrogels have been applied in bone tissue engineering for the repair of encapsulated osteoblasts.[87-89] By utilizing the interaction or attraction between functional groups or inserted bioreceptors in the hydrogel matrix and biomolecules such as adenosine triphosphate (ATP), adenosine diphosphate (ADP) and uridine triphosphate (UTP), hydrogels have also

been applied to monitor multitudinous extracellular activities by recognizing and calculating the concentration of specific biomolecules in tissue engineering.[90-94]

Skin is one of the most vulnerable organs in the human body because of its large surface area and its direct contact with the external environment. Although skin has superior restorative competence after damage, a suitable wound dressing could act as a temporary barrier to accelerate wound healing by isolating external stimuli and bacteria and supporting the regeneration and reorganization of tissue cells. Hydrogels have attracted great interest in wound dressing because of their advanced structures and features, such as their extracellular matrix semblable and their hydrophilic and antimicrobial properties. Among hydrogels, non-covalent hydrogels have been regarded as one of the most competitive materials due to their incredible functionalities and sustainable lifespan. Non-covalent hydrogels with injectable properties could provide many advantages in wound healing, especially in joint tissue wound care. They can easily access deep wound locations, cover irregular wound surfaces without mismatch and release encapsulated drugs in situ. For example, benzaldehyde-terminated Pluronic®F127 (PF127-CHO) micelles have been crosslinked via electrostatic and hydrophobic interactions and the hydrogel synthesized under physiological conditions (in PBS at 37ºC). This could be further applied to in situ gelation on the wound area, and the in vivo experiments showed that the antioxidant drug (curcumin)-loaded hydrogel significantly enhanced the healing process of the wound within a full-scale skin model.[95] This injectable, self-healing and pH-responsible hydrogel provides a novel possibility for wound dressing and also reveals the tendency of multifunctional and integrated hydrogels toward wound healing applications. Furthermore, antibacterial hydrogels can prevent infection in the wound area and consequently reduce the use of antibiotics. Many strategies have been designed to fabricate antibacterial hydrogels, including incorporating nanocomposites such as noble metal nanoparticles, metal oxide

nanoparticles and carbon nanomaterials, noncovalently encapsulating antibiotics and antimicrobials like ciprofloxacin hydrochloride (Cip), Chlorhexidine (CHX) and vancomycin and conjugating antibacterial peptides. One of the most straightforward methods is combining cationic polymers into hydrogel systems. Natural polymer gelatin and semi-synthetic polymer chitosan are two frequently used cationic polymers for wound healing. A good example is a radiation-induced gelatin/carboxymethyl chitosan hydrogel, which was shown to promote the attachment and growth of fibroblasts in vitro, demonstrating great potential for wound healing.[96] An injectable cationic hydrogel was generated with biodegradable poly(L-lactide)-b-poly(ethylene glycol)-b-poly(L-lactide) (PLLA-PEG-PLLA) and noncovalent associated triblock copolymers with D-lactide segments, and this hierarchically structured hydrogel has shown excellent antimicrobial performance in a broad-spectrum range (it completely inhibited the growth of pathogenic microbes including methicillin-resistant S. aureus, vancomycin-resistant enterococci, P. aeruginosa, K. pneumoniae, and C. neoformans and killed almost 100% of the microbes), non-cytotoxicity, non-hemolysis and biocompatibility to mammalian cells which is ideal for wound dressing applications in the clinical treatment of drug-resistant infections.[97] Li et al. reported a self-assembly injectable hydrogel formed through hydrophobic interactions between triblock copolymers. The triblock copolymer consisted of catechol functionalized polyethylene glycol (PEG) as outer blocks and positively charged poly[2(methacryloyloxy)-ethyl] trimethylammonium iodide (PMETA) as central parts. The hydrogel's efficiency at killing *Escherichia coli* (*E. coil*) was more than 99.8% which indicated that the hydrogel had excellent antimicrobial properties by inhibiting the growth of bacteria.[98]

Hydrogels are considered "smart" materials due to their tunable, environment-sensitive and biologically-mimicking properties.[99-100] Hydrogels with stimuli-responsiveness display a significant volume expansion or shrinkage with subtle changes in environmental factors

such as pH, temperature, redox, ionic strength and electric field, which can be used as a trigger method for drug release. Therefore, stimuli-responsive hydrogels have been extensively applied in controlled drug delivery systems as intelligent carriers. For example, modified pH-responsive hydrogels can deliver prescribed medicine to target organs or intracellular vesicles by employing a variation of pH in the human body. Hydrogels containing cationic polymers like chitosan and poly (ethylene imine) (PEI) swell in an acidic medium due to the electrostatic repulsion between positively charged polymer chains, which is caused by the protonation of functional groups (e.g., amino and imine groups). This swelling behavior can be used to deliver drugs to the stomach (pH = 1-3) and to treat gastric ulcers. On the contrary, anionic hydrogels show significant swelling behavior at neutral pH due to the ionization of acidic groups such as carbonyl, carboxyl and phenolic hydroxyl, which can be utilized for intestinal (pH = 6-7.5) drug delivery.[101] Oral insulin delivery is regarded as an alternative to traditional injection therapy for diabetes because it protects patients from infection and inflammation. However, the degradation of insulin in the acidic stomach environment during the oral delivery process is a major problem. Therefore, it is necessary to design drug delivery hydrogels that safely transport drugs past the gastric acid to the intestine. Rasool et al. reported a kappa carrageenan/ acrylic acid hydrogel via novel silane crosslinkers. The hydrogel presented a negligible release profile of insulin in simulated gastric fluid (SGF, pH = 1.2) and sustained a higher release rate in simulated intestinal fluid (SIF, pH = 6.8).[102] Moreover, low amounts (4–8%) of insulin were released from a salicylic acid (SA)-based hydrogel in SGF but achieved 90% release in SIF within 24 h.[103] The pH variation also exists in different cellular compartments such as endosome (pH = 6.2) and lysosome (pH = 5), and the swelling/ deswelling alternation of hydrogels in different pH has been tailored for precision-release drugs or proteins in specific cellular compartments.[104-107]

Temperature-responsive hydrogels are another widely explored candidate for drug delivery systems. The most common example is thermo-sensitive Poly(N-isopropylacrylamide) (PNIPAAm)-based hydrogel. PNIPAAm has an intrinsically low critical solution temperature (LCST) between 32-34 °C. Once the temperature rises above the LCST, the configuration of the PNIPAAm polymer chains will experience a coil-to-globule transition due to the characterized hydrophilic to hydrophobic shift.[108-109] Self-assembled peptide nanofibrils/ PNIPAAm hydrogel undergo reversible sol-gel transition near the body temperature of 37 °C, which indicates that when the hydrogel attaches to human tissues under physiological conditions, it can prevent gelation and perform a sustained linear release of antibacterial peptide.[110]

Molecular recognition is another technique employed in biologically mimicking hydrogels which simulates the recognition process and can be utilized for drug delivery. Those integrated systems have been proven to have tremendous value and have shown enormous potential for enhanced drug delivery systems. Moreover, by incorporating enzymes with hydrogel structures, hydrogels can provide environmental responses to biological analytes, which could enable them to be used as biosensors with drug delivery functions. One practical example is the glucose-responsive drug delivery system. Hydrogels can provide timely release of insulin in response to increased glucose concentration in the blood. In addition, combinations of multi-stimulus responsive hydrogels have flourished within the last two decades. Multi-responsive hydrogels can respond to more than one bio-signal and therefore release specified drugs at a targeted temperature, pH and specific biological analyte with prolonged, sustained and precision drug delivery performance, which provides benefits in multifunctional drug delivery systems.

In conclusion, functional hydrogels have emerged as potential candidates for controlled drug delivery. Their excellent biocompatibility, functionality and

responsiveness have been highly admired and widely employed to create complex, integrated and intellectual platforms with enhanced properties.

1.3.2 24Hydrogels for Biosensing

Wearable biosensing electronics have received extensive attention due to their attractive advantages such as their bio-friendliness, flexibility and stretchability. Enormous progress has been made in this area and a broad range of applications has been developed by monitoring various bio-signals including movement, glucose, insulin and enzymes. Hydrogels emerged for interfacial platforms with biosystems due to their excellent biocompatibility and are considered promising candidates for biosensing electronics. Many features contribute to the popularity of hydrogels for wearable biosensing devices: their water-abundant and soft nature resembles human tissue which can avoid mechanical mismatch; their intermolecular interactions with biological components; their regulating viscoelastic characteristics; their well-developed synthesizing methods for modifying and integrating multifunctional systems, etc. The responsivity of hydrogels to diverse biological signals by changing their selected properties can be used for biosensors. For example, due to the protons admitting or releasing behavior of pH-responsive polymers containing weakly acidic or primary pendant groups (including amine, pyrrolidine, morpholino, imidazole, piperazine, and pyridine groups), pH-sensitive hydrogels respond to the ionic strength alterations in the environment of biosystems. The ionization/deionization behavior relates to the pKa of corresponding polymers, leading to pH-sensitive hydrogels with a negative or positive swelling ratio. A hydroxyethyl cellulose (HEC)/hyaluronic acid (HA) hydrogel containing isoliquiritigenin (ILTG) was designed for the treatment of pH imbalance in the stratum corneum (SC). The natural pH of the

stratum corneum is typically in the range of 5.0–6.0, but when the acid mantle is broken down by skin lesions, the ionization of the carboxyl groups in HA residues caused by the increased pH leads to electrostatic repulsions between polymer chains, which promotes drug release from within the hydrogel and achieves more than 70% releasing efficiency. This hydrogel wound dressing also shows significant inhibition of the growth of Propionibacterium acnes and exhibits excellent skin permeability.[111] Grimes et al. illustrated a wireless magnetoelastic biosensor with biocatalytic precipitation for avidin detection. This bioaffinity-based sensor coupled with a biotinylated poly (ethylene glycol) (PEG)-immobilized surface can bind with streptavidin and cause mass change-based signals. The magnetoelastic sensor then shifts those signals to resonance frequencies for sensitive avidin detections (to a limit of approximately 200 ng/ml).[112]

Hydrogels with a thermo-triggered responsive property are also appealing for biosensing applications. For example, a volume or toughness change upon heating and recovering once cooling below the LCST can be observed in hydrogels built with hydrophilic and hydrophobic fragments. PNIPAAm and PEG are two commonly known polymers used in the creation of thermo-responsive hydrogels. A droplet-based multiplexed platform can provide single-cell secreted protein detection by encapsulating P(NIPAAM-co-AAc) immunosensors into the droplets. The significant high sensitivity is attributed to the thermo-responsive behavior of PNIPAAM-based microgel particles within cells. Body temperature causes the shrink of hydrogels and can therefore concentrate fluorescence signals within a smaller area, thereby instantly achieving signal amplification. Compared with conventional enzymatic reactions, this fluorescence signal amplification has a remarkable intrinsic signal enhancement capability for both sensitivity and detection limits.[113] Polyelectrolyte hydrogels, which respond to electric signals by adjusting the existing charges inside polymer networks, are also commonly used for biosensors.[114]

Besides sensing the pH value of bodily fluids, temperatures and electrical and chemical signals, glucose monitoring for diabetic patients and pregnant women is also a focus for the application of biosensors. For example, by following the theory of glucose oxidases which can convert glucose into gluconic acids, a cationic hydrogel with PEG grafts incorporated with activated glucose oxidase and catalase was used to detect glucose levels. The decreased pH due to the generated gluconic acid caused the volume expansion of the cationic hydrogel and the changed volume ratio gave information about the concentration of glucose. Aside from the intrinsic property change triggered by hydrogel biosensors, bioreceptor immobilized hydrogels are also commonly employed to identify certain bio-signals. Bioreceptors including antigen/antibodies, enzymes, cells and cellular structures, nucleic acids, DNA and biomimetic receptors have been incorporated with porous and high surface-volume ratio hydrogels through diverse methods (e.g., physical adsorption and entrapment, covalent binding, crosslinking techniques, or a combination of two or more) and have been widely used for recognizing small biomolecules such as glucose, lactate, urea and cholesterol.[114-116]

1.4 Objectives and Significance of the Work

Due to their intrinsic water abundant, biomimetic and biocompatible nature, hydrogels have attracted enormous attention in the field of bioengineering in the past three decades, and numerous uses of hydrogels in bioengineering and sensing applications have been demonstrated. Although many featured hydrogels, including mechanically robust, self-healing and stimuli-responsive hydrogels, have been well-studied in the literature, the integration of multifunctionality, enhanced mechanical properties and a facile fabrication process into one highly intelligent hydrogel platform and the exploration of their practical applications (especially in the context of bioengineering) still remain a challenge. The introduction of noncovalent interactions into hydrogel networks not only endows hydrogels with desirable properties such as improved mechanical properties, self-healing capability and stimuli-responsiveness, but also broadens the scope for developing multifunctional, biocompatible and mechanically superior hydrogels. This thesis aims to develop an integrated strategy to facilely fabricate multifunctional hydrogel systems by employing noncovalent interactions, and explore their potential applications in bioengineering, sensing or biomedical areas, such as wound dressing, motion detection and drug delivery. The fabrication methods and the new multifunctional hydrogels synthesized in this work will provide useful implications to develop advanced bioadhesives and self-healing biomaterials to meet the requirements in practical bioengineering and biomedical applications. The followings are three detailed objectives for this thesis work:

(1) Develop a highly stretchable, adhesive and conductive hydrogel network based on multiple noncovalent intermolecular interactions with antibacterial properties for wound dressing and strain-sensing applications.

(2) Develop a stretchable, compressible, and conductive hydrogel with high sensitivity for strain sensing, and demonstrate precise human motion detection in practical applications.

(3) Develop a tough adhesive hydrogel for dual drug delivery and wound healing with pH-responsive microgels and characterize the mechanical, drug-release and antibacterial properties.

1.5 Structure of the Thesis

In Chapter 1, a general introduction to multifunctional hydrogels and noncovalent interactions is presented, followed by a brief literature review of several applications related to bioengineering and sensing of noncovalent force-driven hydrogels.

Chapter 2 explains a hydrogen-bonding-driven hydrogel with self-healing, remodeling and electrical response sensing qualities. The hydrogel was prepared by copolymerizing the PVA/PMVEMA/TA (PPTA) ternary polymers and can be readily achieved and scaled up in both ionic and non-ionic systems. Due to the affluent dynamic hydrogen bonding interaction, this PPTA gel exhibited superior stretchability, fast and highly recovered self-healing ability, the ability to be remodelled into different shapes and robust adhesion properties on diverse substrates. Moreover, the hydrogel's sensing behavior and antibacterial characteristics were evaluated, and the results show great potential as an effective wound treatment material in bioengineering applications.

In Chapter 3, a multifunctional conductive hydrogel strain sensor was fabricated by incorporating a conductive polymer and a mechanically robust double network hydrogel. The mechanical properties were designed to span a broad spectrum by simply tuning the polymer's composition and the number of freezing-thawing cycles of the poly (vinyl

alcohol) (PVA)/ poly (acrylic acid) (PAA) double network (DN) hydrogel substrate. Furthermore, the interpenetrated conductive polymer Poly(3,4-ethylenedioxythiophene)-poly(styrenesulfonate) (PEDOT: PSS) network endowed the hydrogel with high sensitivity to strain sensing. The self-healing and self-adhesive properties resulting from the synergy of the ternary system and multiple reversible hydrogen bonding interactions were characterized toward practical applications, and the fatigue resistance behavior proved that this hydrogel-based strain and pressure sensor has great potential for wearable soft electronic devices.

In Chapter 4, a microgel-embedded drug delivery hydrogel system has been investigated. To fabricate an integrated pH and temperature dual responsive nanocomposite hydrogel for wound dressing, acrylic acid group functionalized microgels—which have been widely reported due to their pKa resulted pH responsiveness—were embedded in a semi-IPN PAAm/CS hydrogel matrix. The in vitro drug loading and releasing behaviors in different pHs and temperatures were analyzed, and the releasing kinetic profile shows that the hydrogel drug delivery system has a better-controlled release profile in the condition of the wound area (pH 7.4@37ºC) with a high-release efficiency (85% − 91%) and a long-release duration (48h). Moreover, the integrated hydrogel shows an excellent antibacterial property (92.50 ± 0.01 %) attributable to the pronated carboxylic groups of CS. In addition, the macroscopic wound healing panorama and the histological study indicated that the hydrogel system accelerated the wound healing process, which shows the great potential of this combined complex for bioengineering and biomedical applications.

In Chapter 5, the major conclusions and contributions of this work are provided. The outlook for future work is also addressed.

CHAPTER 2 Hydrogen Bonding-Driven Multi-Functional Polymer Coacervate Gel Network

2.1 Introduction

Coacervation is a common phenomenon in nature that involves a liquid-liquid phase separation process,[117] which is frequently observed among oppositely-charged polyelectrolyte systems.[118-119] By mixing a polyanion with a polycation, complex coacervate gels can be formed driven by the electrostatic attraction between the opposite charges, which generally depends on the polyelectrolyte concentration and pH of the aqueous solutions.[120-122] Coacervation has been achieved in both natural and synthetic materials systems based on various non-covalent interactions such as hydrogen bonding and hydrophobic interactions,[122-124] which has been employed as a main driving force in constructing many multi-functional hydrogels[125-127] and the formation of supramolecular assemblies or complexes.[128-129]

Tannic acid (TA) is a naturally derived polyphenolic compound[130] and is capable of interacting or cross-linking macromolecules at multiple binding sites through several interactions such as hydrogen bonding, ionic bonding and hydrophobic interaction.[131-132] TA also can form coacervate gel network based on coordination interaction with metal ions,[133] polyerms[134-135] and other functionalmaterials.[136-137] For example, the poly(vinyl alcohol) (PVA)/TA coacervate gel materials has been reported recently based on cooling down the hot solution to room temperature due to their strong hydrogen bonding interactions.[131] TA also can be interacted with a series of polyelectrolytes to form coacervation systems.[51] The coacervate hydrogels resulting from simple mixing of TA and other polymers such as poly(ethylene glycol) (PEG),[138-139] or poly(N-vinylpyrrolidone)

(PVP),[140] were reported to exhibit good adhesion or mechanical properties.

Although there are many examples exist for constructing coacervate gel networks, few of them focus on the biocompatible materials. Copolymers of alternating methyl vinyl ether and maleic anhydride (poly (methyl vinyl ether-*alt*-maleic anhydride), PMVEMA) and their derived forms are biodegradable materials as approved by the United States Food and Drug Administration (FDA), which possess low toxicity and high biocompatibility. PMVEMA has been widely applied in different medical applications such as encapsulation of pharmaceutical reagents in nanoparticles,[141] a thickening agent,[142] dental adhesives, and transdermal patches for wound healing.[143] PMVEMA has shown promising results for the long-term maintenance of human Embryonic stem cells (ESCs)[130] as well as a building block for antibiotic delivery vehicle to aid tissue regeneration at dental root canals. This interesting material inspires us to seek the possibility to use the polyphenols chemistry to engineer high-strength PMVEMA-based coacervates gel network with excellent properties.

In this work, we aim to make highly stretchable, moldable, rapid self-healing coacervate gel with antibacterial performance using the noncovalent interaction of TA-PMVEMA and TA-PVA to improve the performance of coacervate gel network on the basis of the aforementioned properties of TA, PVA and PMVEMA, which were all FDA approved biocompatible components.[144-146] It was designed and fabricated by simply mixing the PVA/PMVEMA/TA (PPTA) ternary polymer mixtures. The formation of the PPTA gel can be readily achieved and scaled up in both ionic and non-ionic systems. Noteworthy, this PPTA gel can be stretched up to more than 135 times of its original size and preparing mechanically strong fibers. Also, it can be remodeled on diverse substrates and different shapes. Moreover, the as-prepared PPTA gel exhibited excellent adhesion on various substrate and appearance valuable antibacterial properties against both *Escherichia coli* (Gram-negative) bacteria and *Methicillin-resistant Staphylococcus Aureus* (*MRSA*)

bacteria. The PPTA gel provides a promising paradigm for the development of biocompatible drug carriers and various biomedical applications.

2.2 Experimental Section

2.2.1 Materials

Poly vinyl alcohol (PVA) (99% hydrolyzed, average Mw = 89,000-98,000 g·mol^{-1}), Poly (methyl vinyl ether-alt-maleic anhydride) (PMVEMA) average Mw = 1,080,000 g·mol-1) Neil Red, glycerol and tannic acid (TA) were procured from Aldrich and were used as received.

2.2.2 Preparation of PPTA Coacervation Gel Network

Poly (methyl vinyl ether-alt-maleic anhydride) hydrolyzed solution was prepared by stirring PMVEMA aqueous suspension liquid (10%, w/w) at 90 ^{o}C for 4 h and cooling down to room temperature for use. PVA was dissolved into 90 ^{o}C deionized water with mechanical agitation for 30 minutes to prepare 10% (w/w) aqueous solution. TA was dissolved in DI water and ultrasonic for 30 minutes to get 10% (w/w) aqueous solution.10 ml homogeneous precursor solution was made by mixing PMVEMA and PVA solutions with volume ratio of 1:1, then 1 mL as prepared TA solution was slowly added into precursor solution to generate the PPTA coacervate gel under drastic stirring. By tuning the feeding mass ratio, different samples were prepared with PMVEMA: PVA= 0.1:1, 0.5:1, 1.5:1 and 2:1 (w/w). The stretched fiber is prepared by stretching a piece of gel sample with the size of 1.0 cm x 0.5 cm x 0.5 cm (Length, Width and Thickness) to 135 cm in length. The fiber is taken and ready for characterization.

2.2.3 Swelling Test

The swelling properties of PPTA coacervate gel were tested under different pH

condition. Aqueous solutions of pH 1, 4, 7, 10 and 13 were prepared and the solution pH was adjusted using HCl and NaOH solutions. PBS buffer were prepared with pH=7.4. The pre-weighted PPTA coacervate gels were soaked into these aqueous solutions. After a certain time, mass changes were monitored and the swelling percentage was calculated with the following equation, where *t* is the soaked time and 0 is the initial mass.

$$Swelling\ percentage\ (\%) = \frac{Mass_t - Mass_0}{Mass_0} \times 100\%$$

2.2.4 Characterization

The homogeneous porous structure of this coacervate gel network was investigated by a Zeiss EVO M10 scanning electron microscopy (SEM) under 10 kV accelerating voltage. All the coacervate gel samples were freeze-dried and coated a thin layer of gold in a gold sputter for 100 seconds before observation. Fourier transform infrared spectroscopy (FTIR, Nicolet iS50, Thermo Scientific) was used to scanning the bonding status of freeze-dried coacervate gel samples, with a resolution of 4 and range from 500 to 4000 cm^{-1}.

2.2.5 Rheological Properties Measurements

Rheological and self-healing properties were carried out with an AR-G2 rheometer (TA Instrument), a 20.0 mm 2.0° cone plate was used for all the characterizations. The shear modulus, G' (storage modulus) and G'' (loss modulus) were determined with an increasing shear frequency from 0.1 to 100 rad/s at a constant strain of 1% and temperature at 20 °C in an oscillatory frequency sweep measurement. The self-healing behavior was performed by strain amplitude sweep (oscillation strain in the range of 0.1-200% with shear frequency equal to 10 rad/s, then go back to 1% strain immediately) through breaking the gel network and observing the network reconstruction. Cyclic tests were also employed to evaluate the repeatable self-healing ability with low strain (1%, 100 s) to high strain (100%,

100 s) steps shifting for 4 times.

2.2.6 Tensile and Adhesion Measurements

Tensile tests and adhesion tests were performed using an AGS-X universal tensile tester (Shimadzu, Japan) with a 50 N load cell, stretching rate was fixed of 50 mm/min, the same as our previous work.[124] For the tensile test, the coacervate gel specimens were prepared by applying a constant pressure (20 kPa) over a molded gel for 15 minutes, then cut into rectangular shape (dimension of length= 20 – 30 mm, width≈ 10 mm, thickness= 2 – 3 mm) with a sample cutting blade. The adhesive strength was examined by lap-shear tests by sandwiching the coacervate between two substrates with an overlap area of around 1cm in length, 2.5 cm in width and 1 mm in thickness, calculated by the division of the maximum shear strength over the bond area.

2.2.7 Electric Resistance Measurement

The electrical resistance of the PPTA coacervate gel was obtained using an electrochemical workstation (CHI920, CH Instruments). The sensing characterization was evaluated by the real-time resistance (R) change (calculated by R= U/I) by recording the I-t (current-time) curves with a 1.5 V output voltage (U). The strain sensitivity was estimated by the variation of electrical resistance change versus strain. Compression, bending, stretching and folding were also examined to evaluate the sensing performances of different applications.

2.2.8 Antibacterial Assays

The antibacterial activities of the PPTA coacervate gels were investigated using *Escherichia coli* (Gram-negative) bacteria, *MRSA* bacteria and in an agar disc test. Blank solutions were used as controls. PPTA coacervate gel samples were placed on the bottom

of 24-well plates and inoculated with 10 μL of a stock bacterial suspension (10^8 CFU/ml and 10^4 CFU/ml) for 3 h, no gel materials applied for control. Then 1 ml of the incubated bacteria suspension was taken and coated on agar substrate and incubated at 37 °C for 24 h with three replicates, and the number of bacteria colonies were determined based on the recorded images. The bacteria inhibitive rate was calculating by the following equation.

$$\text{Bacteria Inhibitive Rate} = \left[1 - \frac{\#\text{ of colonies in control} - \#\text{ of colinies in sample}}{\#\text{ of colonies in control}}\right] \times 100\%$$

2.3 Results and Discussion

PPTA coacervate gel is formed through hydrogen bonding interactions based on the multifunctional binding motif of TA and the pending groups of PMVEMA/PVA polymer mixture, structures are shown in **Figure 2.1a**. Coacervate gel with adjustable component ratio can be prepared by tuning the mass ratio of PMVEMA/PVA. The resulting soft and coacervate gel network can be easily isolated from the original solution. The hydroxide groups of PVA and carboxylic acid groups of PMVEMA can bind with polyphenol groups of TA through intermolecular hydrogen bonding interactions. After preparing the PMVEMA/PVA solution by mixing 10% (w/w) of PMVEMA and 10% (w/w) PVA at room temperature, a homogeneous solution formed under gentle stirring. When certain volume of 10% (w/w) TA solution was injected, a coacervate inhomogeneous solution was formed. However, only clear solution was observed during the mixing of PMVEMA and PVA polymers. The proposed interaction mechanism for the formation of the PPTA coacervate gel is illustrated in **Figure 2.1b**. In order to evaluate the effect of PMVEMA/PVA ratio on the formation of PPTA coacervate gel, experiments were conducted on different cases with PMVEMA: PVA = 0.1:1, 0.5:1, 1.5:1 and 2:1 (w/w). The results (**Figure S1**) show that regardless the PMVEMA content, PPTA could be immediately formed when the three components were mixed.

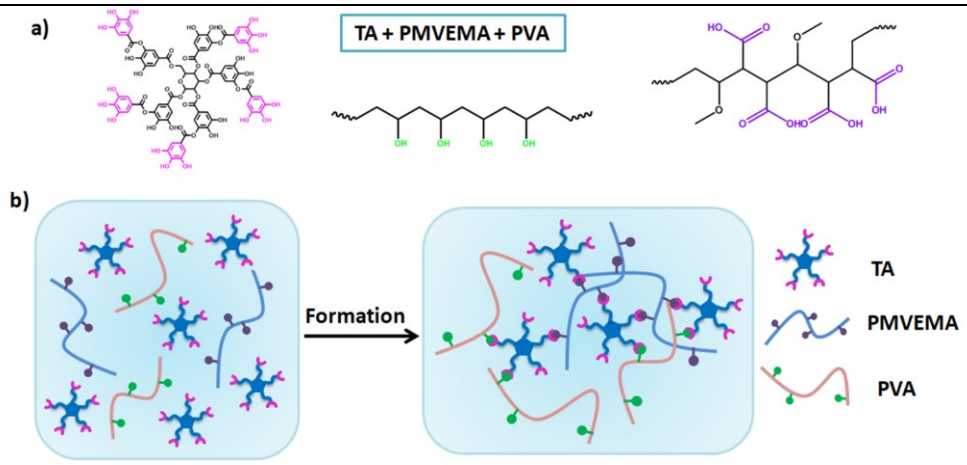

Figure 2.1. Highly stretchable, reprogrammable PPTA coacervate gel formation mechanism. (a) Schematic representation of the coacervate gel network structures of the PPTA. (b) Mechanism representation of PPTA coacervate gel formation.

In **Figure 2.2a**, the SEM images illustrate the porous structure of formed gel network reveals the interactions appear between TA and polymers. The structure of stretched gel fiber was shown in **Figure 2.2b**, which gives the smooth surface with a diameter of ~70 µm. FTIR analysis was carried out to determine the intermolecular interactions between TA and PMVEMA/PVA. In the FTIR spectra shown in **Figure 2.2c**, the peak at around 2950 cm^{-1} is mainly contributed by C-H stretching from PVA, which slight shifts to higher wavenumber possibly due to the interaction between PVA and TA. The peaks at ~1250 cm^{-1} and ~1550 cm^{-1} (indicated with black arrow) are clearly contributed by PMVEMA[147-148] and peak at ~3700 cm^{-1} (dash line) is attributed to the vibration of the phenolic hydroxyl group from TA. The acetal vibration peak (blue arrow) at ~1080 cm^{-1} is possibly due to the presence of chemical reaction.[149-152] These changes suggested that the intermolecular interactions between PMVEMA/PVA and TA exist during the coacervation process.

The swelling properties under different pH condition were evaluated by soaking the prepared PPTA coacervate gels into aqueous solutions with pH value of 1, 4, 7, 10, 13 and

PBS buffer (pH 7.4). The images shown in **Figure S2** clearly present that the gel structure was destroyed under pH 13 after immediate soaking and was completely disappeared after 1 day, which was attributed to the stability of tannic acid that could be readily oxidized under high pH. Moreover, the gel structure was relatively stable under other pH conditions.[153-155] The swelling test (**Figure S3**) up to 12 days shows that the gel slightly shrunk at the beginning (Day 1) and swelled afterward under pH 1. However, a gradually increasing swelling trend was observed for all the other pH cases. The result is possibly induced by the balance of osmotic pressure and tannic acid stability, as well as the pH responsive property of PMVEMA.

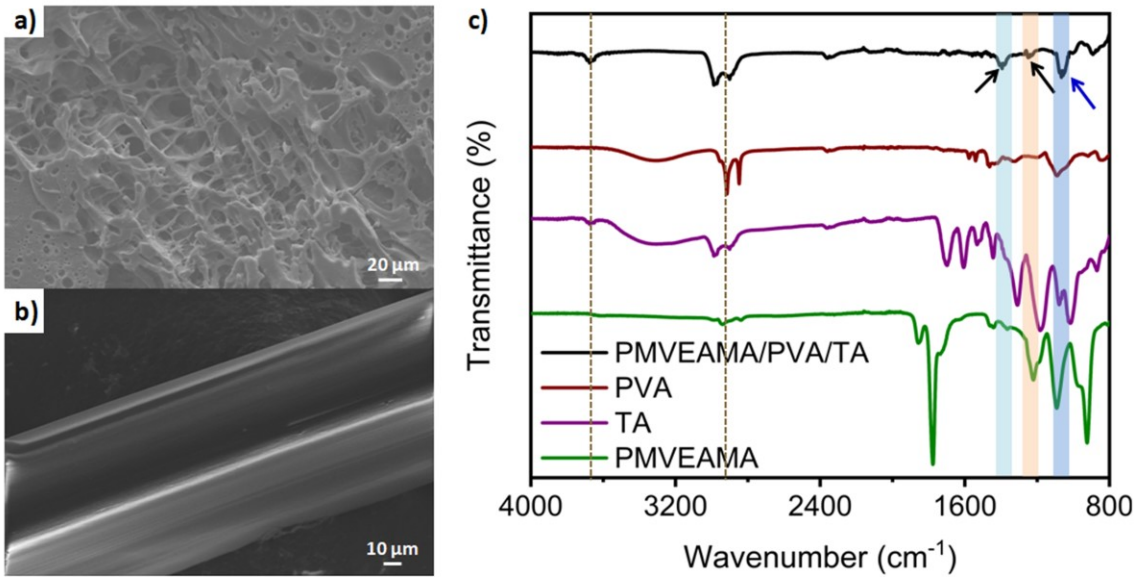

Figure 2.2. SEM images of (a) prepared gel structure and (b) gel fiber with a diameter of ~70 µm. (c) FTIR Spectra of as-prepared PPTA gel, PVA, TA and PMVEAMA. Black and blue arrows indicate the peak positions from PMVEMA. The reddish line shows the peak corresponding to PVA and TA.

To evaluate the highly stretchable properties of prepared PPTA coacervate gel, a gel with diameter of 1.0 cm x 0.5 cm x 0.5 cm (Length x Width x Thickness) was taken and stretched by external force, as shown in **Figure 2.3a**. The gel can be stretched up to

135 times of its original length. The strain-stress curve, conducted on a rectangular shape with the dimension of length 20 – 30 mm, width 10 mm, thickness 2 – 3 mm, shows that this prepared PPTA gel has excellent elongation properties, as shown in **Figure 2.3b**, with the maximum strain reaching ~2300% as compared with that (~1700%) of the pure PVA/TA gel system. It is noted that the stress of the gel shown in Figure 2.3b (~8 kPa) is the nominal stress. Since this material is highly stretchable with large elongation capability, the instantaneous stress changes with the cross-section area that varies during the stretching process. The true stress in the ending of the tensile test was calculated using the force divided by the cross area of the fiber which was formed from the PPTA coacervate gel during the stretching process, as shown in Figure S4 in Supporting Information. Based on the above consideration, the true stress was calculated using the following equation.

$$\text{True stress} = \frac{\text{Force}}{\text{Cross Area}} = \frac{\text{Force}}{\pi(\frac{D}{2})^2} \text{ (D is diameter)}$$

Here, the disruption point force was considered as an example to determine the true stress. From the SEM images in Figure 2.2, the diameter of stretched materials is ~70 μm. Based on the calculation, the true stress reached 7.67 MPa when the PPTA gel achieved the maximum strain. Here we want to stress that the elongations of the PPTA gel are much higher than other types of PVA gels (100-500%) and PVA/TA hydrogel (around 1100%) as reported.[131]

The strong hydrogen bonding interactions between PMVEMA/PVA and TA molecules endow the coacervate gel with high moduli. The amorphous structure and reversible nature of hydrogen bonding provide the gels with an effective energy-dissipating mechanism, leading to their high tensile strengths and elongation behaviors. The amorphous structure was demonstrated in the PVA/TA hydrogel system under different preparation temperatures (25 and -15 °C).[131, 156] In the previous studies, no typical peaks

of PVA crystallites were observed in the XRD spectrum of the PVA/TA system, with only a blunt amorphous peak centered at 2θ = 21.5°.[131, 157] The strong hydrogen bonding interaction between PVA and TA could prevent the formation of PVA crystallites. The stretched fiber exhibited excellent mechanical properties. The tensile strain test of this stretched fiber proves that the stress strength is still higher than 1.3 MPa, as shown in **Figure 2.3c**. The higher tensile strength from stretched fiber compare to the bulk coacervate gel materials may correspond to the water content and alignment of the gel structures, which will be further studied.

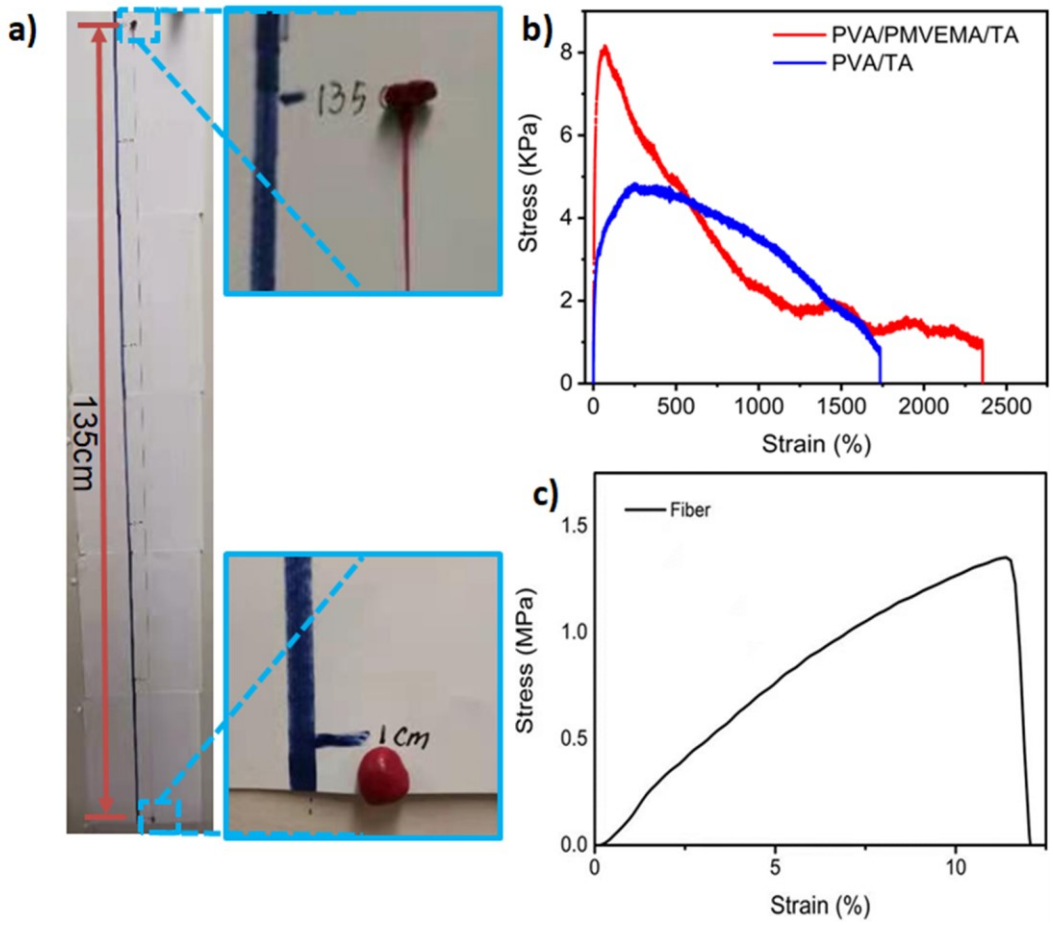

Figure 2.3. Highly stretchable PPTA coacervate gel fiber fabrication and characterization. (a) Elongation of prepared PPTA gel and (b) tensile strain test results of prepared gel structure. (c) Stress-strain test on the prepared PPTA gel fiber in (a).

Next, the viscoelastic properties of the PPTA coacervate gel were examined. Frequency-dependent (at a constant strain of 1%) oscillatory shear rheology (**Figure 2.4a**) of the PPTA coacervate gel shows that G' (storage modulus) is dominant compared to G'' (loss modulus) across the range of experimental frequencies, indicating the solid-like behavior. The continuous step change of the oscillatory strain between 400% and 1% at the same frequency (1 Hz) was given to assess the strain-induced damage and self-healing property of the PPTA coacervate gel (**Figure 2.4b**). The self-healing behavior was performed by strain amplitude sweep (oscillation strain in the range of 0.1-200% with shear frequency equal to10 rad/s, then go back to 1% strain immediately) through breaking the gel network and observing the network reconstruction. A high strain of 200% beyond the critical strain was applied to disrupt the coacervate gel network. As displayed, the G' value of the coacervate gel dropped dramatically along with an inversion of G'' exceeding G'. Following this, a low strain of 1% was applied to inspect the recovery of the gel structure, with the G' value immediately restored to its initial value. Cyclic tests were also employed to evaluate the repeatable self-healing ability with low strain (1%, 100 s) to high strain (100%, 100 s) steps shifting for 4 times. A high-magnitude strain (100%) was applied to break the hydrogel network. a low-magnitude strain (1%) was applied to examine the recovery ability of the coacervate gel network. It is shown that the damaged gel structure can recover quickly over three cycles of breakup and reformation of the network. Then, the shear modulus, G' and G'' of the coacervate gel were determined with an increasing shear frequency from 0.1 to 100 rad/s at a constant strain of 1% and temperature at 20 °C in an oscillatory frequency sweep measurement. **Figure 2.4c** displays the strain-dependent oscillatory rheological behavior of the coacervate gel network. G' curve intersected G'' curve at a certain strain determining the critical point. By further increasing the strain, the G' value decreased and was lower than G'', revealing a collapse of the gel state to a quasi-

liquid state. The storage modulus and loss modulus remain unchanged in the time-dependent test (**Figure 2.4c**, right) and a broad linear viscoelastic region is observed, implying that the PPTA coacervate gel has good stability for a long time.

Cut/heal test was conducted to investigate the self-healing characteristics of the PPTA coacervate gel. As shown in **Figure 2.4d-g**, two pieces of coacervate gel, one dyed with Nile Red, were cut into two parts and then brought into contact at ambient environment without any external intervention (**Figure 2.4d** and **2.4e**). As expected, the fractured two parts could adhere to each other and be holdup in seconds. After stretching the re-adhered gel sample, it still shows the same stretch ability and elongation properties as shown in **Figure 2.4f** and **2.4g**. The self-healing mechanism is explained by the dynamic hydrogen bonding interactions between the hydroxide of PVA, carboxylic acid of PMVEMA and catechol group in TA. When the hydrogel was cut into parts, many reversible hydrogen bonds were cleaved at the cut interfaces. These non-associated groups were exposed and had a strong tendency to link together. Thus, reconstruction of dynamic bonds was facilitated across the cut interfaces once the parts were brought in contact.

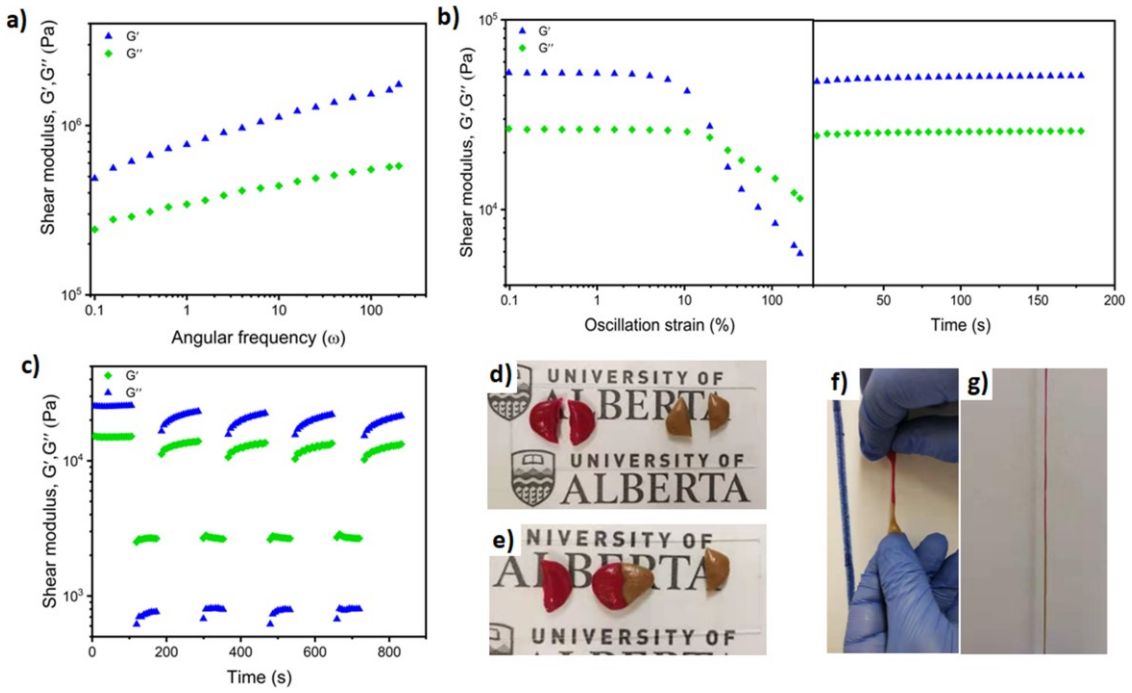

Figure 2.4. Rheological characterizations of PPTA coacervate gel. (a) Frequency-dependent (at a strain of 1%) oscillatory shears rheology of the PPTA coacervate gel. (b) The shear modulus, *G ′*(storage moduli) and *G″*(loss moduli) were determined with an increasing shear frequency from 0.1 to 100 rad/s at a constant strain of 1% and temperature at 20°C in an oscillatory frequency sweep measurement and a time-dependent (at a frequency of 1Hz and strain of 1%) oscillatory shear rheology. (c) The self-healing property of the PPTA coacervate gel demonstrated by the continuous step-strain measurements, which were carried out in steps of 1% and 200% oscillatory strain for four cycles. (d-g) Photographs of the self-healing process of PPTA coacervate gel. Demonstration of merging coacervate gel stained with different colors.

Due to the wide application of hydrogel materials in various areas, they are expected to have not only good mechanical and self-healing properties, but also the ability to adapt to harsh environmental condition. Interestingly, the obtained gel exhibited excellent anti-freezing property and could be readily molded and remolded into various

shapes, as shown in **Figure 2.5**. Glycerol has been widely used as a deicing agent. From **Figure 2.5a** and **2.5b**, it can be seen that the PPTA gel with adding 200 μL of glycerol shows very different appearance as compared to the untreated one after being frozen for 24 h at -20 °C. The treated gel sample can be easily twisted. However, the untreated one was broken to pieces when twisting it under this temperature. It is well known that hydrogen bonding interactions are relatively stable at lower temperature, allowing the gel to maintain a certain shape. The hydrogen bonding cross-linked PPTA gel was moldable and could form different fine structures, as shown in **Figure 2.5c-e**. Without any further treatment, the gel sample can be remodel to any different type of shapes. And their shaped gel samples could remain their shapes without cryogenic cooling.

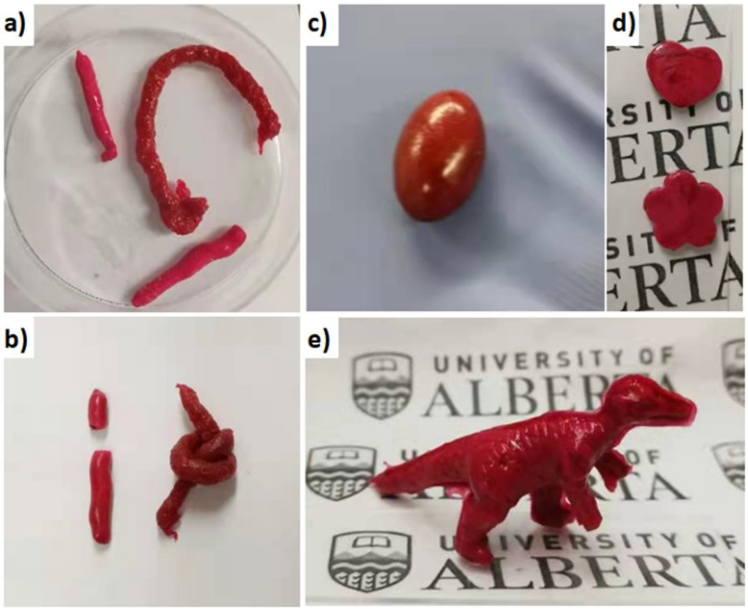

Figure 2.5. (a) Anti-freezing and remodeling properties of the as-prepared PPTA coacervate gel. Photographs of gel samples (a) after staying at -20 ºC for 24 h and (b) showing the anti-freezing properties (which can twist) compare to the untreated one (broken into pieces). The as-prepared gel can be refabricated into different shapes such as (c) egg shape, (d) heart and flower shape and (e) a dinosaur shape. It is noted that the gel was colored using Neil Red dye to better show the illustration.

Apart from the good extensibility and self-healing properties, the PPTA coacervate gel also demonstrated robust adhesion to different substrates such as copper, steel, glass, PTFE, PVC, and PC plate. Lap-shear testing was performed on the samples of two substrate plates coated with an area of around 10 mm x 25 mm PPTA coacervate gel to evaluate the adhesion strength (as shown in **Figure 2.6a**). The average adhesion strengths of PPTA coacervate gel on substrates of copper, steel, glass, PTFE, PVC, and PC plate are 43.86 kPa, 46.74 kPa, 26.80 kPa, 34.77 kPa and 22.69 kPa, respectively. Noteworthy, the contact time is only 10 min for the test, exhibiting the excellent adhesion behavior even under short contact. It is interesting to notice that the time dependence adhesive enhancement behavior which possibly due to the preference of repelling water molecules and mechanical anchorage on these two substrates, resulting in the enhancement of multi-modal hydrogen bonding interactions between adhesives and the substrates, thus improving the adhesive-substrate interfacial interactions, as shown in **Figure 2.6b**. The time-dependent adhesion properties of the PPTA coacervate gel was evaluated using a PC substrate. The adhesion strength increased with longer contacting time. Up to 6 times adhesion strength was achieved within 2 h as compared to the test of 10 min contact time, which could be due to the diffusion of interfacial polymer chains into the porous substrate or more hydrogen bonds formed between the gel and substrates. This result implies that the strong adhesion performance of the PPTA coacervate gel is crucial to its function as a catechol-based adhesive, avoiding its performance degradation upon oxidation.

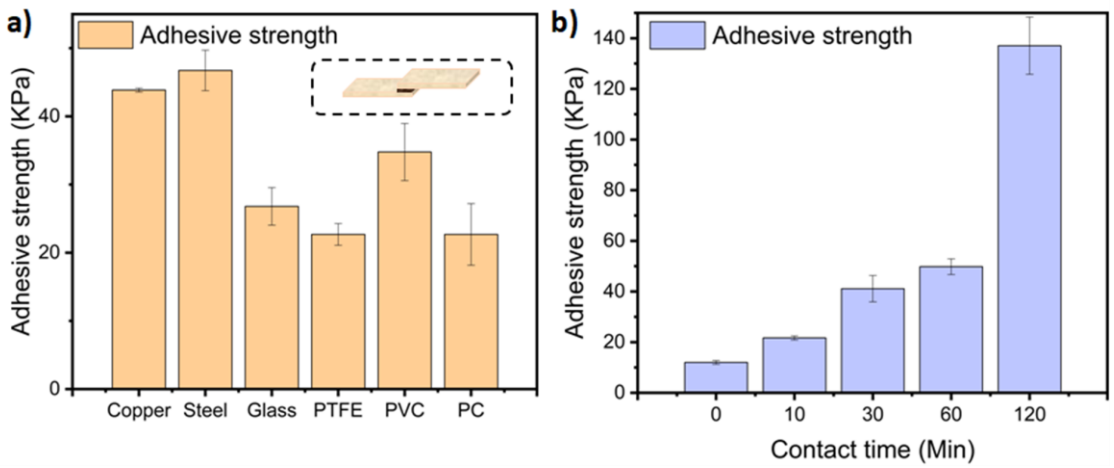

Figure 2.6. (a) Lap-shear adhesive strength of the PPTA coacervate gel adhesives on various substrates in deionized (DI) water after 10 min of contact. (b) Time-dependent adhesion behavior of PPTA coacervate gel on PC substrates.

Furthermore, we evaluate the sensing behavior of prepared PPTA coacervate gel. The electrical resistance signal of the PPTA coacervate gel was obtained using an electrochemical workstation (CHI920, CH Instruments). The sensing characterization was evaluated by the real-time resistance (R) change (calculated by R= U/I) by recording the I-t (current-time) curves with a 1.5 V output voltage (U). The strain sensitivity was estimated by variation of electrical resistance change versus strain. Compression, bending, stretching and folding were also examined to evaluate the sensing performances of different applications. First, we sandwich a piece of PPTA coacervate gel (dimension width x length x height of 10 mm x 10 mm x 5 mm) between two copper foil and connected with electric wire to monitor the current change with time when compression applied, as shown in **Figure 2.7a**. With the stretching of PPTA coacervate gel, the resistance continually increases with the stain increase, providing a great sensitivity on stretching. To better evaluate the sensing performance, we adhesive the piece of PPTA coacervate gel to the surface of partially blown balloon as shown in the inset representative image in Figure 5b. After intermittent inflation of Nitrogen to the balloon, we can observe the controllable

response of resistance change with the pressure increased (**Figure 2.7b**). Next, the bending response is performed by connecting two piece of glass substrate with the PPTA coacervate gel (dimension width x length x height of 10 mm x 20 mm x 5 mm), the resistance signal change was collected based on the bending angle difference, as shown in **Figure 2.7c**. After each angle bending, the set up was keep static and a constant current can be observed, which proving the PPTA coacervate gel is sensitive and stable during the bending sensing performance. With the excellence reprogrammable and stretchable properties of PPTA coacervate gel as we mention previously, a hypothesis comes after evaluating the sensing performance on stretching and bending, whether the response could be reversible after folding the stretched coacervate gel. The results are shown in **Figure 2.7d**. The left part is intermittent stretching one piece of PPTA coacervate gel every 50% elongation until 600% and the right part are adjusting the stretched gel back to the previous length by measuring the length of the gel between the conductive copper foil. We could clearly observe that the resistance change is fully reproducible under folding behaviour. The electrical sensing performance of prepared PPTA coacervate gel network will provide great opportunities for developing sensing device for health, motion or pressure monitor in future.

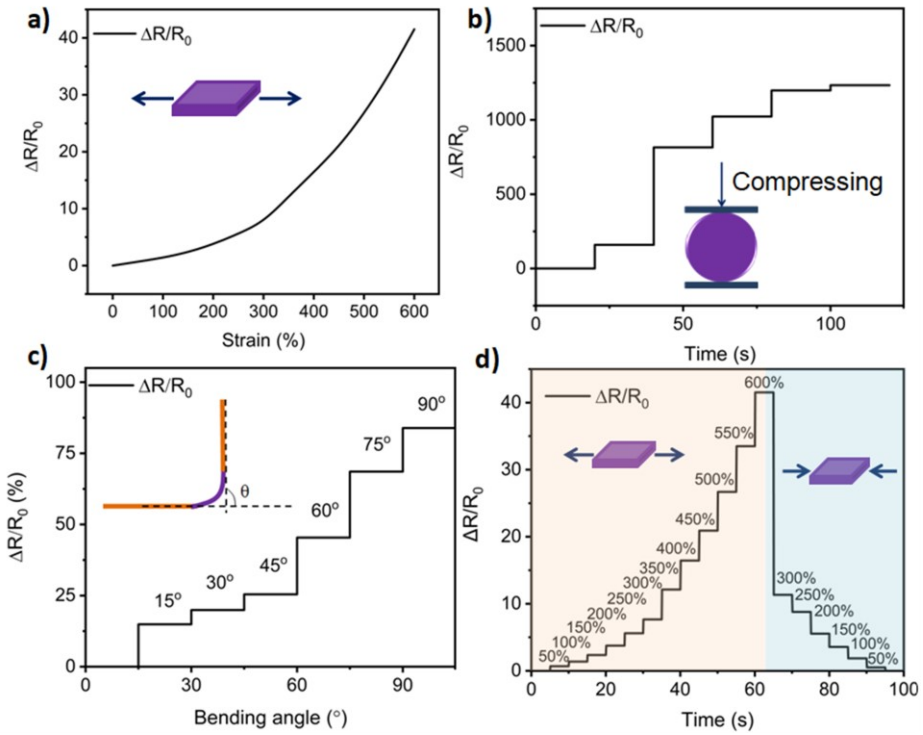

Figure 2.7. Sensing behavior of as-prepared PPTA coacervate gel based on the electrical resistance signal change under stretching, bending, compression and folding operation: (a) resistance changes under continually stretching, (b) electrical signal changes on balloon pressure monitor and (c) bending sensitive performance with different bending angle, and(d) the reversible resistance signal changes with stretching and folding cycling.

Based on the potential broad-spectrum antimicrobial activity of PMVEMA polymer and the polyphenol groups from TA, we also performed antibacterial experiments for the PPTA coacervate gel. As shown in **Figure 2.8**, gram-negative *E. coli* and *MRSA* were used as model bacteria for the agar antibacterial tests. Gram-negative *E. coli*, one of the top five microbes causing surgical infections, and *MRSA*, a group of gram-positive bacteria that has multiple drug resistance were used to evaluate the antimicrobial performance of the developed PPTA coacervate gel. As presented in **Figure 2.8a**, the PPTA coacervate gel displayed a 100% reduction of *E. coli* and *MRSA* for both 10^4 CFU/ml and 10^8 CFU/ml, and this concentration is about 6 orders of magnitude higher than that of an operating theatre in use.

Up to date. the antibacterial mechanism for polyphenol-based materials is still not fully

understood.[158] Several mechanisms have been proposed. For example, it was proposed that the polyphenol-based material could act as an inhibitor of the sugar and amino acid uptake to prevent bacterial growth,[159] or could pass through the bacterial cell wall to kill the bacterial.[160] The antibacterial activity of the PPTA coacervate gel is contributed by both PMVEMA and TA. Strong antibacterial behaviors of these components have been demonstrated previously. For example, a recent study[161] showed that no bacteria could be observed on the surface of TA modified films after 24 h of contact. Thus, with the PMVEMA and TA embedded in the PPTA gel system, strong antibacterial activity would be expected. The antimicrobial activity of the gel material could be ascribed to the presence of both PMVEMA polymer and polyphenol groups from TA, which could efficiently kill *E. coli* and *MRSA* in bacterial counting tests (**Figure 2.8b**).

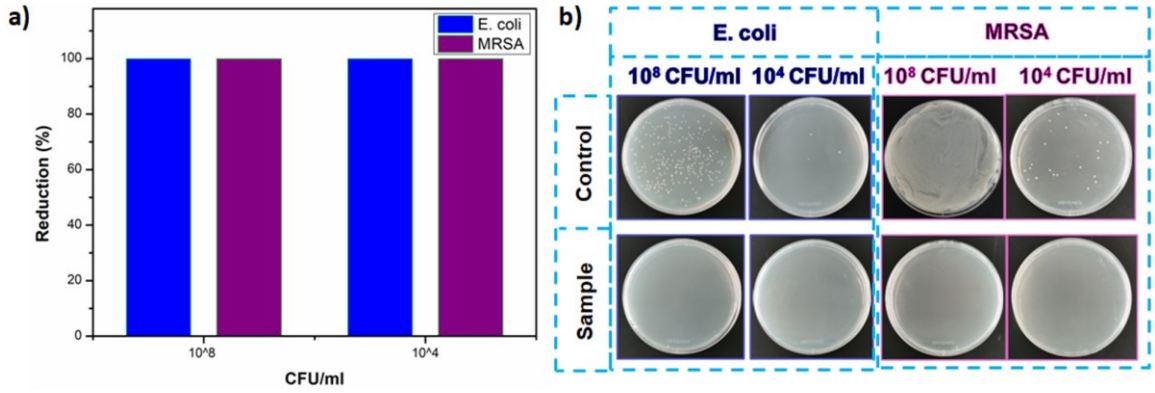

Figure 2.8. Antibacterial performances of PPTA coacervate gel against *E. coli* and *MRSA*. (a) Bacterial inhibition rate for concentrated and diluted bacterial suspension treatment after 24 h incubation. (b) Images of *E. coli* and *MRSA* colonies on an agar plate from a concentrated and diluted bacterial suspension without treatment and treated with PPTA coacervate gel sample.

2.4 Conclusions

In this work, we have developed a novel coacervate gel based on non-covalent

intermolecular interactions via one-step mixing of PMVEMA, PVA and TA aqueous solutions, where the coacervation process is mainly driven by the intermolecular hydrogen bonding interactions between catechol groups of TA and hydroxide groups of PVA and carboxylic acid groups of PMVEMA polymers. This PPTA coacervate gel can be readily scaled up and applied to various applications, including adhesive to different substrates, sensing to compressing, bending and pressure change and antibacterial materials. The one step coacervate gel preparation strategy is facile for practical operation, and the as-prepared coacervate gel is demonstrated as an effective antibacterial material for the treatment of injuries and other related bioengineering applications, which is beneficial for practical surgical treatments. Furthermore, the electric response sensing behaviour could promote the PPTA gel materials as a great candidate for fabricating reusable strain sensors. Noteworthy, this hydrogen bonding-driven coacervate gel also holds great potential in biomedical applications, such as biocompatible tissue glues and wound dressings. The free pending carboxylic acid groups on the PMVEMA polymer chains in the gel network allow further post-functionalization for various potential applications.

CHAPTER 3 Stretchable, Compressible, and Conductive Hydrogel for Sensitive Wearable Soft Sensors

3.1 Introduction

Wearable soft electronics have attracted enormous attention over the past decade with promising applications in health monitoring/sensory devices,[162-163] electronic skins,[164-165] and actuators.[13, 166] Although conventional metal-based electronics show fast responses and signal transitions, they generally suffer from poor mechanical flexibility. Several approaches have been explored to address the issue by integrating soft stretchable polymer films, elastomers or hydrogels with conductive components, including metal nanoparticles [167] or nanowires,[168] liquid metals,[169] graphene oxide,[170] MXene,[171] carbon nanotubes,[172-173] poly(ionic liquid) [174] and conjugated conductive polymers.[175-178] Among them, the strategy of combining hydrogels with conducting polymers (e.g., PEDOT: PSS) show great promises for fabricating conductive hydrogel-based soft electronics due to the biocompatibility of constituted components, tunable functionalities as well as the mechanical match with soft biological tissues.[179-185] However, the weak and brittle nature of conventional hydrogels significantly limit their applications for wearable soft electronics. Double network (DN) hydrogels hold potentials in stretchable soft electronics due to their superior mechanical properties.[186] Liu *et al.* developed a stretchable κ-carrageenan/PAAm DN hydrogel through one-pot photopolymerization. The hydrogel can be stretched up to 10 times of its original length and it could be used for strain sensing.[187] Yang and Yuan designed a conductive agar/PAAm double network hydrogel with over 1600% extension and high toughness (2.2 MJ/m^3) for both thermal and mechanical sensing.[188]

In practical applications, wearable soft electronics are frequently subjected to external stress caused by stretching, compressing, bending or twisting from body movement. The accumulation of stress may lead to the damage of the devices, limiting their lifespan.[173] Therefore, it is desirable to render the conductive hydrogel with self-healing property to improve the material durability and reliability.[189] Hydrogen bonding interactions is one of the most common dynamic intermolecular interactions for constructing self-healing hydrogels due to the abundant hydrogen bonding donors and acceptors (e.g., hydroxyl groups, carboxyl groups, amine groups, etc.) in both natural and synthetic polymers.[11, 190-191] Self-healing hydrogels based on hydrogen bonding interactions demonstrate fast healing efficiency due to the immediate hydrogen bonds dissociation/association.[192-193] In addition, the strong interfacial hydrogen bonding interactions could also provide the hydrogel with self-adhesive property to different substrates, not only allowing the device to be used without the aid of tape or glue, but also preventing the delamination between device and biological tissues for better sensing performance.[194-197] It is of great significance while remains a challenge to fabricate a mechanically robust conductive hydrogel with multifunctionalities using feasible raw material through facile preparation method.

Herein, we report a facile approach for fabricating a stretchable conductive hydrogel by introducing the conducting polymer PEDOT: PSS into a PVA/ PAA double network hydrogel. The hydrogel can be facilely formed through a one-pot free-radical polymerization method, followed by freezing-thawing process. The as-prepared hydrogel sensor could span a wide spectrum of mechanical properties by simply tuning the polymer composition and the number of freezing-thawing cycles. The rich hydrogen bonds within the network not only offer the hydrogel with excellent self-healing property, but also provide self-adhesiveness towards different substrates. Meanwhile, the addition of PEDOT:

PSS endows the hydrogel with good conductivity and high sensitivity to mechanical strain, allowing the as-prepared hydrogel to be used as a strain sensor for detecting various human activities including finger bending, walking, pulse and vocal cord vibration. The as-prepared multifunctional conductive hydrogel sensor holds great promises for wearable sensory devices and electronic skins.

3.2 Experimental Methods

3.2.1 Materials

Poly(vinyl alcohol) (PVA, 99+%, Aldrich), Acrylic acid (AA, 99+%, Aldrich), Poly(3,4-ethylenedioxythiophene)-poly(styrenesulfonate) (PEDOT: PSS, 1.3 wt% dispersion in H_2O, Aldrich), ammonium persulfate (APS, 98%, Aldrich), N, N′-Methylenebis(acrylamide) (MBAA, 99%, Aldrich) and N, N, N′, N′-tetramethylethylenediamine (TEMED, 99%, Aldrich) were used as received.

3.2.2 Preparation of PVA/PAA/PEDOT: PSS Double-Network Hydrogel

A series amount of PVA (0.7, 0.6, 0.5, 0.4,0.3 or 0.2g) was dissolved in 4 mL Milli-Q water at 90°C to prepare the PVA solution. Then AA (0.3, 0.4, 0.5, 0.6, 0.7 or 0.8g), PEDOT: PSS (1 mL), APS (1% w/w), MBAA (0.25% w/w) and TEMED (1 μL) were added into the corresponding PVA solution and stirred at 0°C in an ice bath for 30 min. The homogeneous solution was transferred to a sealed glass mold. The first covalently crosslinked PAA network was formed after heating at 60°C for 5 h. The resulted hydrogel was then frozen at -20°C overnight and thawed at room temperature for 3h to form the second physically crosslinked PVA network. The freezing-thawing cycle was repeated one to three times.

3.2.3 Characterization

The surface morphologies and internal crosslinking structures of hydrogels were captured by a scanning electron microscopy (SEM; Zeiss EVO M10) operated at 5 kV acceleration voltage. Fourier transform infrared (FTIR) spectra was obtained from a Thermo Scientific Nicolet iS50 FTIR spectrometer in the frequency range of 500−4000 cm^{-1}. All the samples prepared for SEM and FTIR inspection were freeze-dried and were cut into proper size.

3.2.4 Mechanical Tests

Both tensile and compression tests were performed on an AGS-X universal tensile testing machine (Shimadzu, Japan). For the tensile test, hydrogel specimens were cut into a rectangular strip (length=12mm, width=8mm, thickness=3mm) and were stretched at a 50mm/min tensile rate with a 50N load cell. Elastic moduli of the hydrogels are calculated by the initial slope of the stress-strain curve and the toughness is calculated by the area under the stress-strain curve. For the compression test, hydrogel specimens (diameter=16mm, height=15mm) were tested by a 2000N load cell at 20mm/min compression rate. The energy dissipation was calculated by the area of hysteresis loop in a loading-unloading compressive stress-compressive strain curve.

3.2.5 Self-Healing Tests

The macroscopic self-healing behavior of the hydrogel was demonstrated by bringing two pieces of separated hydrogels together after heating the cross section on a heat plate for 5 seconds. The recovery of illuminance of a light-emitting diode (LED) bulb and the current change during cyclic cutting/healing process was recorded by an electrochemical workstation (CHI920, CH Instruments, USA) to illustrate the self-

repairing electrical properties of PEDOT: PSS@PVA/PAA hydrogel.

3.2.6 Adhesiveness Tests

The adhesive behavior was visualized using the hydrogel sample to glue different substrates (wood, steel, glass, PTFE, PMMA, pork skin) together. The adhesive strength was conducted on the AGS-X tensile machine following typical lap-shear tests on different substrates. The adhesion strength is calculated by dividing the maximum force during detaching process by the overlap contacting area.[198-199] Hydrogel samples were cut into rectangle shape (L:15mm, W:10mm) and sandwiched between two substrates in same material then pull to separate after compressing for 1 min. The cyclic contact-separate process was performed by placing PEDOT: PSS@PVA/PAA hydrogel specimen between two substrates and contacting for 30s then pulling the upper substrate to fail. The contact and separate process was repeated for 20 times. All the adhesion tests were repeated for at least three times.

3.2.7 Electrical Tests

The electrical resistance of the PEDOT: PSS@PVA/PAA hydrogel was obtained from an electrochemical workstation which recorded the real-time I-t curve, the resistance was calculated through Ohm's law ($R = U/I$) with a constant applied 1.5V voltage. The electrical resistance variation versus compressive strain tendency was evaluated by the electrical resistant data from electrochemical workstation under a certain compressive strain test with 40 mm/min compressive rate which could also be demonstrated through the brightness change of a LED bulb.

The gauge factor (GF) ,[200] representative of the strain sensitivity, can be defined as the slope of resistance change rate ($\frac{R-R_0}{R_0} = \frac{\Delta R}{R_0}$) versus applied strain (λ), formulized as

$GF = \frac{\delta\left(\Delta R/R_0\right)}{\delta\lambda}$ and the sensitivity (S),[201] which indicates the pressure sensitivity, can be defined as the slope of current change ($\frac{I-I_0}{I_0} = \frac{\Delta I}{I_0}$) upon applied pressure (P), formulized as $S = \frac{\delta\left(\Delta I/I_0\right)}{\delta P}$. They are two important parameters to evaluate the sensing ability.

3.2.8 Sensing Tests

The wearable biosensor was assembled by proper sized hydrogel between two formed nickel electrodes and fixed on different parts of human body like finger, wrist, throat, and foot to investigate the sensing ability. The real time I-t curves were recorded to measure the electrical resistant change of human body motions.

3.3 Results and Discussion

3.3.1 Formation of the PEDOT: PSS@PVA/PAA Double-Network Hydrogel

PEDOT: PSS@PVA/PAA double network hydrogel was facilely prepared through a two-step process as shown in **Figure 3.1**. The first covalently crosslinked PAA network was formed through a thermo-triggered free-radical polymerization of the hydrogel precursor solution. In the second step, the second physically crosslinked PVA network was formed after freezing-thawing process because partial condensed PVA chains contribute to the precipitation of PVA crystallites in the freezing process, which act as crosslinkers and form physical network with other PVA chains by the strong hydrogen bonding interactions during the freezing-thawing process.[202-203] In addition, the carboxyl groups of PAA could form multiple hydrogen bonds with the hydroxyl groups of PVA, which could further improve the mechanical properties of the hydrogel. PEDOT: PSS colloidal particles were added as the conductive fillers and were homogenously distributed in the hydrogel network, which could provide high conductive channel for the system.

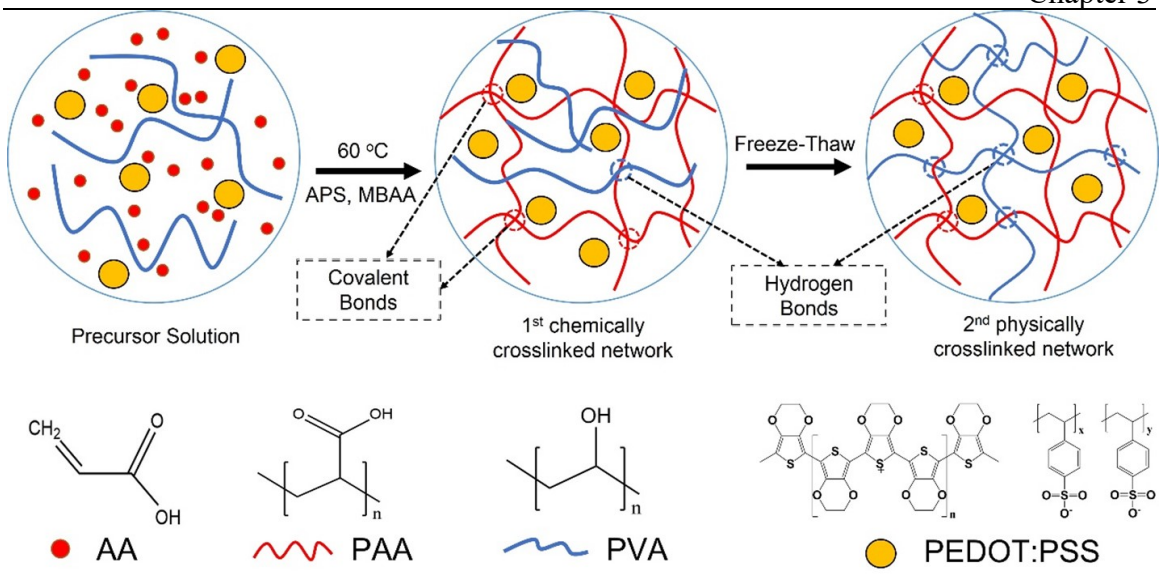

Figure 3.1. Scheme of the preparation process of PEDOT: PSS@PVA/PAA double network hydrogel.

The chemical property of the hydrogels was characterized by FTIR (**Figure S3.1a**). For the PVA/PAA DN hydrogel (blue), the peak at 3350 cm^{-1} could be attributed to the vibration of O-H. The characteristic peaks at 1452 and 1250 cm^{-1} were attributed to the asymmetric and symmetric stretching of COO- and C-O respectively, confirming the presence of PVA and PAA in the hydrogel sample.[204] With the addition of PEDOT: PSS (green), the peak of hydroxyl groups showed a red shift, which could ascribed to the weakening and lengthening of O-H bonds.[205] In addition, the peaks of O-H vibration in PAA shift from 1176 to 1170 cm^{-1}, 1238 to 1230 cm^{-1} and 1417 to 1408 cm^{-1}, indicating the hydrogen bonding interactions between PVA, PAA and PEDOT:PSS. The morphology of the PVA/PAA hydrogel with or without PEDOT: PSS was characterized by SEM (**Figure S3.1b and S3.1c**). Both hydrogels show uniform porous structures, but the pore size became smaller after introducing PEDOT: PSS into this double network system, resulting from a higher polymer fraction in the hydrogel network. The homogeneous distribution of PEDOT:PSS is indicated by the EDS in **Figure S3.2** and **S3.3**.

3.3.2 Mechanical Properties of PVA/PAA/PEDOT: PSS Hydrogels

To investigate the stretchability and elasticity of the hydrogel, a series of hydrogel samples with different PVA/PAA mass ratios were prepared and characterized by tensile tester (total polymer concentration were fixed at 200 mg/mL and weight percentage of PEDOT: PSS was fixed at 2wt%). As show in **Figure 3.2a**, with the increase of PAA weight percent, the maximum fracture strain increases from 400% to over 900%, while the Young's modulus decreases from 38.54 kPa to 7.08 kPa. The mechanical property of the hydrogel can also be fine-tuned by varying the number of freezing-thawing cycles as shown in **Figure 3.2b,** as the number of freezing-thawing cycles increases from one to three, the Young's modulus of PEDOT:PSS@PVA/PAA DN hydrogel (PVA/PAA=6:4) increases from 10.5 kPa to 121.7kPa while the maximum strain decreases from 723% to 563%. This is due to the increase of physical crosslinks formed between PVA crystallites and PVA chains through hydrogen boning interactions.[206] The weight ratio of PVA/PAA=6/4 was chosen and used for the following tests due to the balance of the stretchability and stiffness. The hydrogel (PVA/PAA=6/4) can be stretched up to 6 times of its original length (**Figure 3.2c).** As the strain sensors are constantly subjected to multiple cycles of stretching or bending, the elasticity and fatigue resistance were characterized by cyclic tensile tests with different maximum loading strains (100%, 300% and 600%). Although the as-prepared hydrogel showed a decreased energy dissipation in the second loading cycle at the strain of 100%, the superposition of the successive loading-unloading cycles was observed (**Figure 3.2d**). The maximum tensile stress of the hydrogel remained at 200 kPa after 100 loading-unloading cycles (**Figure 3.2e**).

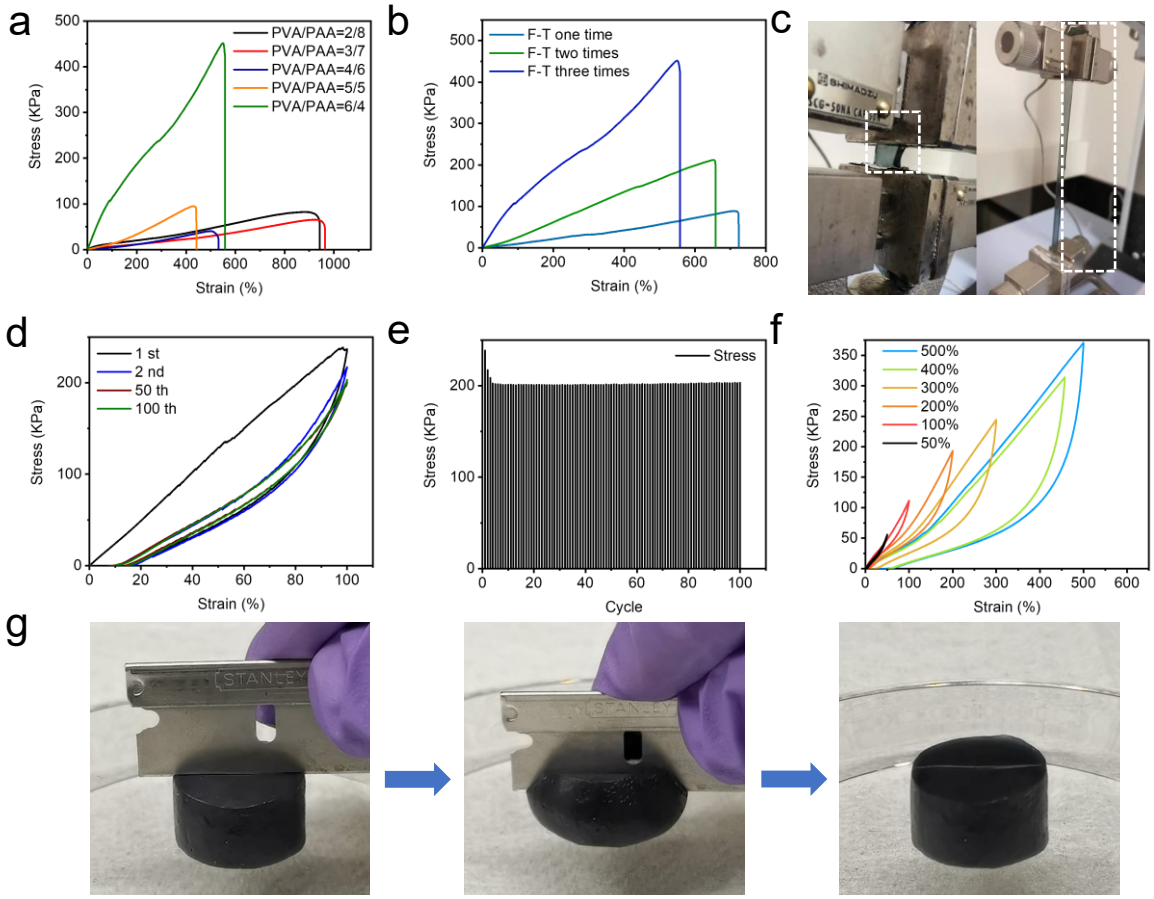

Figure 3.2. (a) Strain-stress curves of PEDOT: PSS@PVA/PAA hydrogels with different PVA/PAA ratios after three freezing-thawing cycles. (b) Strain-stress curves of PEDOT:PSS@PVA/PAA hydrogel (PVA/PAA=6:4) after different number of freezing-thawing cycles. (c) PEDOT: PSS@PVA/PAA hydrogel (PVA/PAA=6:4) before stretch (left) and after stretch (right). (d) Cyclic loading-unloading tensile tests of PEDOT: PSS@PVA/PAA hydrogel (PVA/PAA=6:4) with strain from 0-100%. (e) Tensile stress change in cyclic loading-unloading tensile tests. (f) Loading-unloading tensile test of PEDOT: PSS@PVA/PAA hydrogel (PVA/PAA=6:4) under different strain values. (g) Cutting hydrogel with a blade showing high toughness.

The large hysteresis loop in the first cycle can be attributed to the disassociation of multiple hydrogen bonds within the hydrogel network for energy dissipation and the recovery of the original shape and maximum stress in the successive cycles confirms the

excellent elasticity of the hydrogel. Similar fatigue resistance behavior of the hydrogel was also observed in the cyclic tests using 300% and 600% loading strains (**Figure S3.4a and S3.4b**). Apart from good stretchability and fatigue resistance of the hydrogel, it also shows high toughness as reveled by the loading-unloading tensile cycle tests at different strains from 50% to 600% (**Figure 3.2f**). Larger hysteresis loop can be observed with increasing maximum strain, which indicates a higher degree of energy dissipation due to the rupture of more hydrogen bonds during the mechanical loading. The high toughness allows the hydrogel to preserve structural integrity and recover to its original shape after being cut using a sharp blade from top to bottom (**Figure 3.2g**).

Compression tests were also employed to reveal the excellent mechanical properties of the as-prepared hydrogel. The hydrogel could stand a large compressive deformation and recover to the original shape after releasing the compressive stress **(Figure 3.3a**). The maximum compressive strength can reach from 0.5 MPa to 2.0 MPa and the dissipated energy during the compression can reach up to 6.28 MJ m^{-3} as the compressive strain increased from 50% to 80% (**Figure 3.3b and 3.3c**). The cyclic compression tests show the superposition of the loading-unloading compressive curves, which further demonstrates the elasticity and fatigue resistance of the hydrogel (**Figure 3d**). The maximum compressive strength of the hydrogel was well-remained at 2 MPa after being compressed 100 times (**Figure 3.3e**), which confirmed the remarkable rebound resilience of the PEDOT: PSS@PVA/PAA hydrogel.[207] The excellent mechanical properties of the hydrogel offer advantages to sense different types of motions (e.g., stretching, compressing, bending, etc.). Hammering test (**Figure S3.5, Video S3.1**) was also conducted on hydrogel specimen under a normal pressure of over 1 MPa. After repeating 20 trials, the hydrogel could still retain its original shape, confirming the excellent elasticity.[208]

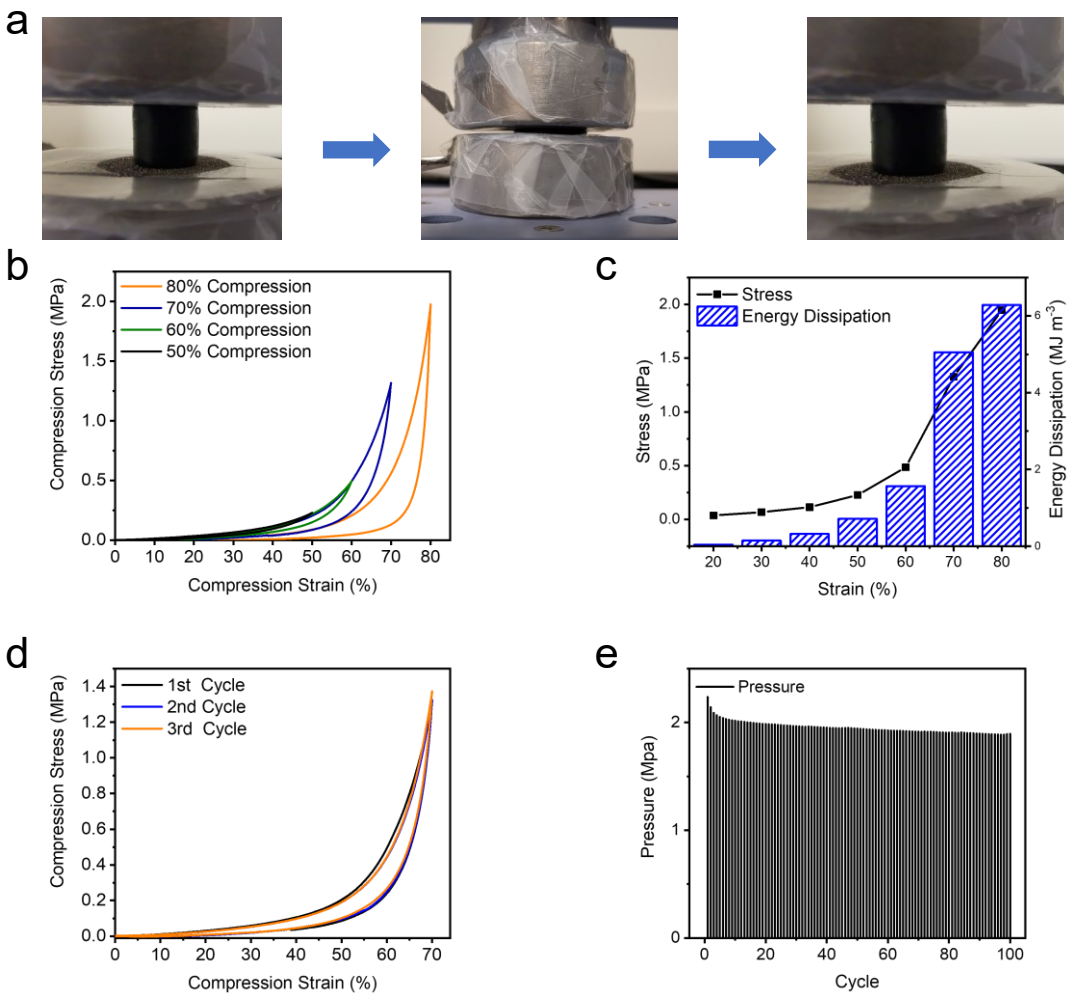

Figure 3.3. (a) Photographs for the compression process of PEDOT: PSS@PVA/PAA double network hydrogel. (b) Typical compressive stress-compressive strain curves under different compressive strain conditions. (c) Maximum compressive stress and energy dissipation during compression process (N=3). (d) Three loading-unloading cyclic curves under 80% compressive strain. (e) Pressure under continuous 100 loading-unloading cycles with 80% compressive strain.

3.3.3 Self-Healing Property

The self-healing process of the hydrogel was shown in **Figure 3.4a**, where two pieces of separated hydrogel could heal and merge into one single piece by first heating the joints then bringing two pieces together. The healed hydrogel can be further stretched

without the rupture at the joint. The excellent self-healing property of our hydrogel sensor can be attributed to the enhanced hydrogen bonding interactions at the interface when the local temperature is increased. The illumination recovery of a LED bulb was also used to demonstrate the self-healing property (**Figure 3.4b**). The LED bulb was illuminated when a piece of PEDOT:PSS@PVA/PAA hydrogel was integrated into the circuit, indicating the conductive nature of the hydrogel. The LED bulb went out when the hydrogel was cut into halves and became bright again after two pieces of hydrogels were brought together. The brightness of the LED bulb can be also adjusted by simply stretching the hydrogel, indicating the change of resistance during the stretching. Real-time current measurement was further employed for studying the self-repairing electrical property (**Figure 3.4c**). The current went to zero when the hydrogel was cut and it recovered to a higher value than the original, which is most likely due to the increased contact area at the re-joined interface.[209] The reproducibility of such self-repairing electrical property was also confirmed by the cyclic cutting-healing process of our hydrogel.

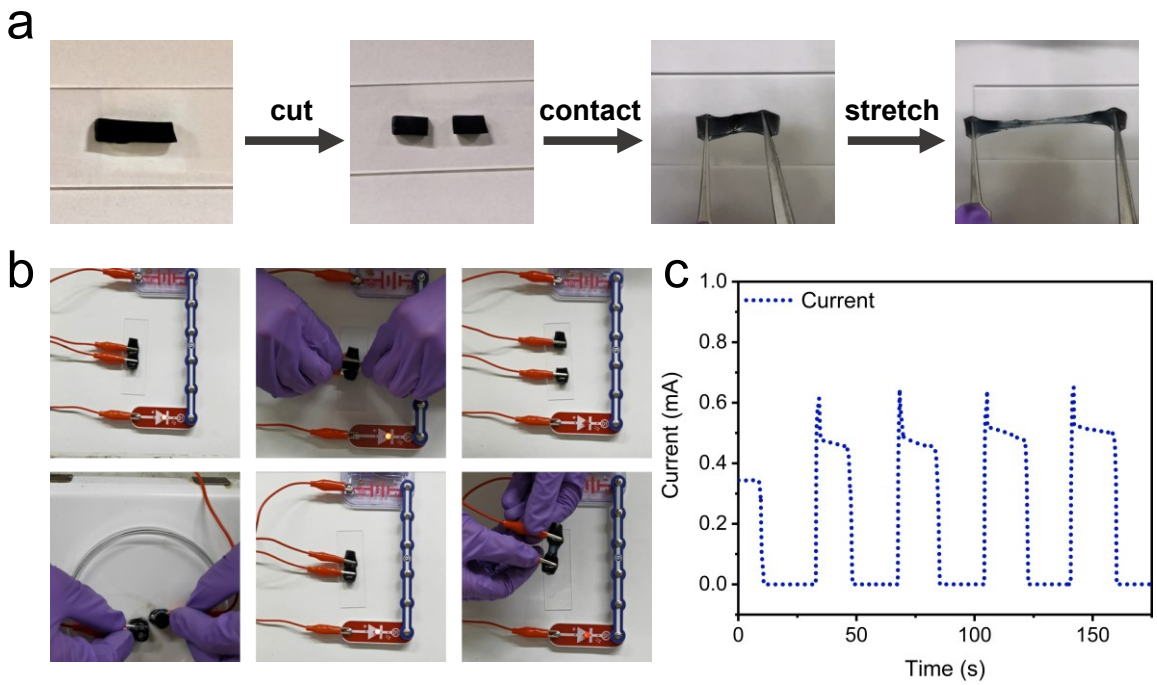

Figure 3.4. (a) Self-healing process of the PEDOT:PSS @PVA/PAA DN hydrogel (PVA/PAA=6:4). (b) The recovery of illuminance of a LED bulb during the hydrogel cutting/healing process. (c) Current change during the cyclic cutting/healing processes.

3.3.4 Self-Adhesiveness of the PEDOT:PSS @PVA/PAA DN Hydrogel

The strong adhesion to various substrates was shown in **Figure 3.5a**. The as-prepared hydrogels could firmly glue a wide range of materials together, including wood, steel, glass, PTFE, PMMA and porcine skin (mimic human tissue).[210] The adhesive strength was measured by lap-shear experiments. As shown in **Figure 3.5b**, the PEDOT:PSS@PVA/PAA hydrogel has highest adhesion with PTFE for 19.8±0.69 kPa and fair adhesion with porcine tissue for 15.9±0.79 kPa. The self-adhesive property of the hydrogel is most likely due to the hydrogen bonding interactions between hydroxyl groups, carboxyl groups of hydrogel and different hydrogen-bonding donor/acceptor groups on the substrates. The macroscopical adhesion was also demonstrated in **Figure S3.6** using PEDOT:PSS@PVA/PAA hydrogel (L×W×T: 10mm×9mm×2mm) sample to glue and lift

a 500-gram weight. Besides, the reversible adhesion to different substrates (glass, PMMA and porcine skin) was studied through normal adhesion tests.

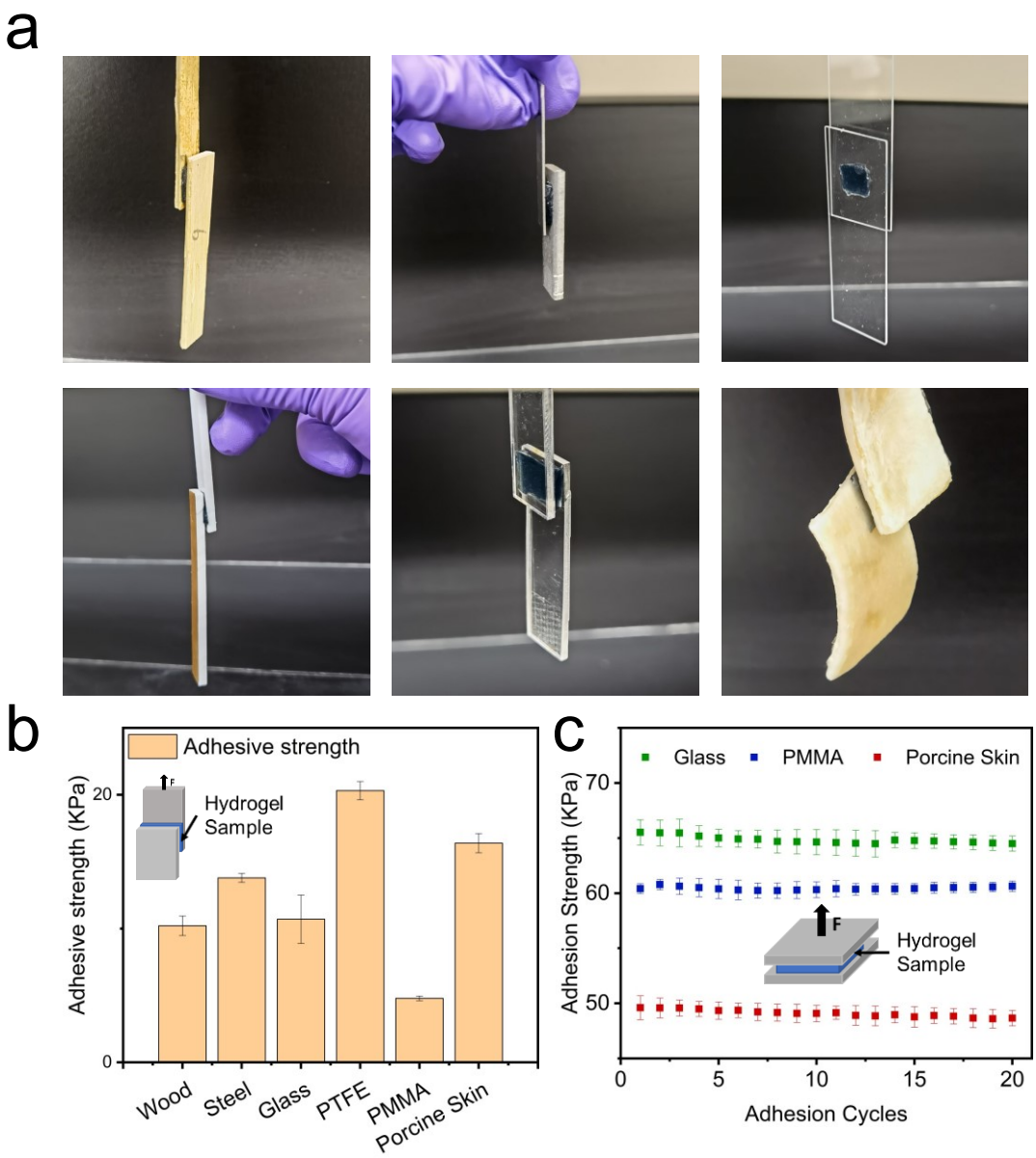

Figure 3.5. (a) Using PEDOT:PSS @PVA/PAA DN hydrogel (PVA/PAA=6:4) to glue different substrates together. (b) Adhesive strength of PEDOT:PSS @PVA/PAA DN hydrogel (PVA/PAA=6:4) on different substrates using lap-shear tests. (c) Reversible adhesive property of PEDOT: PSS @PVA/PAA DN hydrogel on different substrate.

Figure 3.5c shows the normal adhesion strength remained almost the same over 20

cycles on glass, PMMA and porcine skin, demonstrating the dynamic and reversible nature of hydrogen bonding interactions. The good adhesiveness of the hydrogel towards different substrates shows great potential for the self-adhesive soft sensors.

3.3.5 Tensile and Compressive Strain Sensing Ability of the PVA/PAA/PEDOT: PSS DN Hydrogel

The strain sensitivity of the as-prepared hydrogel sensor was investigated by resistance tests. The overall relative resistance change ($\Delta R/R_0$) versus tensile strain is shown in **Figure 3.6a**. The relationship of the relative resistance change with applied strain can almost fit into a polynomial equation:

$$\Delta R/R_0 = 0.01411\varepsilon + 5.51174 \times 10^{-5}\varepsilon^2$$

the gauge factor is calculated to be 2.21 when the strain is less than 150% and it goes up to 3.82 at the strain between 170% to 300%. For the intelligent electronic sensing application, high gauge factor value is required for high sensitivity. Compared with other hydrogel strain sensor systems [14, 187-188, 209, 211-219] as show in **Figure S3.6**, our hydrogel sensor exhibits a higher gauge factor value within 0%-300% strain range (the deformation range of human epidermis is 0%-75%).[220] **Figure 3.6b** shows the identical waveforms of the signal under different tensile strains (50%, 100%, 150% and 200%), indicating the high sensitivity and reliability of sensing response. The current change during one hundred loading-unloading cycles at 100% tensile strain is shown in **Figure 3.6c**, and the current amplitude shows slight decrease in the first several cycles, while remains almost the same in the following successive cycles, suggesting the stable and reproducible signal response. Such signal response can be reflected by the change of brightness of an LED connected in a circuit with a piece of integrated hydrogel being stretched (**Figure 3.6d**). Strain sensing

test for random/ unknow strain values within the working range of PEDOT:PSS@PVA/PAA hydrogel sensor was also conducted. The results (**Figure S3.8**) indicate that the random/ unknown strain can be well detected and agree well with the predicted signal curve of the sensor, which confirms the reliability of the strain sensing of the developed hydrogel.

The hydrogel sensor also has excellent pressure sensing ability. **Figure 3.6e** shows the relationship between current change and applied pressure and it can be fitted by a logistic function, in which the whole tendency can be divide into four areas: 1) when the compressive pressure is less than 100 kPa, the sensitivity is 0.076; 2) when the compressive pressure is between 80 kPa to 170 kPa, the sensitivity goes down to 0.027; 3) when the pressure was during 200 kPa to 300 kPa, the sensitivity is 0.013 and 4) sensitivity is 0.006 as the applied pressure increased further. As shown in **Figure 3.6f**, the current change signal is highly repeatable, stable, and sensitive over a wide compressive range from 10% to 80%. **Figure 3.6g** shows the current change of the hydrogel undergone one hundred cycles with 80% compressive strain. The stable current amplitude indicates the reliable pressure sensing ability of the hydrogel. The relative electrical resistance changes of the hydrogel sensor with the compressive stain from 10% to 80% was also reflected by illumination of a LED. It is clear that the LED becomes brighter with the increasing compressive strain which reflects the decrease of resistance (**Figure 3.6h** and **Video S3.2**).

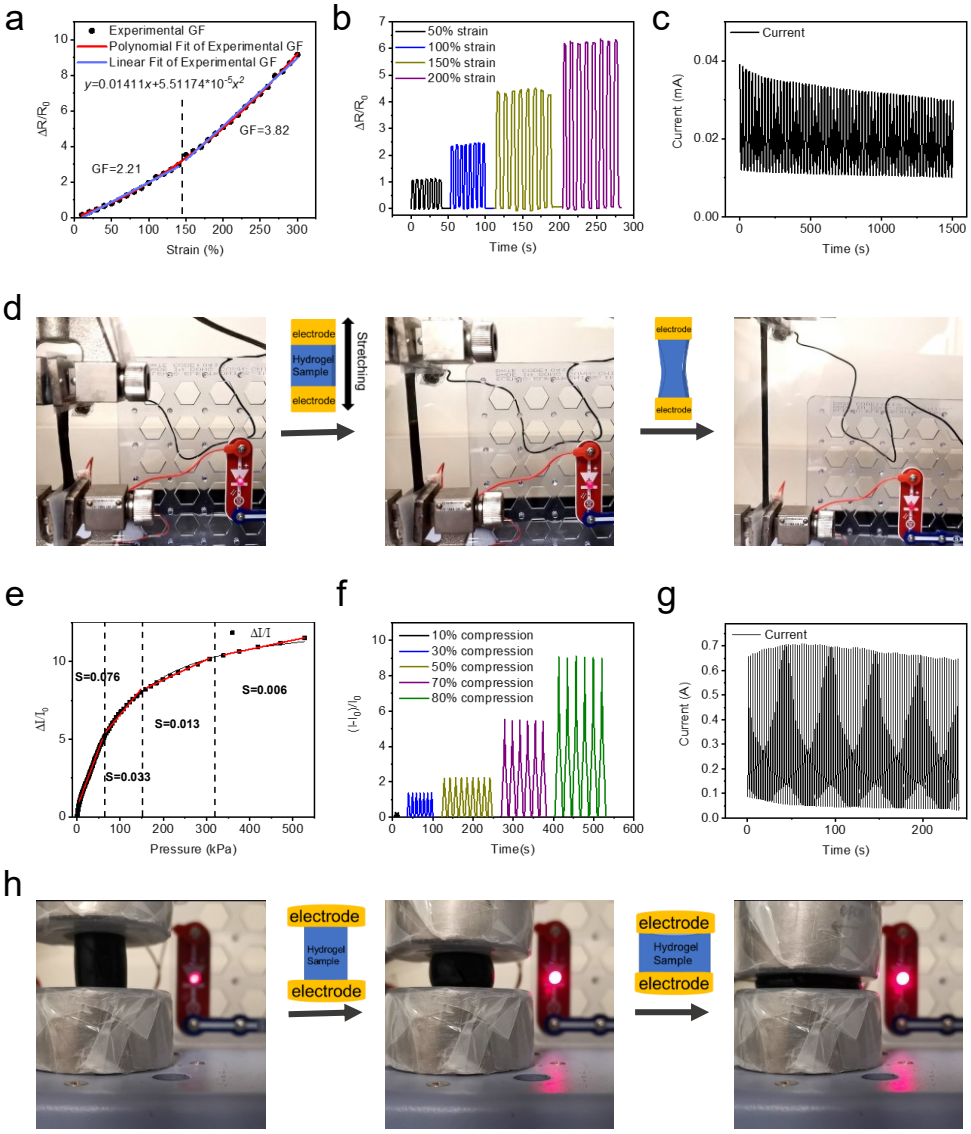

Figure 3.6. (a) Resistance changes vs applied strain (from 0% to 300%) curve. (b) Relative resistance changes of PEDOT:PSS@PVA/PAA DN hydrogel sensor at different strains from 50% to 200%. (c) Current change of loading-unloading process under 100% tensile strain for 100 times (d) The brightness change of LED bulb in circuit under different stretching strain. (e) Relative current change vs applied compressive stress curve. (f) Relative current change of PEDOT:PSS@PVA/PAA hydrogel sensor under the compressive stain of 10% to 80%. (g) Current change of one hundred cycles under 80% compressive strain. (h) The illumination changes of LED bulb during a compression process of 80% compressive strain.

3.3.6 Sensing Ability

Benefiting from the excellent adhesiveness, stretchability, compressibility, and high strain sensitivity, the as-prepared conductive hydrogel can be attached on human tissue and used as a soft sensor device to monitor human activities.[221] **Figure 3.7a** shows the resistance change of the hydrogel with different bending angles. The resistance increases as the hydrogel was bent into a larger angle, resulting in a smaller current. As illustrated in **Figure 3.7b**, when use the hydrogel to detect finger bending, the relative resistance changes of the hydrogel sensor increased significantly from 0.02 to 0.5 as the finger bent from 0 – 15° to 0 – 90°. The same motion-capture ability can also be used to monitor the movement of wrist and foot (**Figure 3.7c-d**). The movement detection was demonstrated by adhering the hydrogel sensor on the sole of a volunteer. As the volunteer was walking (**Video S3.3**), the instantaneous current change was recorded by the electrochemical workstation and displayed on the screen (**Video S3.3**) based on the pressure imprison and release processes. Apart from detecting the large body movements, subtle motions were monitored and demonstrated further. As displayed in **Figure 3.7e**, the hydrogel could detect pulse by over human wrist. The relative resistance change is around 0.03 under resting and the heart rate was determined to be 59 bpm, while after exercise, the higher amplitude of the resistance change signal was obtained and the heart rate went up to 130 bpm. To study the difference of vocal cord vibration when speaking different words, the hydrogel sensor was adhered to the neck to record the related motions. It is clear that there is only one peak when speaking “Hi” and three peaks were repeated showed up when keep saying “How are you” (**Figure 3.7f**). With the successful demonstrations of the human motion detections, this hydrogel-based strain and pressure sensor shows great potential for wearable soft electronic devices with high sensitivity and reliability.

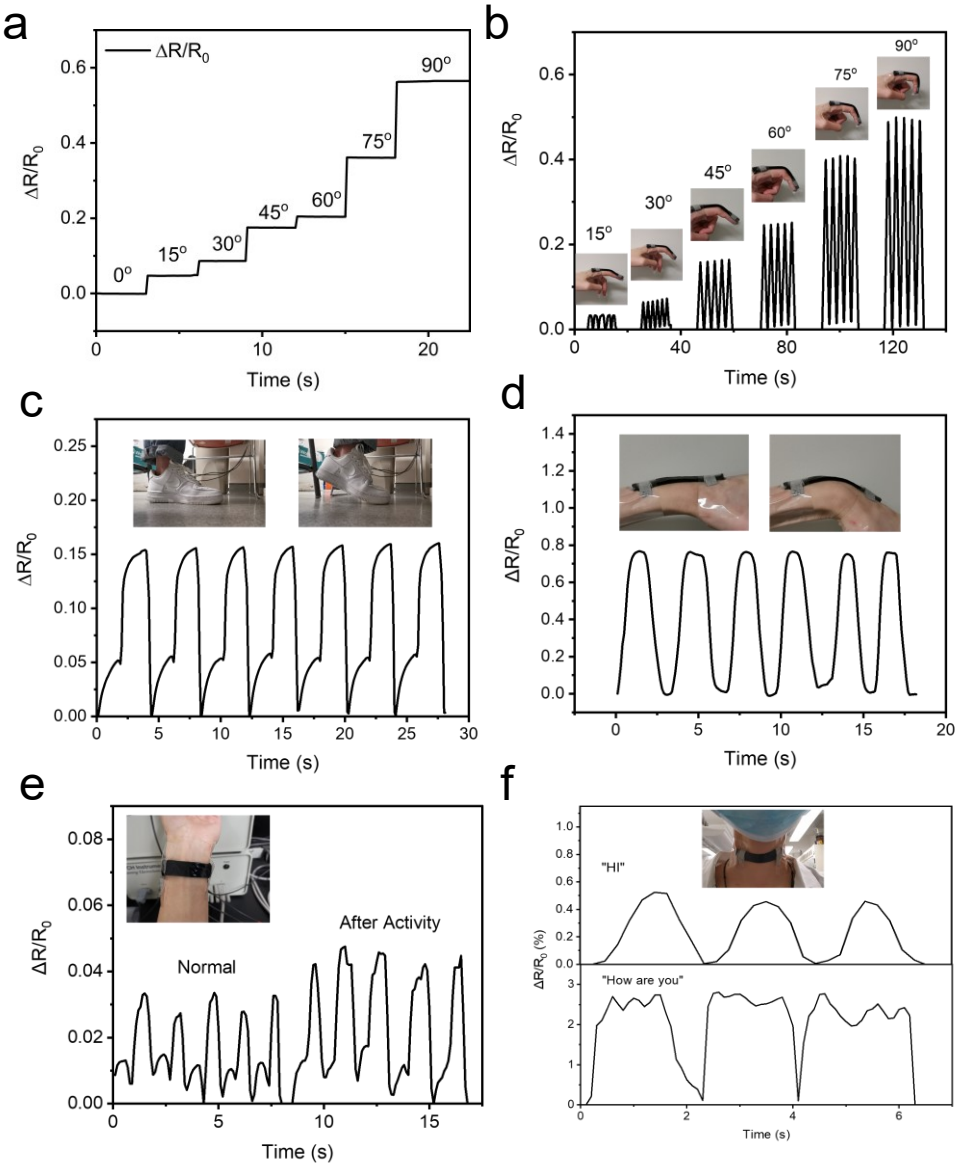

Figure 3.7. (a) Relative resistance changes of DN hydrogel sensor bending from 0 degree to 90 degree. Relative resistance changes of DN hydrogel sensor during monitoring different human activities including (b) Finger bending. (c) Wrist bending. (d) Stepping (e) Heartbeat monitoring, (f) Distinction of pronounce “Hi” and “How are you”.

3.4 Conclusions

In summary, we developed a highly sensitive hydrogel-based strain sensor with excellent self-healing and self-adhesive properties by incorporating a conductive polymer

PEDOT: PSS into a mechanically robust poly(vinyl alcohol) (PVA)/poly(acrylic acid) (PAA) double network (DN) hydrogel via a facile two-step preparation method. The hydrogel sensors could span a wide spectrum of mechanical properties by simply tuning the preparation parameters. Due to the multiple hydrogen bonding interactions between different components within the hydrogel, the hydrogel sensor not only shows improved mechanical properties through an energy dissipation mechanism, but also possesses self-healing capabilities. Such hydrogen bonding interactions are also important for the sensory applications since the strong interfacial hydrogen bonding interactions between hydrogel and tissues can facilitate the robust adhesion of the hydrogel to the skin (and other substrates), which is beneficial to the sensing stability and reliability.

Compared with previously reported mechanically robust hydrogel-based strain sensors, [14, 213, 222] the hydrogel and sensor system developed in this work shows an improved sensitivity (Gauge Factor from 2.21 to 3.82) over the strain range (0-300%), which allows the precise detection of different types of subtle human motions (e.g., pulse and vocal cord vibration). The simple design of our hydrogel-based strain sensor provides useful insights into the development multifunctional conductive hydrogels for flexible screen, electronic skin, and other electrical engineering applications. For further study, nanomechanical force measurement tools (e.g., surface forces apparatus, atomic force microscope) will be used to elucidate the critical roles of dynamic hydrogen bonding interactions among different components in tunning the macroscopic material properties.

CHAPTER 4 A pH and Temperature Dual-Responsive Microgel Embedded Adhesive Tough Hydrogel for Drug Delivery and Wound Healing

4.1 Introduction

Skin is generally considered as the largest multifunctional organ of the human body, and works as the first barrier to defend against the invasion of bacteria.[223] It remains a challenge for the treatment of skin wounds (including injury, chronic disease, surgery, acute trauma, etc.) due to the complexity and dynamic nature of the wound healing process.[224] Advanced wound dressings have attracted much research interest. An ideal wound dressing should meet several requirements: 1) good absorbing ability to clear up wound exudates, 2) providing a good biological environment to transport proteins, ions, minerals, and nutrition for tissue regeneration, 3) drug carrying and releasing capability for pharmacologic interventions, and 4) excellent antibacterial properties to reduce bacterial infection.[225-227] Polymeric hydrogels are promising candidates for wound dressings because of their hydrophilic nature, gas permeability, and fluid absorbing capability. [228-232]

Chitosan (CS), as a natural polysaccharide, has broad-spectrum antibacterial activities because its protonated amino groups can bind to the negatively charged bacterial cell wall, leading to the permeability change of the cell membrane and thus a sterilization effect. CS has been investigated as a wound dressing material.[233-234] CS also owns interesting mechanical and biological properties such as mucoadhesive,[235] excellent biocompatibility,[236-238] biodegradability,[239-240] anticholesterolemic,[241] antimicrobial capacity,[242] antioxidative,[243] and healingstimulation.[244-245] As a result, CS has been used to manufacture biosensors and drug delivery systems and also plays a role in promoting drugs

to pass through biological barriers.[246-247] Traditional CS hydrogels are generally weak and lack of functionality. Therefore, various approaches have been adopted to enhance the mechanical performances and endow the hydrogel with multiple functions to fulfill the increasing needs of modern biomedical materials. Coupling CS with other biocompatible crosslinked polymers to form semi-interpenetrated networks (semi-IPN), which refers to the networks crosslinked by the first polymer with a second linear or branched polymer dispersed in, provides a facile and feasible method to fabricate functional biomaterials to broaden the application of CS, which has been demonstrated by introducing and polymerizing hydrophilic monomers in the presence of CS inside the hydrogel system.[248] Because of their nontoxicity, biodegradability, biocompatibility and antibacterial properties with potential biotechnological and biomedical applications, CS semi-IPN hydrogels have received considerable attention.[249] By incorporating various polymeric networks such as poly(N-isopropylacrylamide),[250] alginate,[251] polyacrylamide,[252-253] and modified cellulose networks,[254] multitudinous CS-based semi-IPN hydrogels have been prepared and displayed excellent mechanical properties, antibacterial capacities and adhesive features.[255-258] However, CS semi-IPN hydrogels usually display pH and composition-dependent swelling behaviour, which influences the drug release kinetics and impairs the wound healing performances. Meanwhile, the electric charge properties of the hydrogel materials can influence the drug loading efficiency and the type of drug loaded, which hinders the critical drug loading and delivery for wound dressing applications with pharmacologic interventions.

On the other hand, stimuli-responsive microparticle-based drug delivery systems have attracted much attention owing to their high drug loading and controlled and sustained drug release behaviors.[247, 259-260] Attributed to the reversible temperature responsible behavior, tian (PNIPAAm) based microgels have been employed to release various

therapeutic agents including drugs and proteins in a passive and nondenaturing manner.[64, 261-262] Chemically modification of the PNIPAAm microgels with diverse functional molecules are commonly used to render the microgels with responsiveness to various stimuli. For example, pH and temperature dual-responsive microgels have been developed by copolymerizing acrylic acid (AAc) with NIPAAm to form microgels (PNIPAm-co-AAc microgels).[263-264] At pH higher than its pKa value (i.e., pH 4.25), deprotonation of AAc groups could occur, which makes the polymer chains negatively charged. At pH < 4.25, the PAAc chains are protonated and become neutralized.[265-266] The anionic charge property of the microgels also enables their interaction with cationic proteins.[267] For example, high protein drug (cytochrome c) loading capacity (more than 9.7 × 105 protein molecules/ microgel particle) has been achieved in a previous study due to the formation of the polymer (PNIPAAm-co-AAc)-protein complexes and the porous structure of the microgels.[268] However, direct administration of microgels as drug carriers faces problems like rapid clearance by human's renal and reticuloendothelial systems (RES).[269] By incorporating stimuli-responsive microgels (e.g., PNIPAAm-co-AAc microgels) into bulk hydrogel networks, composite hydrogels with enhanced drug loading capacity, intelligent and sustained delivery and broadened types of loading drugs can be achieved. Although microgel-embedded hydrogel systems have been reported in previous studies, most of them focused on the physical characteristics of the hydrogels.[270-271] Developing functional microgel-embedded hydrogels with potential biomedical applications (e.g., carriers for drug delivery, wound dressing) is of both fundamental and practical importance.

In this work, we have developed a pH and temperature dual-responsive nanocomposite hydrogel by entrapping PNIPAAm microgels functionalized with acrylic acid inside a semi-IPN PAM/CS hydrogel and successfully applied it as a drug delivery carrier and a wound dressing. The structure, swelling ratio, mechanical, adhesive and

antimicrobial properties of the dual-responsive nanocomposite hydrogel were investigated. The drug loading and releasing behaviors of both the PNIPAAm-co-AAc microgels and the semi-IPN PAM/CS hydrogel were investigated under different pH and temperature conditions, which were compared with that of the microgel@PAM/CS hydrogel to determine their synergistic effect. The composite hydrogel demonstrated sensitive stimuli-responsive and sustained release behaviors. We further evaluated the wound healing performance of the hydrogel using a rat model, and the hydrogel demonstrated significant enhancement of the healing process. These results suggest that the microgel@PAM/CS hydrogel has great potential in bioengineering applications such as drug delivery and wound healing.

4.2 Experimental Section

4.2.1 Materials

N-Isopropylacylamide (NIPAAM, 99%, Aldrich), acrylic acid (AAc, 99%, Aldrich), ammonium persulfate (APS, 99%, Aldrich), N,N-Methylenebis(acrylamide) (Bis-acrylamide, BIS), acrylamide (AAm, ≥99%, Aldrich), Chitosan (CS, high molecular weight,>75% deacetylated, Aldrich), acetic acid (1 M CH3COOH, Aldrich), poly(ethylene glycol) diacrylate (PEGDA, average Mn 700, Aldrich), Bovine Serum Albumin (BSA, Aldrich), Sulfamethoxazole (SMZ, Aldrich), 1, 1-diphenyl-2-picrylhydrazyl free radical (DPPH, 95%, Thermo Scientific), phosphate-buffered saline (PBS, Aldrich) tablets were used as received. Irgacure 2959 (I 2959, 98%, Aldrich) was used as a photo initiator.

4.2.2 Microgel Synthesis

Microgels composed of poly (N–isopropylacrylamide)-co-acrylic acid (PNIPAAm-co-AAc) were synthesized via free radical precipitation polymerization as described

previously.[272] Briefly, a 3-necked round bottom flask was fitted with a reflux condenser, nitrogen inlet, and temperature probe, and charged with a solution of NIPAAm (11.9 mmol) and BIS (0.703 mmol) in 99 mL deionized water, previously filtered through a 0.2 μm filter. The solution was bubbled with N_2 gas and allowed to heat to 70 °C over ~1 hour. AAc (1.43 mmol) was added to the heated reaction mixture in one aliquot. The reaction was then initiated with a solution of APS (0.2 mmol) in 1 mL of deionized water. The reaction was allowed to proceed at 70 °C for 4 h under nitrogen. The resulting suspension was allowed to cool overnight, and then it was filtered through a Whatman #1 paper filter to remove any large aggregates. The microgel solution was then distributed into centrifuge tubes and purified via centrifugation at ~8300 rcf to form a pellet, followed by removal of the supernatant and resuspension with deionized water for 6 times. The cleaned microgels were recombined and stored in a brown glass jar.

4.2.3 UV-Photopolymerized Microgel-Hydrogel

The microgel-embedded chitosan/PAM hydrogel was prepared through free radical polymerization via UV irradiation. Typically, PNIPAAm-co-AAc (0.3 g) was added into 10 mL CS/acetic acid (0.2 M) solution (1 wt%) and stirred overnight to obtain a homogenous solution, and then an AAm (1.76 g) solution containing crosslinker (PEGDA, 0.0088 g) and UV photo initiator (Irgacure 2959,0.0176 g) was mixed with the previous CS solution. The mixture was sonicated for 30 minutes and degassed for 10 minutes at 0 ºC. The resultant solution was transferred to a sealed glass mold and exposed to UV light (wavelength of 365 nm) for 5 h. Equivalent weight of hydrogels with only PAM and without PNIPAAm-co-AAc microgels were also polymerized to serve as controls. Hydrogel specimens were washed three times in distilled water to remove residual unreacted chemicals and stored for further use.

4.2.4 Sample Characterization

The internal morphologies and structures of hydrogel samples were characterized using a Zeiss EVO M10 Scanning Electron Microscopy operated at an acceleration voltage 20 kV. Fourier transform infrared (FTIR) spectra were obtained using a Thermo Scientific Nicolet iS50 FTIR spectrometer, and the testing frequency range was from 500 to 4000 cm-1. All the samples for both SEM and FTIR analysis were prepared by freeze-drying method, and the freeze-dried pieces were coated with a thin gold layer by sputtering for SEM imaging.

4.2.5 Swelling Test

Swelling ratio (SR) and equilibrium water content (EWC) were measured to test the stability of the microgel@PAM/CS hydrogel under a wet environment. The swelling ratio of the hydrogel was evaluated in PBS (pH 7.4, 10 mM) and water at 37°C. In addition, a hydrogel sample swollen in PBS for 1 hour and transferred to water was used as a control group to investigate the effect of ions on crosslinking degree. The cured hydrogel samples (with radius R=10 mm, and height H=10 mm) were washed with DI water three times; after the superficial water was removed, the samples were weighed immediately (W0) for later evaluation. Then samples were immersed into 20 mL PBS in sealed vials. The swelling ratio (SR) was determined using the following equation: SR=(Wt-W0)/W0×100%, where W0 and Wt are the weight of hydrogel samples at initial stage and after a specific swelling time, respectively. The equilibrium water content (EWC) was calculated by equation 1.

$$EWC=(W_s-W_d)/W_d\times 100\% \quad (4\text{-}1)$$

where W_s and W_d are the weight of hydrogel samples swollen for 48 h and after dried, respectively.[225]

4.2.6 Evaporative Water Loss Test

Freshly prepared hydrogel samples were placed in an oven with a constant temperature of 37 °C and relative humidity of 35%. Specimens were taken out and weighed every hour for a total of 6 h, and the weight after 12 h evaporation was also recorded as reference. The percentage of the weight remaining was calculated using the following equation 2:

$$\text{Water weight remaining (\%)} = (W_t - W_{t\ last})/ (W_0 - W_{t\ last}) * 100\% \quad (4\text{-}2)$$

Where W_0, W_t and W_t last are initial weight, weight after time ‘‘t” and weight after 12 h, respectively. All the experiments were performed in triplicate.

4.2.7 Mechanical Tests

Both tensile and compressive properties of the microgel@ PAM/CS hydrogels were characterized using an AGS-X universal tensile tester (Shimadzu, Japan) at room temperature. For tensile tests, hydrogel specimens (thickness of 2 mm) were cut into a dumbbell shape with a standard JIS-K-6251 cutter and stretched at an extension rate of 30 mm/min with a 50 N loading cell. The engineering tensile stress σ was estimated using the following equation: $\sigma=F/A_0$, where F was the real-time force applied on the hydrogel specimen and A_0 was the original area of the cross-section. The elastic modulus (E) was calculated as the slope of the stress-strain curve over the almost linear regime (strain range between 0-10%). The toughness was calculated by integrating the area under the stress-strain curve until fracture. For compression tests, cylindrical hydrogel specimens (diameter = 16mm, height = 15mm) were tested using a 2000 N load cell at a 10 mm/min compression rate. The compressive stress was obtained from the applied force F divided by the initial cross-section area. The compressive strain was calculated by dividing the compressed height (h) over the original height (h_0). The energy dissipation was determined by the

hysteresis loop area in a loading-unloading compressive stress-compressive strain curve.[273]

4.2.8 Adhesion Measurement

The adhesion tests were conducted on an AGS-X universal tensile tester (Shimadzu, Japan) with a 50 N load cell and 24 mm/min displacement rate at room temperature. All the specimens were cut into strips of a size of 70 ×15 × 2 mm. Fresh porcine skin, heart, liver, intestine and kidney were cut into the size of 100×20×2 mm, washed by deionized water with the free water on the specimen surface removed gently using a tissue paper via adsorption for future use. Both lap shearing adhesion test and normal adhesion test were employed to measure the lap shear strength and normal adhesion strength, respectively, which was determined by dividing the maximum (shear or normal adhesion) force measured during the detaching process by the contacting cross-section area. For both lap shearing adhesion and normal adhesion tests, microgel@PAM/CS hydrogels were first sandwiched between the substrates and compressed under a pressure of 15 kPa for 10 mins before the tests in the air. The impact of hydrogel swelling on its adhesion performance was investigated as follows: the hydrogel sample was sandwiched into substrates of porcine tissues and adhered under a pressure of 15 kPa for 10 mins, then the whole hydrogel and substrates were immersed in water or PBS at 37 °C for 30 mins and taken out for the normal adhesion tests to monitor the change of adhesion strength. The influence of the pre-load condition was also investigated by applying different pressure (1, 5, 10, 20, 30, 50, 75,100 kPa) for 10 mins before normal adhesion tests. Cyclic contact-separation test was performed by placing a hydrogel specimen between two porcine skin substrates, which were kept in contact under 15 kPa pressure in water or PBS for 10 min, and then pulled apart until detachment occurs in the air. The contact-separation process was repeated 15 times with pre-loaded 15kPa pressure for 1 min in the air. All the adhesion tests were

repeated at least three times.

4.2.9 BSA Loading in Microgel

Bovine serum albumin (BSA) was used as a model protein to evaluate the protein drug loading efficiency in the PNIPAAm-co-AAc microgels. Dried microgel particles were incubated in BSA solution (PBS) at room temperature, and the solution was adjusted to pH 4 to facilitate the loading process according to the literature.[274] In a typical process, 50 mg of BSA was added to 20 mL of PBS solution (pH=4) (BSA in PBS solution, 2.5 mg/mL) containing 1 g of microgel and placed on a shaker at 30 rpm and room temperature for 48 h. The sample solution was centrifuged at 12000 rpm for 30 min after a predetermined time (1, 2, 6, 12, 24, 48 h), then 3 mL of the supernatant was collected and measured spectrophotometrically on a Thermo Scientific Evolution 300 UV-Vis spectroscopy. The UV-Vis spectrum of a standard BSA solution (BSA in PBS solution, 2.5 mg/mL) was also measured for reference. The absorbance at 280 nm was used for the calculation of the BSA loading efficiency following equation 3 as follows.

$$\text{BSA loading efficiency (\%)} = (A_r - A_s)/A_r * 100\% \quad (4\text{-}3)$$

where A_r and A_s are the absorbances at 280 nm of the reference solution and the supernatant, respectively.

4.2.10 BSA Loading in PAM/CS Hydrogel

To determine the loading efficiency of the bulk microgel@PAM/CS hydrogel, the initial BSA in PBS (2.5 mg/mL) was measured using the UV-vis spectrophotometer and regarded as the reference. A piece of cylindrical hydrogel sample (R=10 mm, H=10 mm) was immersed in a 10 mL BSA solution (pH= 4) for a predetermined time of 1, 3, 6, 12, 24 and 48 h. Then the hydrogel sample was removed, and the remained solution was measured using UV-vis spectroscopy for the calculation of the BSA loading efficiency

following equation 3.

4.2.11 BSA Release Kinetics from The Microgel

The BSA loaded microgel, which was obtained in the previous loading test, was used for the BSA releasing test. 0.25 g of microgel was incubated under different environment conditions (pH=6.3 at 22 °C, pH=6.3 at 37 °C, pH=7.4 at 22 °C, pH=7.4 at 37 °C) for a specific time (1, 3, 6, 12, 24 and 48 h) and centrifuged at 12000 rpm for 30 min, and the supernatant was collected and then characterized using a UV-vis spectrophotometer to determine the BSA releasing kinetics.[109] 10 mL of PBS was chosen as the release medium, and the total PBS volume was adjusted to 10 mL after each sample collection to keep the incubation condition consistent. The BSA release kinetics was also examined by monitoring the characteristic absorbance of BSA at 280 nm. The releasing efficiency was characterized by the amount of released BSA from microgel particles divided by the total amount of entrapped BSA in microgel which was first measured in the BSA loading test as mentioned before.

4.2.12 BSA Release Kinetics from PAM/CS Hydrogel

The PAM/CS hydrogels obtained in the BSA loading test were employed for the BSA releasing experiment. The hydrogels were incubated under two PBS solutions of pH 4 and pH 7.4 at 37 °C, respectively. 3 mL of the release solution was collected at a time of 1, 3, 6, 12, 24 and 48 h which was characterized using a UV-vis spectrophotometer to determine the BSA releasing efficiency.

4.2.13 In Vitro Drug Release of Microgel@PAM/CS Hydrogel

Drug release studies were conducted using cylindric hydrogel samples (radius R=10 mm, height H=10 mm) containing 20 mg Sulfamethoxazole and 20 mg BSA-loaded microgel in 20 mL PBS, under the following environmental conditions: (1) pH=6.3 at 22 °C, (2) pH=6.3 at 37 °C, (3) pH=7.4 at 22 °C, and (4) pH=7.4 at 37 °C. The SMZ was loaded

into the hydrogel system by directly dispersing the drug in precursory solution. The samples and the solution media were sealed in vials and kept under constant temperature conditions using a water bath. 2 mL of the solution medium (i.e., PBS) was collected from each vial at different time intervals (0.5, 1, 1.5, 2. 4, 5, 6, 12, 24 and 48 h) and refilled to the same total volume (i.e., 20 mL) by fresh medium solution under relevant temperature conditions. The drug-releasing effect was monitored by characterizing the sample solutions using UV spectroscopy (particularly at wavelength of 209 and 280 nm). The releasing efficiency was obtained using the following equation.

$$\text{Releasing efficiency (\%)} = (m_t - m_0)/m_0 * 100\% \quad (4\text{-}4)$$

where m_t is the mass of the drug released from the hydrogel at time t, and m_0 is the mass of the drug-loaded into the hydrogel. All the experiments were examined in triplicate.

4.2.14 Antimicrobial Assay

The inhibiting effect of the hydrogel on microbial growth was evaluated by the spread plate method. SMZ-loaded microgel@PAM/CS hydrogel samples were firstly incubated with 1 ml *E. coli* suspension (106 colony forming units/mL) in a 12 well plate and gently shaken for 4 h at 37 °C, then 150 μL of the suspension was spread on Luria-Bertain (LB) agar plates and stored at 37 °C for 14 h for incubation. Pure PAM hydrogel was used for the control test, and the number of colonies was analyzed using Image J software.

4.2.15 Animal Skin Trauma Modelling

A total of 8 female Sprague Dawley (SD) rats weighing between 250 and 300 g were used for the experiments. To let the newly purchased SD rats acclimate, they were raised in the Specific Pathogen Free (SPF) animal house for one week by providing water ad libitum and rationed rat food at a constant ambient temperature (24-26 °C). SD rats with no adverse reactions were employed for the experiments.

Rats were individually anesthetized via an Intraperitoneal (IP) injection（2% pentobarbital sodium）for later induction of wounds. The back area and hair of rats were disinfected using 75% ethanol, and hairs were removed with a shaver. After that, the bare skin of rats was perforated with a special puncher (diameter of 1.5 cm in diameter) and the damaged tissue was removed to create a wound. The wound was dressed with microgel@PAM/CS hydrogel in the experimental group and 1×PBS solution in the control group.

4.2.16 Evaluation of Wound Healing Processes

The skin wound area swelling, color, size and growth of granulation tissue were observed on the 1^{st}, 3^{rd}, 5^{th}, 7^{th}, 9^{th}, 11^{th}, 13^{th} and 15^{th} day, respectively. A digital camera was used to monitor the wound healing process, and image analysis software ImageJ was used to measure the sizes of wound area. The wound closure rate was obtained by the following formula: wound closure rate=$(D_1-D_n)/D_1\times100(\%)$, where D_1 is the area of full-thickness circular skin wound on day 1, and D_n is the dimension of wound area on day n (3, 5, 7, 9, 11, 13 and 15).

4.2.17 Study of Histology

The treated full-thickness skins from wounds area in both groups were taken on the 7th and 15th day, respectively. Histologic sections under 4% neutral paraformaldehyde solution fixation, 70-100% gradient alcohol dehydration, paraffin embedding and sectioning (3-5 μm), and finally stained with hematoxylin and eosin (H&E). The histopathological changes in the skin wound, including inflammatory cell infiltration, angiogenesis, the proliferation of fibroblasts and the degree of epithelialization, were also observed under an optical microscope.

4.2.18 Statistical Analysis

GraphPadPrism 8.0 was used for plotting the data and statistical analysis was conducted through SPSS Statistics 25.0. The experimental data were expressed as mean±standard error of the mean, and the comparison between the two groups was conducted by t test ($P<0.05$ indicated the statistically significant, and $P<0.01$ indicated the highly statistically significant).

4.3 Results and Discussion

4.3.1 Characterizations of Hydrogels

PAM and CS were chosen in this work due to their biocompatible, hydrophilic, high-water uptake and economic features. The formation of PAM/CS semi-IPN hydrogels was reported previously. **Figure 4.1** illustrates the fabrication process of the microgel@PAM/CS hydrogel. Briefly, 20 mg/mL AAc-NIPAAm microgel was added to 10 mL of 1 wt% chitosan solution, and 150 mg/mL AM, PEGDA, and photo initiator (I2959) were then added into the microgel/CS solution. The polymerization process was initiated using UV light. The homogeneous mixture was transferred to a glass mold and exposed to UV light for 5 h. Pure PAM and PAM/CS hydrogels with the same PAM monomer concentration were also prepared as the control groups.

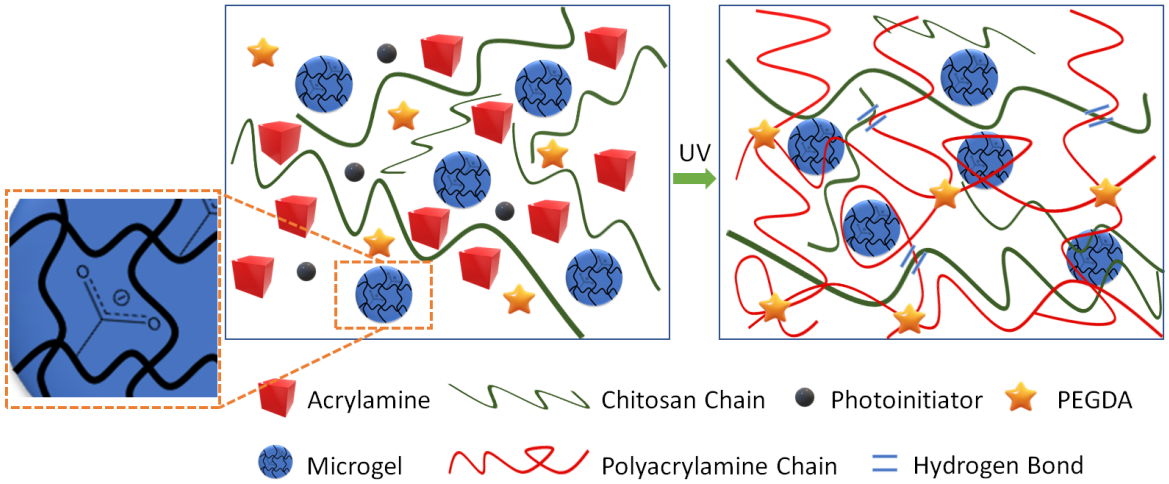

Figure 4.1. Illustration for the fabrication of PNIPAAm-co-AAC microgel-embedded PAM/CS composite hydrogel.

High uniformity and porosity are two important and desired properties for hydrogels used in wound dressing applications. A dense pore distribution corresponds to close space between polymer chains with high degree of crosslinkers. **Figure 4.2a-d** shows the SEM images of freeze-dried PAM, PAM/CS, microgel@PAM/CS and swollen microgel@PAM/CS (hydrogel sample immersed in water for 2h) hydrogels, respectively. All the four hydrogel samples show uniform pore distribution. The microgel@PAM/CS hydrogel displays relatively higher porosity (with relatively smaller and denser pores, **Figure 4.2c**) than pure PAM and PAM/CS hydrogels (**Figure 4.2a** and **4.2b**). The high porosity of the microgel@PAM/CS hydrogel suggests its high crosslinking density, which could be attributed to the intermolecular hydrogen bonding between carboxylic groups of microgels (or chitosan chains) and amino groups of PAM chains. The microgel@PAM/CS hydrogel shows a larger pore size after swelling treatment (**Figure 4.2d**), as compared to **Figure 4.2c** due to the expansion of a strongly hydrated polymer network. Such network expansion associated with the hydrogel swelling allows fast ion diffusion with high water permeability through the hydrogel network, indicating that the swollen process of

microgel@PAM/CS hydrogel will promote the release of drug molecules from the hydrogel carrier during practical applications.

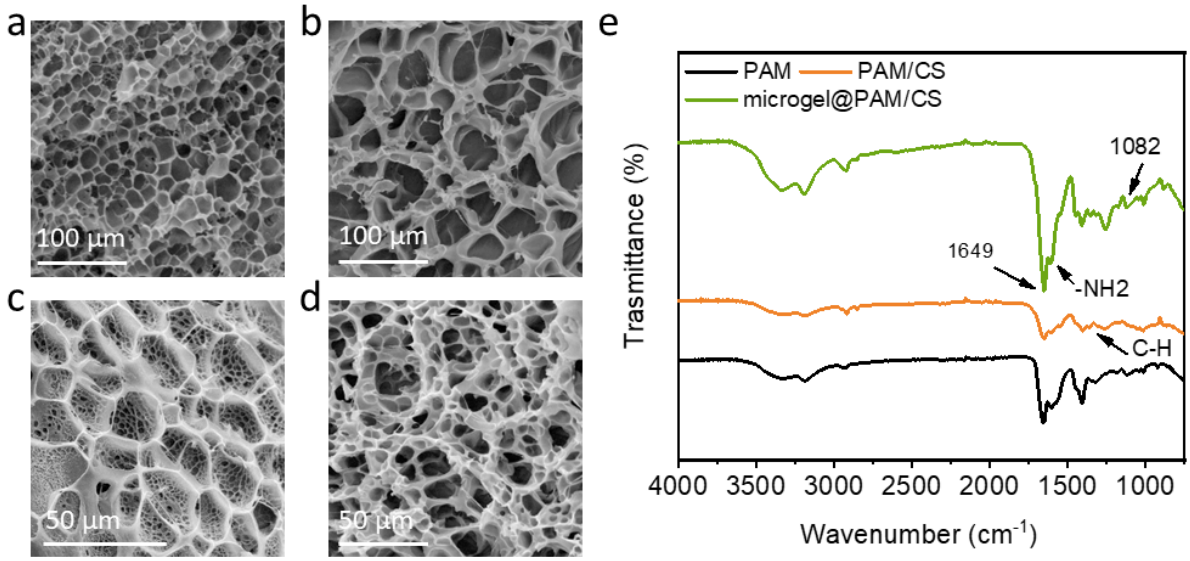

Figure 4.2. SEM images of (a) bare PAM, (b) PAM/CS, (c) microgel@PAM/CS and (d) swollen microgel@PAM/CS hydrogels. (e) FTIR spectra of PAM, PAM/CS, microgel@PAM/CS hydrogels.

The FTIR spectra of PAM, PAM/CS and microgel@PAM/CS hydrogel were shown in **Figure 4.2e**. The characteristic peaks of the CS in its FTIR spectrum at 1658 cm^{-1}, 1595 cm^{-1} and 1314 cm^{-1} are attributed to Amide I, -NH_2 and C-H bending vibration, respectively. The stretching vibration of the acetyl group and the bending vibration of the N-H of 2-aminoglucouse primary amines showed characteristic peaks at 1658 cm^{-1} and 1598 cm^{-1}, respectively, and the bending vibration of alkane C-H displayed characteristic peaks at 1421 cm^{-1} and 1380 cm^{-1}, while the characteristic peaks at 1154, 1082 and 1032 cm^{-1} were assigned to antisymmetric stretching of the C–O–C bridge and skeletal vibrations involving the C–O stretching, respectively. The FTIR spectrum of PAM exhibits a broad peak at around 3339 cm^{-1} and a characteristic peak at 3186 cm^{-1} due to the N-H stretching vibration. The significant characteristic peaks at 1649 cm^{-1} and 1606 cm^{-1} correspond to the C=O stretching

vibration (Amide I) and N-H bending vibration (Amide II), respectively. The C-N stretching vibration exhibits a characteristic peak at 1338 cm^{-1}.[275-276] All the spectra show broad and strong signals in the range from 3500 to 3200 cm^{-1}due to the overlapping of the O-H stretching vibration of the carbohydrate and the N-H bending vibration from primary amine bonds. All the major characteristic peaks of PAM and CS could be observed in the microgel@PAM/CS spectra, but the shift of characteristic peaks of Amide I and II indicate the inter- and/or intramolecular interactions among microgels, PAM and CS via hydrogen bonding and possible covalent bonding due to residual monomers in the microgels.

4.3.2 Study of Swelling Behavior

Swelling behavior is significant for hydrogels because it affects the mechanical properties and is highly related to the drug delivery behavior of hydrogel systems.[277-278] Two key parameters affect the swelling properties: the hydrophilicity of the functional groups present in the hydrogel and its crosslinking degree. For the microgel@PAM/CS hydrogel, various hydrophilic groups affect its swelling behavior with the hydrophilicity of the moieties following the order: $–COO^–$ > –COOH > $–CONH_2$ > –OH.[279-280] **Figure 4.3a** shows the swelling ratio of microgel@PAM/CS hydrogel under different swelling times in (1) PBS, (2) water, and (3) in PBS for 1 hour and then transferred into the water. It was found that the swelling rates were very similar under the three solution conditions, the hydrogels reached a swelling equilibrium after 40 h with the equilibrium swelling ratio of around 250%, suggesting the hydrogel's ability to absorb fluid, but it will not absorb too much liquid to lose its mechanical robustness and affect surrounding tissues.[281] The swelling behaviors observed in **Figure 3a** suggest that the presence of salts (i.e., in PBS solution) could enhance the swelling of microgel@PAM/CS hydrogel or its adsorption of water, which could be achieved through their influence on the electrostatic interactions

among the charged functional groups (e.g., -COO^-) and the association and dissociation of hydrogen bonds within the hydrogel network.[282] **Figure 4.3b** shows the water weight remaining associated with the evaporative water loss test for 12 h under a constant temperature of 37 °C and relative humidity of 35%, which indicates that water was evaporated steadily from the hydrogel. Noticeably the dehydrated hydrogel could recover to the same hydration stage after swelling or immersion in water for 2 h. The reversible dehydration-hydration behavior indicates that the microgel@PAM/CS hydrogel maintains its network structure during this process to support its potentially cyclic use in practical applications.

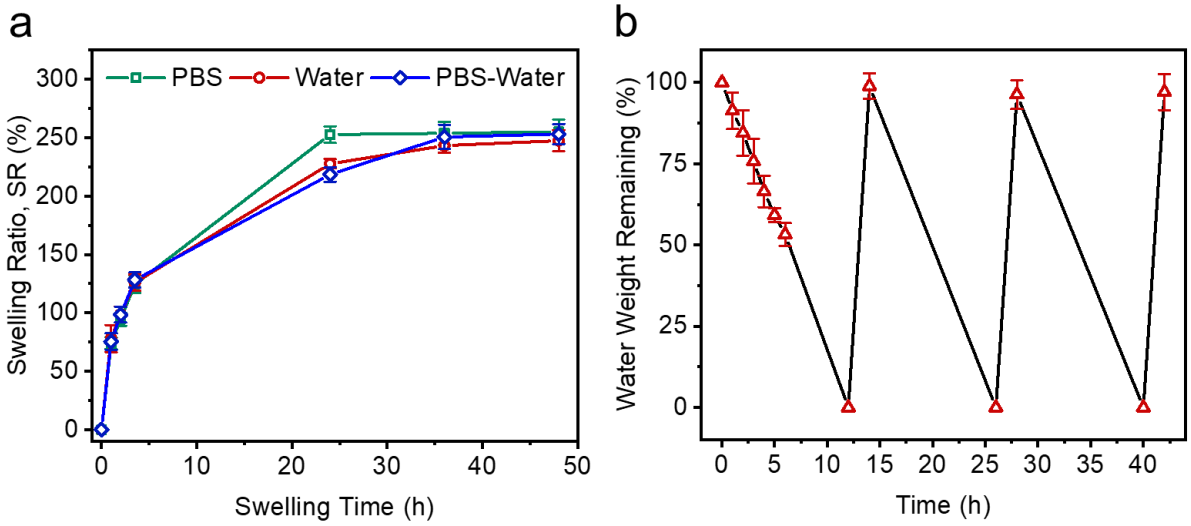

Figure 4.3. (a) Swelling ratio of microgel@PAM/CS hydrogel in PBS, water and a hydrogel sample swollen in PBS for 1 hour and transferred to water was used as a control group (PBS-Water). (b) Water weight remaining of microgel@PAM/CS hydrogel after evaporative water loss test for 12 h under a constant temperature of 37 °C and relative humidity of 35% and rehydration in water for 2 h and repeated 2 times.

4.3.3 Mechanical Properties

Mechanical properties of the hydrogels with different compositions were investigated and the results were shown in **Figure 4.4**. **Figure 4.4a** shows the typical

tensile strain-stress curves of the hydrogels. PAM hydrogel possesses the poorest strength and stretchability mainly due to its single network structure. It could only be stretched over two times its initial length. The semi-IPN PAM/CS hydrogel demonstrates greatly enhanced fracture strength (~ 70 kPa) and stretchability (over 600% strain at break). The improved tensile stretchability and strength are mainly attributed to the hydrogen bonding interactions between PAM and CS chains in the network, which enable the elongation of polymer network and prohibit the propagation of microcracks under tensile loads. The incorporation of the microgels into the hydrogel network further significantly improved the tensile performances of the hydrogel (microgel@PAM/CS), that is, the gel can withstand more than ~850% strain and reach a high tensile strength of around 160 kPa. As biomaterials like wound dressings are generally used under wet conditions, the mechanical properties of microgel@PAM/CS after swelling were also studied. As shown in **Figure 4a**, after swelling in water for 2 h, the microgel@PAM/CS keeps an excellent stretchability of over 900% and a good fracture strength of ~ 80 kPa, suggesting its good mechanical performances in wet conditions and thus its potential in practical biomedical applications. The calculated elastic modulus (E) and toughness of the hydrogels were demonstrated in **Figure 4.4b**. According to the figure, the microgel@PAM/CS hydrogel possesses an elastic modulus up to 28 kPa and a toughness of 483.0 kJ/m^3. The toughness of the composite hydrogels reached twice of the PAM/CS hydrogel and more than ten times of the PAM hydrogel. Such significantly enhanced mechanical properties of the microgel@PAM/CS hydrogel can be possibly attributed to the formation of hydrogen bonding among the carboxylic groups of PNIPAAm-co-AAc microgels, amide groups of PAM chains, as well as the hydroxyl and amine groups of chitosan. The interactions of the embedded PNIPAAm-co-AAc microgels with the surrounding polymers in the microgel@PAM/CS hydrogel introduce additional cross-linkages among the polymer

matrix, resulting in a relatively dense network structure, as confirmed by the SEM images (**Figure 4.2a-d**), which contribute to its excellent mechanical properties. As compared to the freshly prepared microgel@PAM/CS hydrogel, the swollen microgel@PAM/CS hydrogel exhibits only slightly impaired stretching stiffness (22% less) and toughness (15% less).

Cyclic tensile loading-unloading tests under a maximum stretching strain of 100%, without rest between the cycles, were conducted to evaluate the anti-fatigue property of the microgel@PAM/CS hydrogel. As shown in **Figure 4.4c**, the curves of different cycles almost overlapped and only slight hysteresis was detected during the loading-unloading cycles even when there was no rest time between the successive cycles, which indicates the excellent elasticity of the microgel@PAM/CS hydrogel due to both reversible molecular interactions (e.g., hydrogen bonding) and covalent crosslinkings.[283] **Figure 4.4d** shows the energy dissipation (i.e., the area of the loading-unloading hysteresis loop) associated with the 20 loading-unloading tensile cycles. The energy dissipation value was fairly low of only 38 J/m^3 for the first cycle. The value dropped to 15 J/m^3 for the second cycle and remained almost constant (around 16 J/m^3) for following cycles, which suggests the stabilized network after the second cycle. Cyclic compression tests were also conducted for the microgel@PAM/CS hydrogel with 60% maximum compression strain applied. As shown in **Figure 4.4e**., the maximum compression stress gradually decreased from 110 kPa for the first cycle to about 80 kPa for the fifth cycle and kept almost unchanged for the next 15 cycles, indicating the pressure tolerance was mostly maintained when the sample was subjected to successive compressing loading-unloading processes. The energy dissipation in cyclic compression tests was shown in **Figure 4.4f.** The value decreased from 8 kJ/ m^3 to 5 kJ/m^3 after the first cycle. However, the subdued decreasing tendency of dissipated energy in the next cycles indicates that the hydrogel kept most of its structural integrity to

resist the external pressures.[284]

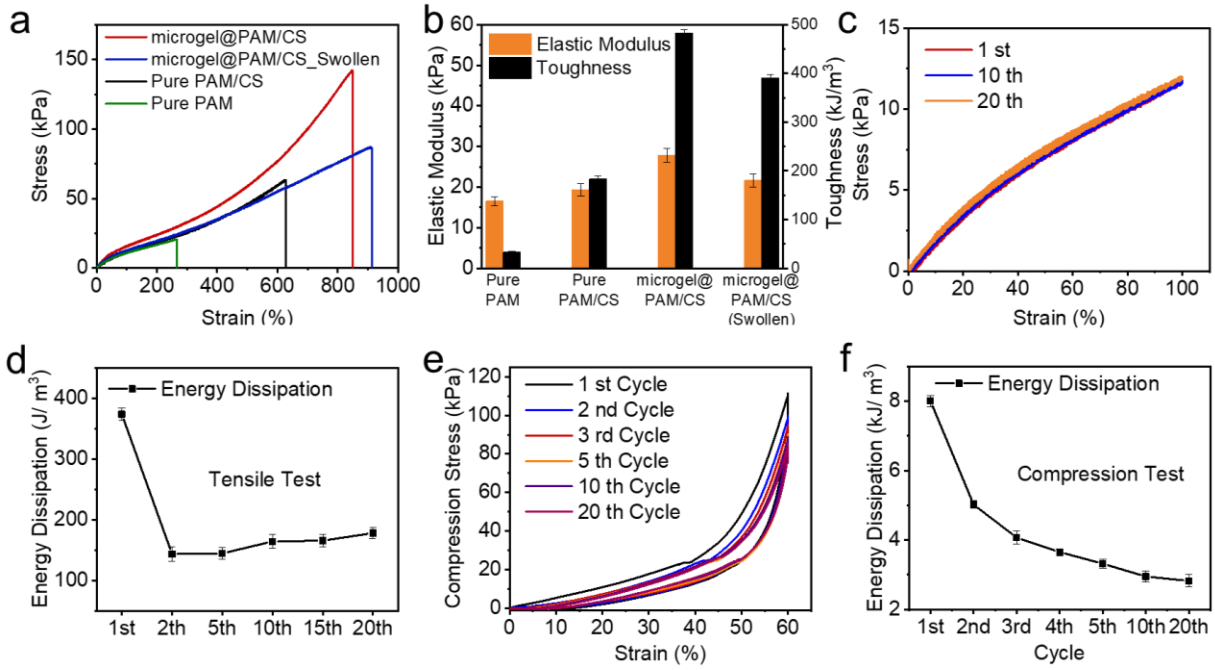

Figure 4.4. (a) Typical strain-stress curve of PAM, PAM/CS, microgel@PAM/CS, and swollen microgel@PAM/CS hydrogels. (b) Elastic modulus and toughness of the hydrogels. (c) Tensile strain-stress curves of 20 loading-unloading cycles of the microgel@PAM/CS hydrogel with a maximum tensile strain of 100%. (d) Energy dissipation changes in cyclic tensile tests of the microgel@PAM/CS hydrogel. (e) Compressive stress-compressive strain curves of 20 loading-unloading cycles of the microgel@PAM/CS hydrogel with a maximum compression strain of 60%. (f) Change of energy dissipation in cyclic compression tests of the microgel@PAM/CS hydrogel.

4.3.4 Adhesion

Robust adhesion is an important property which allows dressing materials to attach to diverse tissue surfaces. As shown in **Figure 4.5a**, the as-prepared microgel@PAM/CS hydrogel could adhere to various porcine tissues (e.g., heart, kidney, liver, intestine and skin) and the adhesion is sufficiently strong to hold the weight of respective tissues. The

microgel@PAM/CS hydrogel could also glue two separated organs together as shown in **Figure 4.5b**. **Figure 4.5c** shows the illustration for the experimental setup of the normal adhesion strength measurements between the microgel@PAM/CS hydrogel and different porcine tissues. As demonstrated in **Figure 5d**, after applying a small pressure of 15 kPa for 10 min, the microgel@PAM/CS hydrogel can firmly adhere to all the tested porcine tissues with the normal adhesion strength reaching from ~55 kPa with liver to 70 kPa with kidney. In practical applications, stable adhesion between wound dressing materials and tissues in physiological environment is also required. Therefore, the influence of hydrogel swelling on its adhesion performance was also investigated. From **Figure 4.5e**, after the microgel@PAM/CS hydrogels were immersed in water or PBS solution for 30 min, the normal adhesion strengths remain almost the same as the untreated cases in **Figure 4.5c**, which suggests that the adhesion properties of the hydrogels are not sensitive to swelling treatment. The adhesion of the microgel@PAM/CS hydrogel also shows a pressure-sensitive manner. As shown in **Figure 4.5f**, the normal adhesion strength of the hydrogel and porcine skin increased from ~25 to ~173 kPa with the preload increasing from 1 to 100 kPa. The repeatability of the adhesive process with the porcine skin was characterized by cyclic contact-separation test in both water and PBS with a short preloading contact time of 1 min after the first cycle and a preload pressure of 15 kPa. The adhesion strength kept high values of 62 and 59 kPa in PBS and water after 15 cycles, respectively, indicating the hydrogel's stable and repeatable adhesion to porcine skin. The high lap shear strengths shown in **Figure S4.1** also proved the excellent adhesion between the hydrogel and various tissue surfaces.

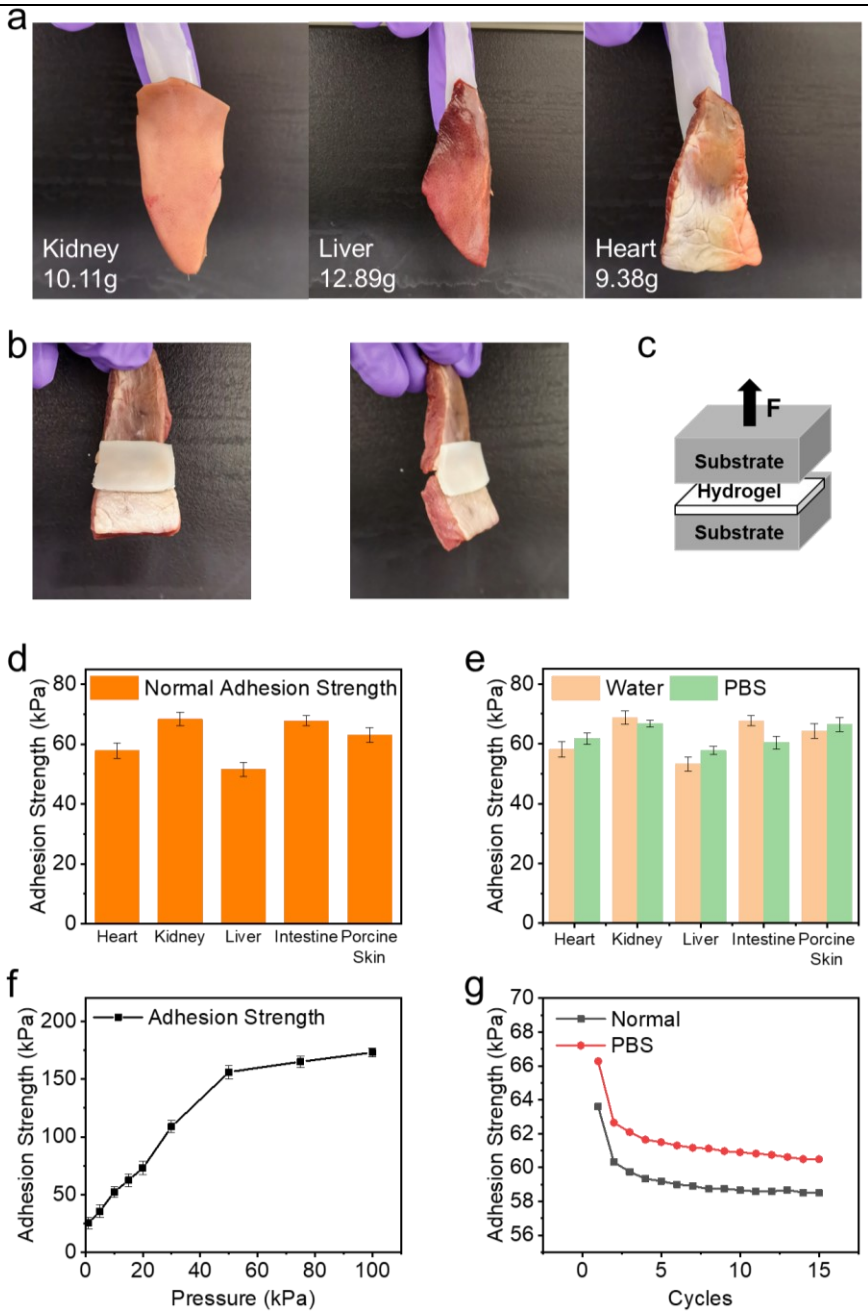

Figure 4.5. (a) Pictures for demonstrating the adhesive properties of microgel@PAM/CS hydrogel glued with different tissue surfaces. (b) Pictures for demonstrating that the microgel@PAM/CS hydrogel can glue two separated tissues together. (c) Scheme of normal adhesion test and (d) experimental results of adhesion strength between the microgel@PAM/CS hydrogel and various porcine tissues (e.g., heart, kidney, liver, intestine and skin) measured in air. (e) Normal adhesion strength measured in air between the microgel@PAM/CS hydrogels and various porcine tissues after immersed in water or PBS for 30 min. (f) Normal adhesion strength between the microgel@PAM/CS hydrogels and porcine skin measured under different preloading. (g) The adhesion strength of the microgel@PAM/CS hydrogels on porcine skin during cyclic attaching-detaching process after immersed in both water and PBS.

4.3.5 *In Vitro* Drug Release

The stimuli-responsive *in vitro* drug release behaviors of the microgel@PAM/CS hydrogels were studied using two model drugs, one model protein, BSA, and a small molecular antibiotic, SMZ. First, the BSA loading and releasing efficiency of the PNIPAAm-co-AAc microgel and the PAM/CS semi-IPN hydrogel were investigated. The loading of the BSA in these two gels were conducted under acidic pH of 4 for different time periods. As shown in **Figure 4.6a** and 4.**6b**, the loading of BSA in the microgels is much faster than that in the PAM/CS semi-IPN hydrogel with the efficiency reaching as high as 72% in the first 12 h for microgels compared to ~65% for bulk PAM/CS gel. Both gels gradually reached plateaus with the further increase of the incubation time to 48 h, with the final BSA loading efficiencies to be 80% and 71% for PNIPAAm-co-AAc microgel and PAM/CS bulk gel, respectively. The higher loading efficiency of the microgels is mainly due to the electrostatic attractions between the partially negatively charged PNIPAAm-co-AAc and the positively charged BSA under pH 4 which is lower than the isoelectric point of BSA (~4.7).[285-286]

To better understand the role of the stimuli-responsive microgels in the drug delivery behaviors of the hydrogels, the BSA releasing from the microgels and the PAM/CS bulk gels were studied using PBS as the medium under pH of 4 and 7.4 and temperature of 22 and 37 °C, and the results were shown in **Figure 4.6c** and 4.**6d**. From **Figure 4.6c,** the PNIPAAm-co-AAc microgels release the model protein in an obviously pH-sensitive manner, i.e., the release in pH 7.4 PBS much faster than that in pH 4 PBS, with the releasing efficiency to be 46% and 10.2% at 37 °C under neutral and acidic pH, respectively. This can be ascribed to the electrostatic repulsion between the copolymers and the protein under neutral pH that is much higher than the pKa of AAc and isoelectric point of BSA, as well as the looser gel network due to the stronger repulsion among the

polymer chains at pH 7.4. Temperature also poses an influence on the BSA release profiles from the microgels. BSA was released slightly faster at body temperature compared with that at room temperature, which may be due to the partial dewatering of the PNIPAAm at temperatures higher than its lower critical solution temperature (LCST, around 32 °C) and the higher mobility of molecules at higher temperatures. In contrast, the effects of pH and temperature on the release of BSA from the PAM/CS semi-IPN hydrogel are less pronounced, as shown in **Figure 4.6d**. The different plateau BSA releasing efficiencies from the PAM/CS bulk gel and the microgels might be caused by the different crosslinking degrees and pore sizes. As the PNIPAAm-co-AAc microgels demonstrated excellent protein loading efficiency and dual-stimuli sensitive protein release, the BSA model drug was loaded in the microgels for the investigation of the drug release behaviors of the composite hydrogel.

Next, the drug release behaviors of the composite microgel@PAM/CS were studied with two model drugs co-loaded into the hydrogel, i.e., SMZ in the matrix and BSA in the microgels. Typical dual drug release profiles of SMZ and BSA from microgel@PAM/CS hydrogel as a function of pH and temperature are shown in **Figure 4.6e** and 4.**6f**, respectively. According to these figures, rapid release behaviors of the SMZ were observed with the releasing efficiency reaching ~90% in 6 h. The enlarged inserted figures show that the release rates of SMZ in acidic (pH=4) and warm (37ºC) environment are slightly faster than those in neutral and cooler solutions which are correlated with the swelling behavior of microgel@PAM/CS hydrogel. Compared with the short-term release of SMZ, the releasing profiles of BSA feature sustained and long-term release, and high dependence on the environmental pH and temperature. **Figure 4.6e** shows that the releasing efficiency of BSA is much higher at pH 4 than that at pH 7.4, and the increased temperature also accelerates the release rate and slightly affects the final release efficiency of BSA as

shown in **Figure 4.6f**, which is in good agreement with the BSA releasing behaviors of the microgels, indicating that the microgels control the BSA release in this composite system. The results indicate that the PBS with pH of 7.4 and temperature of 37^{o}C, which simulates the condition of human tissue, provides an ideal environment for both SMZ and BSA release with intelligent and controlled dual drug release profiles.

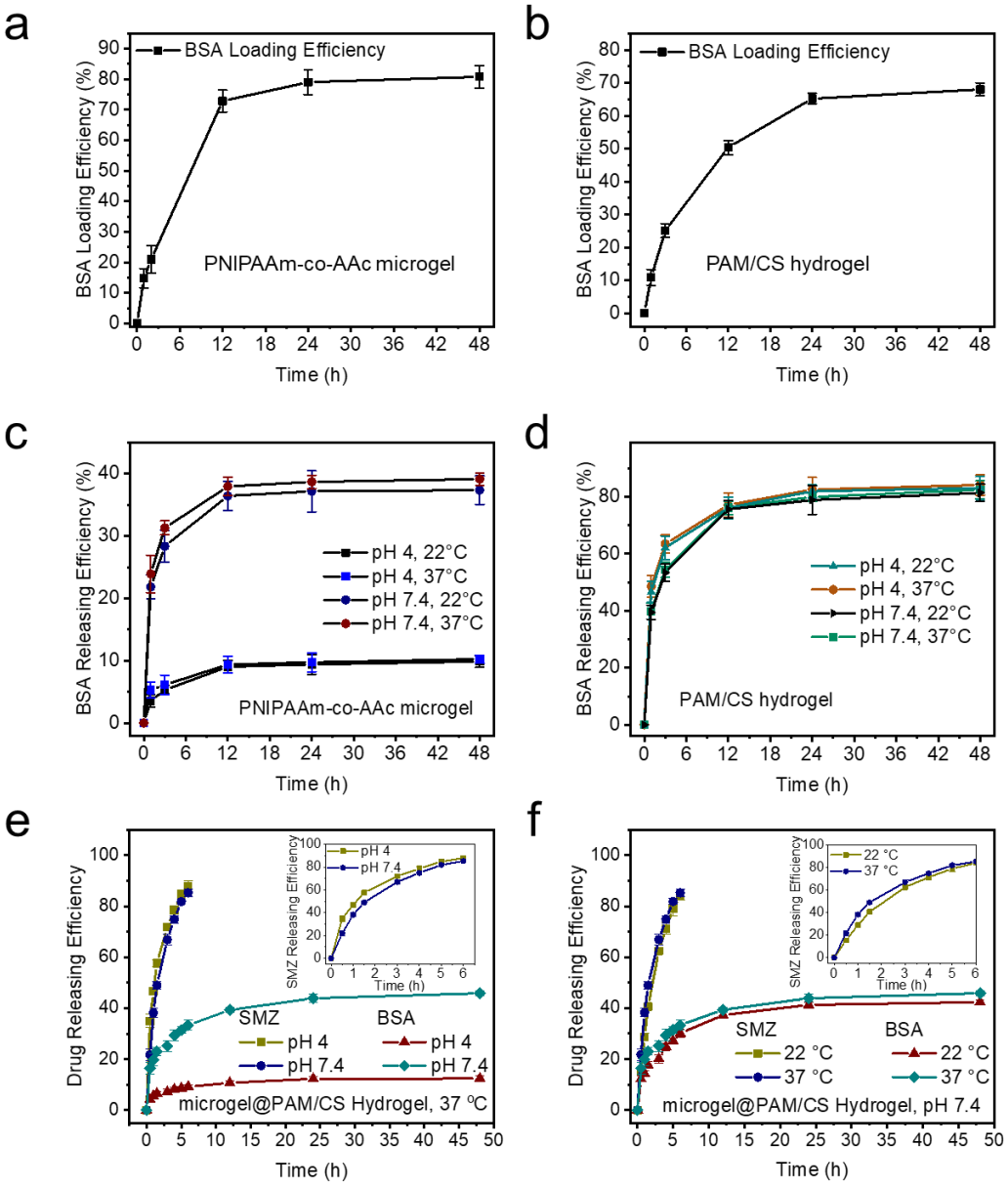

Figure 4.6. (a) BSA loading efficiency of PNIPAAm-co-AAc microgel in pH 4 PBS at 22 ºC. (b) BSA loading efficiency of PAM/CS hydrogel in pH 4 PBS at 22 ºC. (c) BSA releasing efficiency of PNIPAAm-co-AAc microgel in pH 4 and 7.4 PBS at 22 and 37 ºC. (d) BSA releasing efficiency of PAM/CS hydrogel in pH 4 and 7.4 PBS at 22 and 37 ºC. (e) SMZ and BSA releasing efficiency of microgel@PAM/CS hydrogel in pH 4 and 7.4 PBS at 37 ºC. (f) SMZ and BSA releasing efficiency of microgel@PAM/CS hydrogel in pH 7.4 PBS at 22 and 37 ºC.

4.3.6 Antimicrobial Tests

It is critical for wound dressing materials to possess antimicrobial property, which can act as the first barrier to damaged tissue. The antimicrobial property of the microgel@PAM/CS hydrogel was evaluated by counting the inhibited number of *E. coli* through the spread plate method.[287] *E. coli* suspension was treated with SMZ-loaded microgel@PAM/CS and PAM (as a control) hydrogels for 4 h, and then transferred to Luria-Bertani (LB) agar plates for another 14 h incubation. **Figure 4.7a** shows a 92.50 ± 0.01 % reduction of colonies for the SMZ-loaded microgel@PAM/CS hydrogel treated agar plates as compared to those treated by bare PAM hydrogel. The excellent antimicrobial properties were also demonstrated by images showing the inhibition of the growth of *E. coli* colonies in **Figure 4.7b**. The significant inhibition of *E. coli* can be attributed to the antibiotic effect of SMZ as well as the pronated amino groups of CS chains.

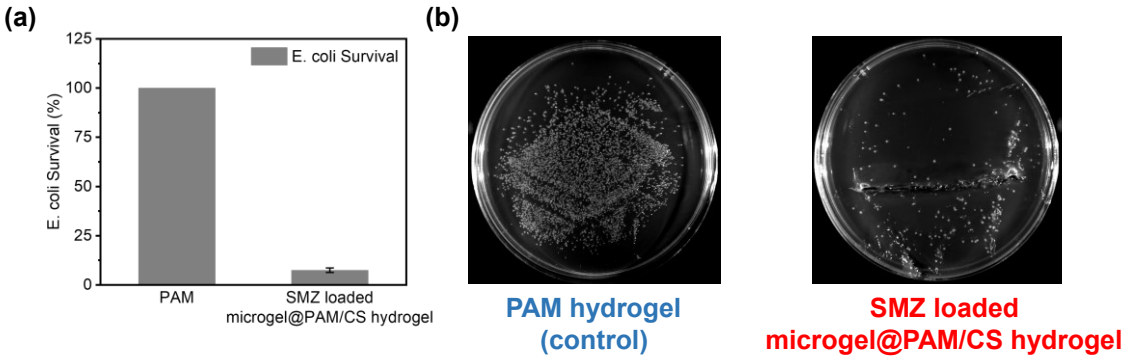

Figure 4.7. Antibacterial properties of SMZ-loaded microgel@PAM/CS hydrogel. (a) Statistical *E. coil* survival rate (n=3, $p < 0.001$) and (b) Optical images of *E. coli* colonies after incubation with PAM hydrogel (left) and SMZ loaded microgel@PAM/CS hydrogel (right) for 4 h.

4.3.7 Wound Healing Process Enhanced by the Microgel@PAM/CS Hydrogel Dressing

Figure 4.8a shows the pictures of typical macroscopic wound healing panorama of wound surfaces of rats treated with the as-prepared SMZ-loaded microgel@PAM/CS hydrogel (denoted as the experimental group) and without the hydrogel (denoted as the control group) over 15 days. The wound area of rats in both experimental group and control group gradually healed, but the healing rate of each group was significantly different. On the 7^{th} day, compared with the control group, the experimental group which was treated with the microgel@PAM/CS hydrogel showed reduced wound size, with no apparent redness, inflammation, or eschar in the wound areas. On the 11^{th} day, epithelialization could be observed in the wound areas, and the new epithelium and the healing of wounds were more evident in the experimental group. On the 13^{th} day, epithelialization was almost completed in the experimental group, while the control group still had residual eschar. On the 15^{th} day, the wound shrinkage rate achieved the highest and the wound was nearly healed. The wound dressed with microgel@PAM/CS hydrogel showed a faster closure rate than the control group, indicating the hydrogel dressing accelerated the wound healing.

Meanwhile, the wound closure rate of different days was calculated by GraphPad prism 8.0 software, as shown in **Figure 4.8b.** The wound closure rate of the experimental group was significantly different from that of the control group on the 7^{th} day, and the difference was statistically significant ($P<0.05$). Specifically, on the 11^{th} day, the wound healing effect of the hydrogel group was significant ($P<0.01$), and the results on the 13^{th} and 15^{th} days were statistically significant ($P<0.05$). These results demonstrated that the experimental group treated with the microgel@PAM/CS hydrogel improved the wound healing, as compared to the control group.

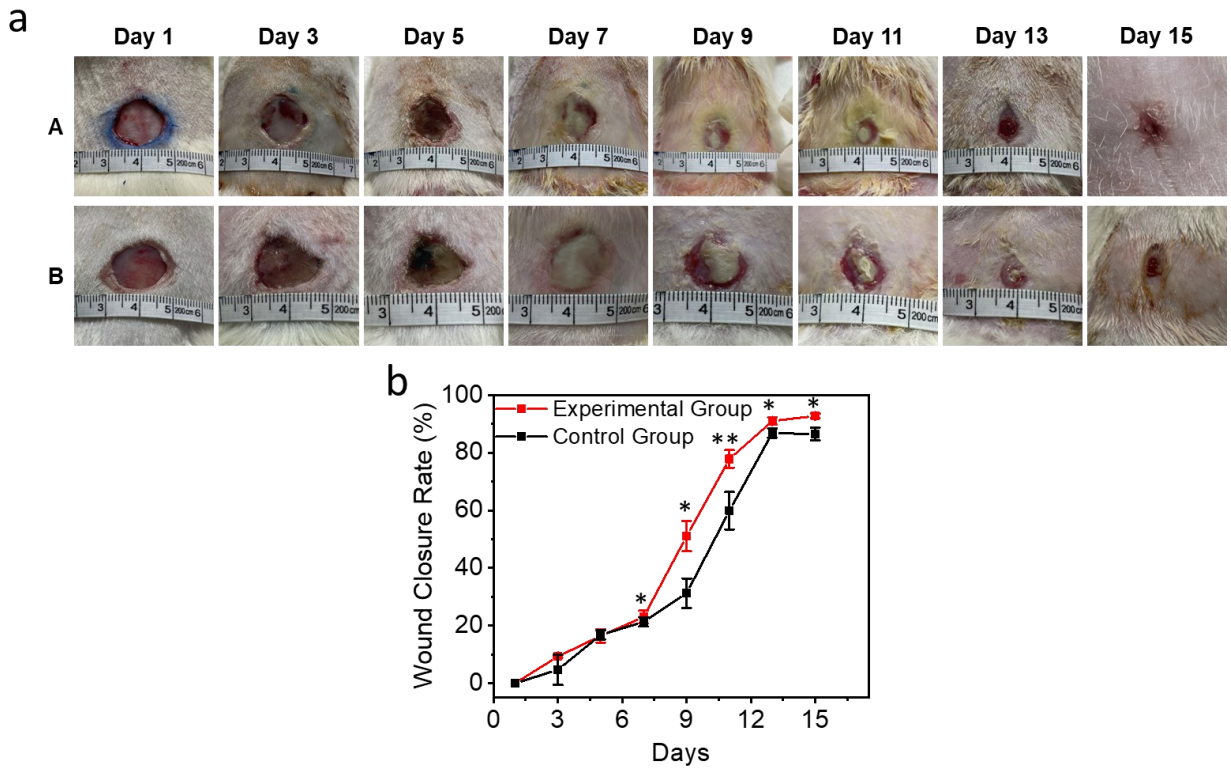

Figure 4.8. (a) Typical macroscopic wound healing panorama with different treatments over 15 days. (A) represents the experimental group treated with the as-prepared microgel@PAM/CS hydrogel, and (B) represents the control group treated with 1×PBS, without the hydrogel material. (b) Wound closure rate with time (Hydrogel vs Control*P<0.05, **P<0.01).

4.3.8 Histological Study

Figure 4.9 shows the results of the histological study. Compared with the control group (without hydrogel treatment), the experimental group (treated with the microgel@PAM/CS hydrogel) had fewer neutrophils and other inflammatory cells, more capillaries, and fibroblasts. New epidermis began to form in the experimental group as compared with the control group, which still showed mild necrosis of the epidermis on the 7^{th} day of the wound repair procedure. On the 15^{th} day, there were a few inflammatory cells and many fibroblasts in both groups, and skin appendages (hair follicles) were visible. The

fibroblasts and collagen fibers were neatly arranged in the experimental group, and the epithelium was basically formed with a denser tissue structure and complete wound healing.

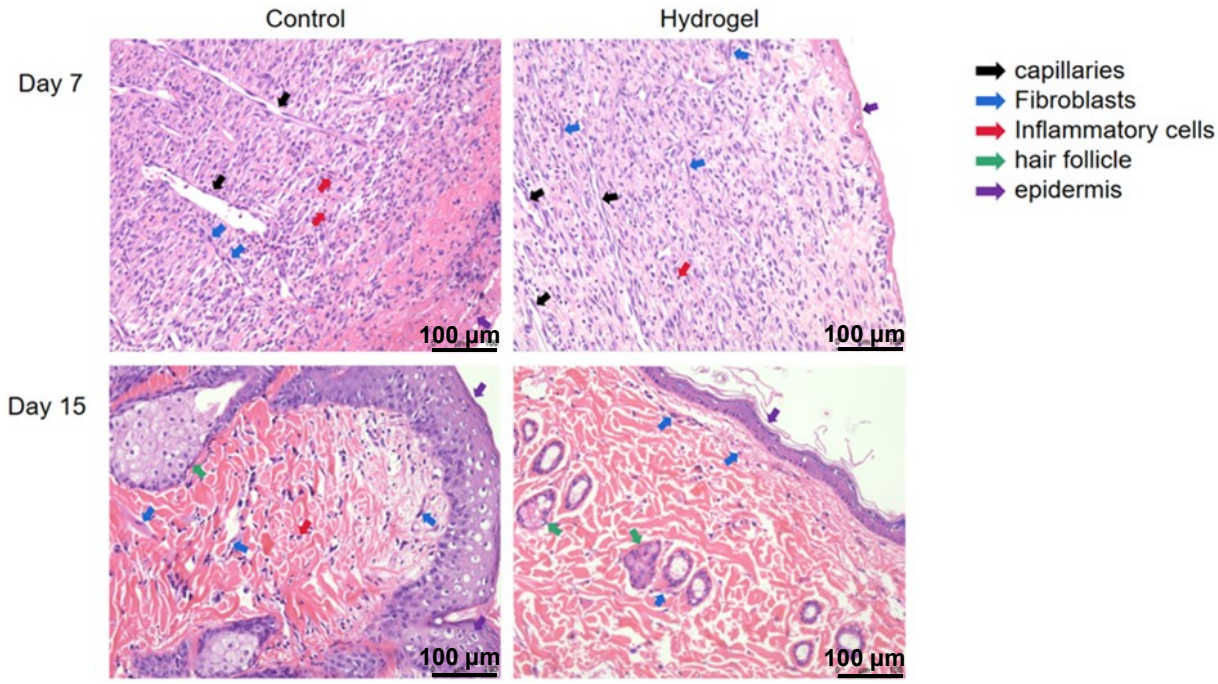

Figure 4.9. HE staining results for the control group (without hydrogel treatment, left panels) and the experimental group (treated using the microgel@PAM/CS hydrogel, right panels) on the 7th and 15th days (scale bars: 100 μm).

4.4 Conclusions

In this work, we have fabricated a pH and temperature dual-responsive microgel-embedded hydrogel, microgel@PAM/CS, via a facile approach by incorporating PNIPAAm-co-AAc microgel particles to PAM/CS semi-IPN hydrogel. The microgel@PAM/CS hydrogel shows reversible swelling-dewatering capability while maintains its structure integrity, and also possesses excellent mechanical properties, i.e., reaching a tensile strength of 150 kPa, withstanding more than 800% strain and repeatedly recovering from tensile and compressive strains. The microgel@PAM/CS hydrogel also shows strong and reversible adhesion to different tissue surfaces such as porcine skin,

kidney, intestine, liver and heart, and is able to encapsulate and release both BSA (as a model protein) and SMZ. The as-prepared microgel@PAM/CS hydrogels demonstrated high protein drug loading efficiency (more than 80%), controllable drug-releasing behaviors and sustained drug-releasing duration over 2 days, showing advantages over the traditional oral, injection and smear medication methods. The macroscopic wound healing tests by monitoring the wound surfaces of rats treated with and without the microgel@PAM/CS hydrogels demonstrated that the microparticle-embedded hydrogels can significantly enhance the wound healing process and also possess good antimicrobial properties. Our results have demonstrated a facile and feasible approach for building multifunctional stimuli-responsive microparticle-embedded hydrogel materials, and microgel@PAM/CS hydrogels fabricated hold potential applications in the bioengineering field as smart wound dressing materials.

CHAPTER 5 Conclusions and Future Work

5.1 Major Conclusions and Contributions

In this thesis work, various noncovalent interactions have been incorporated into hydrogel systems, and three integrated multifunctional hydrogels demonstrating stretchability, adhesion and self-healing capacity were developed for different bioengineering and sensing applications. The major conclusions and original contributions are listed as follows.

(1) An ultra-stretchable hydrogel with strain-sensing and antibacterial properties was fabricated based on multiple hydrogen bonding interactions between catechol moieties of TA, hydroxide groups of PVA, and carboxylic acid groups of PMVEMA by facilely mixing the ternary polymer system. The gel showed fast and highly recovered healing behavior from fractures. Moreover, the stable swelling properties in different pH conditions, anti-freezing and remodeling characteristics indicated that the hydrogel could be used in a variety of conditions. Moreover, the hydrogel's substantial adhesive property on diverse substrates made it a promising vehicle for the delivery of drugs in suit by immobilizing it in regions like wounds, vessels and tumors. Due to the affluent dynamic hydrogen bonding interaction, this hydrogel exhibited superior stretchability, which also broadened the strain sensing range. We further demonstrated the electrical sensing performance of the prepared hydrogel network under stretching, bending, compression and folding behaviors, which provides great potential for developing sensing devices for health, motion, or pressure monitoring. In addition, the PMVEMA polymer and the polyphenol groups from TA provided the hydrogel with excellent antibacterial properties, resulting in great opportunities for wound dressing and other bioengineering applications.

(2) An adhesive, stretchable, self-healing and conductive hydrogel was fabricated by one-pot polymerization as a multifunctional strain sensor. The mechanical property of the hydrogel can be adjusted by the density of hydrogen bonding crosslinks in the PVA/PAA double network structure. The mechanically robust hydrogel was stretched up to 6 times its original length, withstood over 80% compressive strain and maintained a stable performance after 100 loading-unloading cycles. The self-healing and strong adhesion to diverse surfaces of the as-prepared hydrogel also contributed to the reversible nature of hydrogen bonding interactions, showing advantages for self-adhesive soft sensors. Notably, the incorporated conductive PEDOT: PSS polymer network endowed the hydrogel with high sensitivity of a gauge factor range from 2.21 to 3.82. Precise detection of diverse human activities, including finger bending, wrist bending, and stepping was demonstrated. In addition, the as-prepared hydrogel sensor distinguished many subtle human motions, such as pulse changes and vocal cord vibration, which provided valuable insights into the development of conductive hydrogel-based wearable soft electronics.

(3) A pH-responsive hydrogel was developed by incorporating modified PNIPAAm microgel particles and a tough CS/PAAm hydrogel for adhesive drug delivery and other bioengineering applications. The pH and temperature-sensitive properties of the hydrogel resulted from the deprotonation of the AAc groups caused by the increased pH and the hydrophilic-hydrophobic transition of the collapsed PNIPAAm caused by the elevated temperature. The synthesized hydrogel can be stretched over 800% and compressed over 60% strain. The highly overlapping loading-unloading stress-strain curves indicate the high resilience, anti-fatigue and reliability of the hydrogel system. The adhesion to various surfaces of porcine tissues (e.g., heart, kidney, liver, intestine and skin)

and the pressure-sensitive behaviors make this material advantageous for attaching to tissue surfaces in biomedical applications. Moreover, the as-prepared hydrogel shows a higher drug release efficiency and longer release duration in the wound area (pH=7.4 @ 37 °C) due to the shrinking of microgel networks and the protonation of functional groups. In addition, the hydrogel has excellent antibacterial properties and has remarkably accelerated wound healing in experimental SD rats. This microgel-embedded hydrogel provides insights conducive to developing multifunctional biomaterials with various biomedical and bioengineering applications.

5.2 Future Work

In this work, we have explored the integration of various noncovalent interactions with different hydrogel structures and introduced functional networks into the hydrogel systems, endowing the hydrogels with improved mechanical properties, specific responsiveness and multifunctionalities. The applications of those hydrogel systems in the areas of bioengineering and sensing have also been investigated. The possible areas of future work include the followings:

(1) Although noncovalent interactions have been well identified by many types of nanomechanical force measurement tools such as Atomic Force Microscopy (AFM), Surface Forces Apparatus (SFA), nano tribometer, etc., it is still necessary to investigate the leverage of noncovalent interactions in macroscopic systems (e.g., polymers, elastomers, hydrogels, etc.) for the development of design strategies and tuned properties or functionalities. Novel multifunctional hydrogels could be discovered based on the identification of the role noncovalent interactions play within the whole system.

(2) Despite the much effort devoted to applying hydrogels in diverse areas, there

are still numerous modification strategies and synthesis methods that could be used to broaden the applied ranges of functional hydrogels. For example, by modifying conductive hydrogels, portable wireless soft devices can be achieved to meet the practical needs of intelligent wearable electronics. For applications such as wound dressing and postoperative treatment materials, hydrogels with drug delivery capacity could be further improved to provide strong adhesion with tissue in wet conditions since tissues or organs are usually surrounded by bodily fluids.

(3) Even though hydrogels are well-known as ideal candidates for biomedical applications, they can be further elevated by being incorporated with macromolecules such as DNAs, RNAs and enzymes to improve their biocompatibility and biodegradability. In addition, optimizing the mechanical properties of hydrogels toward mimicking the character of real tissue is also critical for their applications in bioengineering. Nevertheless, because the practical application of these novel multifunctional materials could have a considerable effect on human health, in vivo tests with large animal models should be conducted to further evaluate the medical outcomes of these materials.

Bibliography

(1) Wichterle, O.; Lim, D. Hydrophilic gels for biological use. *Nature communications* **1960,** *185* (4706), 117-118.

(2) Wichterle, O.; Chromeček, R. In *Polymerization of ethylene glycol monomethacrylate in the presence of solvents*, Journal of Polymer Science Part C: Polymer Symposia, Wiley Online Library: **1967**; pp 4677-4686.

(3) Skardal, A.; Devarasetty, M.; Kang, H.-W.; Mead, I.; Bishop, C.; Shupe, T.; Lee, S. J.; Jackson, J.; Yoo, J.; Soker, S. A hydrogel bioink toolkit for mimicking native tissue biochemical and mechanical properties in bioprinted tissue constructs. *Acta biomaterialia* **2015,** *25*, 24-34.

(4) Li, S.; Dong, S.; Xu, W.; Tu, S.; Yan, L.; Zhao, C.; Ding, J.; Chen, X. Antibacterial hydrogels. *Advanced science* **2018,** *5* (5), 1700527.

(5) Zhao, C.; Zhou, L.; Chiao, M.; Yang, W. Antibacterial hydrogel coating: Strategies in surface chemistry. *Advances in Colloid Interface Science* **2020,** *285*, 102280.

(6) Ekblad, T.; Bergström, G.; Ederth, T.; Conlan, S. L.; Mutton, R.; Clare, A. S.; Wang, S.; Liu, Y.; Zhao, Q.; D'Souza, F. Poly (ethylene glycol)-containing hydrogel surfaces for antifouling applications in marine and freshwater environments. *Biomacromolecules* **2008,** *9* (10), 2775-2783.

(7) Nicodemus, G. D.; Bryant, S. J. Cell encapsulation in biodegradable hydrogels for tissue engineering applications. *Tissue Engineering Part B: Reviews* **2008,** *14* (2), 149-165.

(8) Li, R. H.; Altreuter, D. H.; Gentile, F. T. Transport characterization of hydrogel matrices for cell encapsulation. *Biotechnology bioengineering* **1996,** *50* (4), 365-373.

(9) Bhattacharya, M.; Malinen, M. M.; Lauren, P.; Lou, Y.-R.; Kuisma, S. W.; Kanninen, L.; Lille, M.; Corlu, A.; GuGuen-Guillouzo, C.; Ikkala, O. Nanofibrillar cellulose hydrogel promotes three-dimensional liver cell culture. *Journal of controlled release* **2012,** *164* (3), 291-298.

(10) Grinstaff, M. W. Designing hydrogel adhesives for corneal wound repair. *Biomaterials* **2007,** *28* (35), 5205-5214.

(11) Liu, H.; Li, M.; Ouyang, C.; Lu, T. J.; Li, F.; Xu, F. Biofriendly, stretchable, and reusable hydrogel electronics as wearable force sensors. *Small* **2018,** *14* (36), 1801711.

(12) Luo, X.-L.; Xu, J.-J.; Zhang, Q.; Yang, G.-J.; Chen, H.-Y. J. B.; Bioelectronics. Electrochemically deposited chitosan hydrogel for horseradish peroxidase immobilization through gold nanoparticles self-assembly. **2005,** *21* (1), 190-196.

(13) Yuk, H.; Lin, S.; Ma, C.; Takaffoli, M.; Fang, N. X.; Zhao, X. Hydraulic hydrogel actuators and robots optically and sonically camouflaged in water. *Nature communications* **2017,** *8* (1), 1-12.

(14) Zhang, J.; Wan, L.; Gao, Y.; Fang, X.; Lu, T.; Pan, L.; Xuan, F. Highly stretchable and self‐healable MXene/polyvinyl alcohol hydrogel electrode for wearable capacitive electronic skin. *Advanced Electronic Materials* **2019,** *5* (7), 1900285.

(15) Wei, X.; Tian, T.; Jia, S.; Zhu, Z.; Ma, Y.; Sun, J.; Lin, Z.; Yang, C. J. Target-responsive DNA hydrogel mediated “stop-flow” microfluidic paper-based analytic device for rapid, portable and visual detection of multiple targets. *Analytical chemistry* **2015,** *87* (8), 4275-4282.

(16) Oyen, M. Mechanical characterisation of hydrogel materials. *International Materials Reviews* **2014,** *59* (1), 44-59.

(17) Gong, J. P.; Katsuyama, Y.; Kurokawa, T.; Osada, Y. Double‐network hydrogels with extremely high mechanical strength. *Advanced materials* **2003,** *15* (14), 1155-1158.

(18) Gong, J. P. Why are double network hydrogels so tough? *Soft Matter* **2010,** *6* (12), 2583-2590.

(19) Chen, Q.; Zhu, L.; Zhao, C.; Wang, Q.; Zheng, J. A robust, one‐pot synthesis of highly mechanical and recoverable double network hydrogels using thermoreversible sol‐gel polysaccharide. *Advanced materials* **2013,** *25* (30), 4171-4176.

(20) Nakajima, T.; Sato, H.; Zhao, Y.; Kawahara, S.; Kurokawa, T.; Sugahara, K.; Gong, J. P. A universal molecular stent method to toughen any hydrogels based on double network concept. *Advanced functional materials* **2012,** *22* (21), 4426-4432.

(21) Fu, F.; Wang, J.; Zeng, H.; Yu, J. J. A. M. L. Functional conductive hydrogels for bioelectronics. **2020,** *2* (10), 1287-1301.

(22) Chen, Z.; To, J. W.; Wang, C.; Lu, Z.; Liu, N.; Chortos, A.; Pan, L.; Wei, F.; Cui, Y.; Bao, Z. A three‐dimensionally interconnected carbon nanotube–conducting polymer hydrogel network for high‐performance flexible battery electrodes. *Advanced energy materials* **2014,** *4* (12), 1400207.

(23) Baei, P.; Jalili-Firoozinezhad, S.; Rajabi-Zeleti, S.; Tafazzoli-Shadpour, M.; Baharvand, H.; Aghdami, N. Electrically conductive gold nanoparticle-chitosan thermosensitive hydrogels for cardiac tissue engineering. *Materials Science Engineering: C* **2016,** *63*, 131-141.

(24) Ahn, Y.; Lee, H.; Lee, D.; Lee, Y. Highly conductive and flexible silver nanowire-based microelectrodes on biocompatible hydrogel. *ACS applied materials interfaces* **2014,** *6* (21), 18401-18407.

(25) Lin, J.; Tang, Q.; Wu, J.; Hao, S. J. R.; Polymers, F. The synthesis and electrical conductivity of a polyacrylate/graphite hydrogel. **2007,** *67* (4), 275-281.

(26) Zhang, L.; Shi, G. J. T. J. o. P. C. C. Preparation of highly conductive graphene hydrogels for fabricating supercapacitors with high rate capability. **2011,** *115* (34), 17206-17212.

(27) Wang, M.; Chen, Y.; Khan, R.; Liu, H.; Chen, C.; Chen, T.; Zhang, R.; Li, H. A fast self-healing and conductive nanocomposite hydrogel as soft strain sensor. *Colloids and Surfaces a-Physicochemical and Engineering Aspects* **2019,** *567*, 139-149, DOI: 10.1016/j.colsurfa.2019.01.034.

(28) Guiseppi-Elie, A. J. B. Electroconductive hydrogels: synthesis, characterization and biomedical applications. **2010,** *31* (10), 2701-2716.

(29) Zheng, Y.; Yang, Y.; Chen, S.; Yuan, Q. Smart, stretchable and wearable supercapacitors: prospects and challenges. *CrystEngComm* **2016,** *18* (23), 4218-4235.

(30) Tang, Q.; Wu, J.; Sun, H.; Fan, S.; Hu, D.; Lin, J. J. C. p. Superabsorbent conducting hydrogel from poly (acrylamide-aniline) with thermo-sensitivity and release properties. **2008,** *73* (3), 473-481.

(31) Balint, R.; Cassidy, N. J.; Cartmell, S. H. Conductive polymers: Towards a smart biomaterial for tissue engineering. *Acta biomaterialia* **2014,** *10* (6), 2341-2353.

(32) Ismail, Y. A.; Martínez, J. G.; Al Harrasi, A. S.; Kim, S. J.; Otero, T. F. J. S.; Chemical, A. B. Sensing characteristics of a conducting polymer/hydrogel hybrid microfiber artificial muscle. **2011,** *160* (1), 1180-1190.

(33) Snook, G. A.; Kao, P.; Best, A. S. J. J. o. p. s. Conducting-polymer-based supercapacitor devices and electrodes. **2011,** *196* (1), 1-12.

(34) Lu, B.; Yuk, H.; Lin, S.; Jian, N.; Qu, K.; Xu, J.; Zhao, X. Pure PEDOT:PSS hydrogels. *Nature Communications* **2019,** *10* (1), 1043, DOI: 10.1038/s41467-019-09003-5.

(35) Ruel-Gariepy, E.; Leclair, G.; Hildgen, P.; Gupta, A.; Leroux, J.-C. J. J. o. C. R. Thermosensitive chitosan-based hydrogel containing liposomes for the delivery of hydrophilic molecules. **2002,** *82* (2-3), 373-383.

(36) Chen, S.-C.; Wu, Y.-C.; Mi, F.-L.; Lin, Y.-H.; Yu, L.-C.; Sung, H.-W. A novel pH-sensitive hydrogel composed of N, O-carboxymethyl chitosan and alginate cross-linked by genipin for protein drug delivery. *Journal of Controlled Release* **2004,** *96* (2), 285-300.

(37) Lei, Z.; Wang, Q.; Sun, S.; Zhu, W.; Wu, P. J. A. M. A bioinspired mineral hydrogel as a self‐healable, mechanically adaptable ionic skin for highly sensitive pressure sensing. **2017,** *29* (22), 1700321.

(38) Samai, S.; Sapsanis, C.; Patil, S. P.; Ezzeddine, A.; Moosa, B. A.; Omran, H.; Emwas, A.-H.; Salama, K. N.; Khashab, N. M. J. S. m. A light responsive two-

component supramolecular hydrogel: a sensitive platform for the fabrication of humidity sensors. **2016,** *12* (11), 2842-2845.

(39) Zhao, B.; Moore, J. S. J. L. Fast pH-and ionic strength-responsive hydrogels in microchannels. **2001,** *17* (16), 4758-4763.

(40) Kim, S. J.; Yoon, S. G.; Lee, S. M.; Lee, S. H.; Kim, S. I. J. J. o. A. P. S. Electrical sensitivity behavior of a hydrogel composed of polymethacrylic acid/poly (vinyl alcohol). **2004,** *91* (6), 3613-3617.

(41) Satarkar, N. S.; Hilt, J. Z. J. J. o. C. R. Magnetic hydrogel nanocomposites for remote controlled pulsatile drug release. **2008,** *130* (3), 246-251.

(42) Dahman, Y. *Nanotechnology and Functional Materials for Engineers*, Elsevier: 2017.

(43) Zhu, Z.; Wu, C.; Liu, H.; Zou, Y.; Zhang, X.; Kang, H.; Yang, C. J.; Tan, W. An aptamer cross‐linked hydrogel as a colorimetric platform for visual detection. *Angewandte Chemie* **2010,** *122* (6), 1070-1074.

(44) Berggren, M.; Richter-Dahlfors, A. Organic Bioelectronics. **2007,** *19* (20), 3201-3213, DOI: 10.1002/adma.200700419.

(45) Johnson, E. R.; Keinan, S.; Mori-Sánchez, P.; Contreras-García, J.; Cohen, A. J.; Yang, W. Revealing noncovalent interactions. *Journal of the American Chemical Society* **2010,** *132* (18), 6498-6506.

(46) Soderberg, T. *Organic chemistry with a biological emphasis*, 2012.

(47) Müller-Dethlefs, K.; Hobza, P. Noncovalent interactions: a challenge for experiment and theory. *Chemical Reviews* **2000,** *100* (1), 143-168.

(48) Weinhold, F.; Klein, R. A. What is a hydrogen bond? Mutually consistent theoretical and experimental criteria for characterizing H-bonding interactions. *Molecular Physics* **2012,** *110* (9-10), 565-579.

(49) Grabowski, S. J. *Hydrogen bonding: new insights*, Springer: 2006; Vol. 3.

(50) Chen, Y.-N.; Peng, L.; Liu, T.; Wang, Y.; Shi, S.; Wang, H. Poly (vinyl alcohol)–tannic acid hydrogels with excellent mechanical properties and shape memory behaviors. *ACS applied materials interfaces interfaces* **2016,** *8* (40), 27199-27206.

(51) Fan, H.; Wang, J.; Jin, Z. Tough, swelling-resistant, self-healing, and adhesive dual-cross-linked hydrogels based on polymer–tannic acid multiple hydrogen bonds. *Macromolecules* **2018,** *51* (5), 1696-1705.

(52) Zhang, H.; Xia, H.; Zhao, Y. Poly (vinyl alcohol) hydrogel can autonomously self-heal. *ACS Macro Letters* **2012,** *1* (11), 1233-1236.

(53) Shao, Y.; Jia, H.; Cao, T.; Liu, D. Supramolecular hydrogels based on DNA self-assembly. *Accounts of chemical research* **2017,** *50* (4), 659-668.

(54) Dankers, P. Y.; Harmsen, M. C.; Brouwer, L. A.; Van Luyn, M. J.; Meijer, E. A modular and supramolecular approach to bioactive scaffolds for tissue engineering. *Nature materials* **2005,** *4* (7), 568-574.

(55) Chen, J.; Peng, Q.; Thundat, T.; Zeng, H. Stretchable, injectable, and self-healing conductive hydrogel enabled by multiple hydrogen bonding toward wearable electronics. *Chemistry of Materials* **2019,** *31* (12), 4553-4563.

(56) Lin, F.; Wang, Z.; Chen, J.; Lu, B.; Tang, L.; Chen, X.; Lin, C.; Huang, B.; Zeng, H.; Chen, Y. A bioinspired hydrogen bond crosslink strategy toward toughening ultrastrong and multifunctional nanocomposite hydrogels. *Journal of Materials Chemistry B* **2020,** *8* (18), 4002-4015.

(57) Han, Y. L.; Yang, Y.; Liu, S.; Wu, J.; Chen, Y.; Lu, T. J.; Xu, F. Directed self-assembly of microscale hydrogels by electrostatic interaction. *Biofabrication* **2013,** *5* (3), 035004.

(58) Criado-Gonzalez, M.; Wagner, D.; Rodon Fores, J.; Blanck, C.; Schmutz, M.; Chaumont, A.; Rabineau, M.; Schlenoff, J. B.; Fleith, G.; Combet, J. Supramolecular hydrogel induced by electrostatic interactions between polycation and phosphorylated-Fmoc-tripeptide. *Chemistry of Materials* **2020,** *32* (5), 1946-1956.

(59) Hill, A.; Candau, F.; Selb, J. Properties of hydrophobically associating polyacrylamides: influence of the method of synthesis. *Macromolecules* **1993,** *26* (17), 4521-4532.

(60) Tuncaboylu, D. C.; Sari, M.; Oppermann, W.; Okay, O. Tough and self-healing hydrogels formed via hydrophobic interactions. *Macromolecules* **2011,** *44* (12), 4997-5005.

(61) Kakuta, T.; Takashima, Y.; Nakahata, M.; Otsubo, M.; Yamaguchi, H.; Harada, A. Preorganized hydrogel: self-healing properties of supramolecular hydrogels formed by polymerization of host-guest-monomers that contain cyclodextrins and hydrophobic guest groups. *Adv. Mater.* **2013,** *25* (20), 2849-53, DOI: 10.1002/adma.201205321.

(62) Fan, X.; Wang, T.; Miao, W. The preparation of pH-sensitive hydrogel based on host-guest and electrostatic interactions and its drug release studies in vitro. *Journal of Polymer Research* **2018,** *25* (10), 1-10.

(63) Chen, Y.; Pang, X. H.; Dong, C. M. Dual Stimuli‐Responsive Supramolecular Polypeptide‐Based Hydrogel and Reverse Micellar Hydrogel Mediated by Host‐Guest Chemistry. *Advanced Functional Materials* **2010,** *20* (4), 579-586.

(64) Zhang, G.; Chen, Y.; Deng, Y.; Ngai, T.; Wang, C. Dynamic supramolecular hydrogels: regulating hydrogel properties through self-complementary quadruple hydrogen bonds and thermo-switch. *ACS Macro Letters* **2017,** *6* (7), 641-646.

(65) Nakahata, M.; Takashima, Y.; Yamaguchi, H.; Harada, A. Redox-responsive self-healing materials formed from host–guest polymers. *Nature communications* **2011,** *2* (1), 1-6.

(66) Peng, L.; Zhang, H.; Feng, A.; Huo, M.; Wang, Z.; Hu, J.; Gao, W.; Yuan, J. Electrochemical redox responsive supramolecular self-healing hydrogels based on host–guest interaction. *Polymer Chemistry* **2015,** *6* (19), 3652-3659.

(67) Nakahata, M.; Takashima, Y.; Hashidzume, A.; Harada, A. Redox‐generated mechanical motion of a supramolecular polymeric actuator based on host–guest interactions. *Angewandte Chemie* **2013,** *52* (22), 5731-5735.

(68) Ouellette, R. J.; Rawn, J. D. 1-structure and bonding in organic compounds. *Organic Chemistry* **2014**, 1-39.

(69) Rowley, J. A.; Madlambayan, G.; Mooney, D. J. Alginate hydrogels as synthetic extracellular matrix materials. *Biomaterials* **1999,** *20* (1), 45-53.

(70) Andersen, T.; Auk-Emblem, P.; Dornish, M. 3D cell culture in alginate hydrogels. *Microarrays* **2015,** *4* (2), 133-161.

(71) Ozawa, F.; Ino, K.; Shiku, H.; Matsue, T. Electrochemical hydrogel lithography of calcium-alginate hydrogels for cell culture. *Materials* **2016,** *9* (9), 744.

(72) Zhang, Z.; Zhang, R.; Zou, L.; McClements, D. J. J. F. H. Protein encapsulation in alginate hydrogel beads: Effect of pH on microgel stability, protein retention and protein release. **2016,** *58*, 308-315.

(73) Kang, S.-M.; Lee, J.-H.; Huh, Y. S.; Takayama, S. Alginate microencapsulation for three-dimensional in vitro cell culture. *ACS Biomaterials Science Engineering* **2020,** *7* (7), 2864-2879.

(74) Gao, F.; Zhang, Y.; Li, Y.; Xu, B.; Cao, Z.; Liu, W. Sea cucumber-inspired autolytic hydrogels exhibiting tunable high mechanical performances, repairability, and reusability. *ACS applied materials interfaces* **2016,** *8* (14), 8956-8966.

(75) Fan, H.; Wang, J.; Gong, J. P. Barnacle cement proteins‐inspired tough hydrogels with robust, long‐lasting, and repeatable underwater adhesion. *Advanced Functional Materials* **2021,** *31* (11), 2009334.

(76) Wang, S.; Guo, G.; Lu, X.; Ji, S.; Tan, G.; Gao, L. Facile soaking strategy toward simultaneously enhanced conductivity and toughness of self-healing composite hydrogels through constructing multiple noncovalent interactions. *ACS applied materials interfaces* **2018,** *10* (22), 19133-19142.

(77) He, X.; Liu, L.; Han, H.; Shi, W.; Yang, W.; Lu, X. Bioinspired and microgel-tackified adhesive hydrogel with rapid self-healing and high stretchability. *Macromolecules* **2018,** *52* (1), 72-80.

(78) Feng, Z.; Zuo, H.; Gao, W.; Ning, N.; Tian, M.; Zhang, L. A Robust, Self‐Healable, and Shape Memory Supramolecular Hydrogel by Multiple Hydrogen Bonding Interactions. *Macromolecular rapid communications* **2018,** *39* (20), 1800138.

(79) Ikada, Y. Challenges in tissue engineering. *Journal of the Royal Society Interface* **2006,** *3* (10), 589-601.

(80) Jo, Y.; Hwang, S. H.; Jang, J. Employing Extracellular Matrix-Based Tissue Engineering Strategies for Age-Dependent Tissue Degenerations. *International Journal of Molecular Sciences* **2021,** *22* (17), 9367.

(81) Khademhosseini, A.; Langer, R. Microengineered hydrogels for tissue engineering. *Biomaterials* **2007,** *28* (34), 5087-5092.

(82) Sefton, M.; May, M.; Lahooti, S.; Babensee, J. Making microencapsulation work: conformal coating, immobilization gels and in vivo performance. *Journal of Controlled Release* **2000,** *65* (1-2), 173-186.

(83) Spicer, C. D. Hydrogel scaffolds for tissue engineering: The importance of polymer choice. *Polymer Chemistry* **2020,** *11* (2), 184-219.

(84) Demirtaş, T. T.; Irmak, G.; Gümüşderelioğlu, M. A bioprintable form of chitosan hydrogel for bone tissue engineering. *Biofabrication* **2017,** *9* (3), 035003.

(85) Zhu, J.; Marchant, R. E. Design properties of hydrogel tissue-engineering scaffolds. *Expert review of medical devices* **2011,** *8* (5), 607-626.

(86) Cheng, T.-Y.; Chen, M.-H.; Chang, W.-H.; Huang, M.-Y.; Wang, T.-W. Neural stem cells encapsulated in a functionalized self-assembling peptide hydrogel for brain tissue engineering. *Biomaterials* **2013,** *34* (8), 2005-2016.

(87) Burdick, J. A.; Anseth, K. S. Photoencapsulation of osteoblasts in injectable RGD-modified PEG hydrogels for bone tissue engineering. *Biomaterials* **2002,** *23* (22), 4315-4323.

(88) Alsberg, E.; Anderson, K.; Albeiruti, A.; Franceschi, R.; Mooney, D. Cell-interactive alginate hydrogels for bone tissue engineering. *Journal of dental research* **2001,** *80* (11), 2025-2029.

(89) Place, E. S.; Rojo, L.; Gentleman, E.; Sardinha, J. P.; Stevens, M. M. Strontium-and zinc-alginate hydrogels for bone tissue engineering. *Tissue Engineering Part A* **2011,** *17* (21-22), 2713-2722.

(90) Santos-Cancel, M.; Simpson, L. W.; Leach, J. B.; White, R. J. Direct, real-time detection of adenosine triphosphate release from astrocytes in three-dimensional culture using an integrated electrochemical aptamer-based sensor. *ACS chemical neuroscience* **2019,** *10* (4), 2070-2079.

(91) Shih, Y.-R. V.; Hwang, Y.; Phadke, A.; Kang, H.; Hwang, N. S.; Caro, E. J.; Nguyen, S.; Siu, M.; Theodorakis, E. A.; Gianneschi, N. C. Calcium phosphate-bearing matrices induce osteogenic differentiation of stem cells through adenosine signaling. *Proceedings of the National Academy of Sciences* **2014,** *111* (3), 990-995.

(92) Latifi, N.; Asgari, M.; Vali, H.; Mongeau, L. A tissue-mimetic nano-fibrillar hybrid injectable hydrogel for potential soft tissue engineering applications. *Scientific reports* **2018,** *8* (1), 1-18.

(93) Jahan, K.; Mekhail, M.; Tabrizian, M. One-step fabrication of apatite-chitosan scaffold as a potential injectable construct for bone tissue engineering. *Carbohydrate polymers* **2019,** *203*, 60-70.

(94) Marler, J. J.; Upton, J.; Langer, R.; Vacanti, J. P. Transplantation of cells in matrices for tissue regeneration. *Advanced drug delivery reviews* **1998,** *33* (1-2), 165-182.

(95) Qu, J.; Zhao, X.; Liang, Y.; Zhang, T.; Ma, P. X.; Guo, B. Antibacterial adhesive injectable hydrogels with rapid self-healing, extensibility and compressibility as wound dressing for joints skin wound healing. *Biomaterials* **2018,** *183*, 185-199.

(96) Yang, C.; Xu, L.; Zhou, Y.; Zhang, X.; Huang, X.; Wang, M.; Han, Y.; Zhai, M.; Wei, S.; Li, J. A green fabrication approach of gelatin/CM-chitosan hybrid hydrogel for wound healing. *Carbohydrate polymers* **2010,** *82* (4), 1297-1305.

(97) Li, Y.; Fukushima, K.; Coady, D. J.; Engler, A. C.; Liu, S.; Huang, Y.; Cho, J. S.; Guo, Y.; Miller, L. S.; Tan, J. P. Broad‐spectrum antimicrobial and biofilm‐disrupting hydrogels: stereocomplex‐driven supramolecular assemblies. *Angewandte Chemie International Edition* **2013,** *52* (2), 674-678.

(98) Li, L.; Yan, B.; Yang, J.; Huang, W.; Chen, L.; Zeng, H. Injectable Self-Healing Hydrogel with Antimicrobial and Antifouling Properties. *ACS Appl. Mater. Interfaces.* **2017,** *9* (11), 9221-9225, DOI: 10.1021/acsami.6b16192.

(99) Vashist, A.; Vashist, A.; Gupta, Y.; Ahmad, S. Recent advances in hydrogel based drug delivery systems for the human body. *Journal of Materials Chemistry B* **2014,** *2* (2), 147-166.

(100) Peppas, N. A. Hydrogels and drug delivery. *Current opinion in colloid interface science* **1997,** *2* (5), 531-537.

(101) Rizwan, M.; Yahya, R.; Hassan, A.; Yar, M.; Azzahari, A. D.; Selvanathan, V.; Sonsudin, F.; Abouloula, C. N. pH sensitive hydrogels in drug delivery: Brief history, properties, swelling, and release mechanism, material selection and applications. *Polymers* **2017,** *9* (4), 137.

(102) Rasool, N.; Yasin, T.; Heng, J. Y.; Akhter, Z. Synthesis and characterization of novel pH-, ionic strength and temperature-sensitive hydrogel for insulin delivery. *Polymer Chemistry* **2010,** *51* (8), 1687-1693.

(103) Demirdirek, B.; Uhrich, K. E. Salicylic acid-based pH-sensitive hydrogels as potential oral insulin delivery systems. *Journal of Drug Targeting* **2015,** *23* (7-8), 716-724.

(104) Mitragotri, S.; Burke, P. A.; Langer, R. Overcoming the challenges in administering biopharmaceuticals: formulation and delivery strategies. *Nature reviews Drug discovery* **2014,** *13* (9), 655-672.

(105) Langer, R. Drug delivery and targeting. *Nature communications* **1998,** *392* (6679 Suppl), 5-10.

(106) Storrie, H.; Mooney, D. J. Sustained delivery of plasmid DNA from polymeric scaffolds for tissue engineering. *Advanced drug delivery reviews* **2006,** *58* (4), 500-514.

(107) Duncan, R. The dawning era of polymer therapeutics. *Nature reviews Drug discovery* **2003,** *2* (5), 347-360.

(108) Ashraf, S.; Park, H.-K.; Park, H.; Lee, S.-H. Snapshot of phase transition in thermoresponsive hydrogel PNIPAM: Role in drug delivery and tissue engineering. *Macromolecular Research* **2016,** *24* (4), 297-304.

(109) Ramanan, R. M. K.; Chellamuthu, P.; Tang, L.; Nguyen, K. T. J. B. p. Development of a temperature‐sensitive composite hydrogel for drug delivery applications. **2006,** *22* (1), 118-125.

(110) Cao, M.; Wang, Y.; Hu, X.; Gong, H.; Li, R.; Cox, H.; Zhang, J.; Waigh, T. A.; Xu, H.; Lu, J. R. Reversible thermoresponsive peptide–PNIPAM hydrogels for controlled drug delivery. *Biomacromolecules* **2019,** *20* (9), 3601-3610.

(111) Kwon, S. S.; Kong, B. J.; Park, S. N. Physicochemical properties of pH-sensitive hydrogels based on hydroxyethyl cellulose–hyaluronic acid and for applications as transdermal delivery systems for skin lesions. *European journal of pharmaceutics biopharmaceutics* **2015,** *92*, 146-154.

(112) Ruan, C.; Zeng, K.; Varghese, O. K.; Grimes, C. A. A magnetoelastic bioaffinity-based sensor for avidin. *Biosensors Bioelectronics* **2004,** *19* (12), 1695-1701.

(113) Hsu, M. N.; Wei, S. C.; Guo, S.; Phan, D. T.; Zhang, Y.; Chen, C. H. Smart hydrogel microfluidics for single‐cell multiplexed secretomic analysis with high sensitivity. *Small* **2018,** *14* (49), 1802918.

(114) Tavakoli, J.; Tang, Y. Hydrogel based sensors for biomedical applications: An updated review. *Polymers* **2017,** *9* (8), 364.

(115) Grieshaber, D.; MacKenzie, R.; Vörös, J.; Reimhult, E. Electrochemical biosensors-sensor principles and architectures. *Sensors* **2008,** *8* (3), 1400-1458.

(116) Naresh, V.; Lee, N. J. S. A review on biosensors and recent development of nanostructured materials-enabled biosensors. **2021,** *21* (4), 1109.

(117) Sing, C. E.; Perry, S. L. Recent progress in the science of complex coacervation. *Soft Matter* **2020,** *16* (12), 2885-2914.

(118) Kizilay, E.; Kayitmazer, A. B.; Dubin, P. L. Complexation and coacervation of polyelectrolytes with oppositely charged colloids. *Advances in colloid interface science* **2011,** *167* (1-2), 24-37.

(119) Kelly, K. D.; Schlenoff, J. B. Spin-coated polyelectrolyte coacervate films. *ACS applied materials interfaces* **2015,** *7* (25), 13980-13986.

(120) Thomson, J. A.; Schurtenberger, P.; Thurston, G. M.; Benedek, G. B. Binary liquid phase separation and critical phenomena in a protein/water solution. *Proceedings of the National Academy of Sciences* **1987,** *84* (20), 7079-7083.

(121) Dompé, M.; Cedano‐Serrano, F. J.; Heckert, O.; van den Heuvel, N.; van der Gucht, J.; Tran, Y.; Hourdet, D.; Creton, C.; Kamperman, M. Thermoresponsive Complex Coacervate‐Based Underwater Adhesive. *Advanced Materials* **2019,** *31* (21), 1808179.

(122) Chang, L.-W.; Lytle, T. K.; Radhakrishna, M.; Madinya, J. J.; Vélez, J.; Sing, C. E.; Perry, S. L. Sequence and entropy-based control of complex coacervates. *Nature communications* **2017,** *8* (1), 1-8.

(123) Okesola, B. O.; Smith, D. K. Applying low-molecular weight supramolecular gelators in an environmental setting–self-assembled gels as smart materials for pollutant removal. *Chemical Society Reviews* **2016,** *45* (15), 4226-4251.

(124) Peng, Q.; Chen, J.; Wang, T.; Gong, L.; Peng, X.; Wu, M.; Ma, Y.; Wu, F.; Yang, D.; Zhang, H. Coacervation-driven instant paintable underwater adhesives with tunable optical and electrochromic properties. *Journal of Materials Chemistry A* **2021,** *9* (22), 12988-13000.

(125) Wang, A.; Wang, Y.; Zhang, B.; Wan, K.; Zhu, J.; Xu, J.; Zhang, C.; Liu, T. Hydrogen-bonded network enables semi-interpenetrating ionic conductive hydrogels with high stretchability and excellent fatigue resistance for capacitive/resistive bimodal sensors. *Chemical Engineering Journal* **2021,** *411*, 128506.

(126) Fan, H.; Wang, J.; Tao, Z.; Huang, J.; Rao, P.; Kurokawa, T.; Gong, J. P. Adjacent cationic–aromatic sequences yield strong electrostatic adhesion of hydrogels in seawater. *Nature communications* **2019,** *10* (1), 1-8.

(127) Lee, J. N.; Lee, S. Y.; Park, W. H. Bioinspired self-healable polyallylamine-based hydrogels for wet adhesion: synergistic contributions of catechol-amino functionalities and nanosilicate. *ACS Applied Materials Interfaces* **2021,** *13* (15), 18324-18337.

(128) Appel, E. A.; del Barrio, J.; Loh, X. J.; Scherman, O. A. Supramolecular polymeric hydrogels. *Chemical Society Reviews* **2012,** *41* (18), 6195-6214.

(129) Balu, R.; Dutta, N. K.; Dutta, A. K.; Choudhury, N. R. Resilin-mimetics as a smart biomaterial platform for biomedical applications. *Nature Communications* **2021,** *12* (1), 1-15.

(130) Wu, G.; Schöler, H. R. Role of Oct4 in the early embryo development. *Cell Regeneration* **2014,** *3* (1), 1-10.

(131) Chen, Y.-N.; Peng, L.; Liu, T.; Wang, Y.; Shi, S.; Wang, H. Poly (vinyl alcohol)–tannic acid hydrogels with excellent mechanical properties and shape memory behaviors. *ACS applied materials interfaces* **2016,** *8* (40), 27199-27206.

(132) Xu, Y.; Rothe, R.; Voigt, D.; Hauser, S.; Cui, M.; Miyagawa, T.; Patino Gaillez, M.; Kurth, T.; Bornhäuser, M.; Pietzsch, J. Convergent synthesis of diversified reversible network leads to liquid metal-containing conductive hydrogel adhesives. *Nature communications* **2021,** *12* (1), 1-19.

(133) Ejima, H.; Richardson, J. J.; Liang, K.; Best, J. P.; van Koeverden, M. P.; Such, G. K.; Cui, J.; Caruso, F. One-step assembly of coordination complexes for versatile film and particle engineering. *Science* **2013,** *341* (6142), 154-157.

(134) Fan, H.; Wang, J.; Zhang, Q.; Jin, Z. Tannic acid-based multifunctional hydrogels with facile adjustable adhesion and cohesion contributed by polyphenol supramolecular chemistry. *ACS omega* **2017,** *2* (10), 6668-6676.

(135) Fan, H.; Wang, L.; Feng, X.; Bu, Y.; Wu, D.; Jin, Z. Supramolecular hydrogel formation based on tannic acid. *Macromolecules* **2017,** *50* (2), 666-676.

(136) Björnmalm, M.; Wong, L. M.; Wojciechowski, J. P.; Penders, J.; Horgan, C. C.; Booth, M. A.; Martin, N. G.; Sattler, S.; Stevens, M. M. In vivo biocompatibility and

immunogenicity of metal–phenolic gelation. *Chemical science* **2019,** *10* (43), 10179-10194.

(137) Kaczmarek, B.; Mazur, O.; Miłek, O.; Michalska-Sionkowska, M.; Osyczka, A. M.; Kleszczyński, K. Development of tannic acid-enriched materials modified by poly (ethylene glycol) for potential applications as wound dressing. *Progress in biomaterials* **2020,** *9* (3), 115-123.

(138) Chen, C.; Geng, X.-w.; Pan, Y.-h.; Ma, Y.-n.; Ma, Y.-x.; Gao, S.-z.; Huang, X.-j. Synthesis and characterization of tannic acid–PEG hydrogel via Mitsunobu polymerization. *RSC advances* **2020,** *10* (3), 1724-1732.

(139) Zhang, D.; Xu, Z.; Li, H.; Fan, C.; Cui, C.; Wu, T.; Xiao, M.; Yang, Y.; Yang, J.; Liu, W. Fabrication of strong hydrogen-bonding induced coacervate adhesive hydrogels with antibacterial and hemostatic activities. *Biomaterials science* **2020,** *8* (5), 1455-1463.

(140) Nam, H. G.; Nam, M. G.; Yoo, P. J.; Kim, J.-H. Hydrogen bonding-based strongly adhesive coacervate hydrogels synthesized using poly (N-vinylpyrrolidone) and tannic acid. *Soft Matter* **2019,** *15* (4), 785-791.

(141) Pawlaczyk, M.; Schroeder, G. Dual-Polymeric Resin Based on Poly (methyl vinyl ether-alt-maleic anhydride) and PAMAM Dendrimer as a Versatile Supramolecular Adsorbent. *ACS Applied Polymer Materials* **2021,** *3* (2), 956-967.

(142) Stewart, S. A.; Backholm, M.; Burke, N. A.; Stöver, H. D. Cross-linked hydrogels formed through Diels–Alder coupling of furan-and maleimide-modified poly (methyl vinyl ether-alt-maleic acid). *Langmuir* **2016,** *32* (7), 1863-1870.

(143) Caló, E.; de Barros, J. M.; Fernández-Gutiérrez, M.; San Román, J.; Ballamy, L.; Khutoryanskiy, V. V. Antimicrobial hydrogels based on autoclaved poly (vinyl alcohol) and poly (methyl vinyl ether-alt-maleic anhydride) mixtures for wound care applications. *Rsc Advances* **2016,** *6* (60), 55211-55219.

(144) Baker, M. I.; Walsh, S. P.; Schwartz, Z.; Boyan, B. D. A review of polyvinyl alcohol and its uses in cartilage and orthopedic applications. *Journal of Biomedical Materials Research Part B: Applied Biomaterials* **2012,** *100* (5), 1451-1457.

(145) Sileika, T. S.; Barrett, D. G.; Zhang, R.; Lau, K. H. A.; Messersmith, P. B. Colorless multifunctional coatings inspired by polyphenols found in tea, chocolate, and wine. *Angewandte Chemie* **2013,** *125* (41), 10966-10970.

(146) Arbós, P.; Wirth, M.; Arangoa, M.; Gabor, F.; Irache, J. Gantrez® AN as a new polymer for the preparation of ligand–nanoparticle conjugates. *Journal of controlled release* **2002,** *83* (3), 321-330.

(147) Torres-Figueroa, A. V.; Pérez-Martínez, C. J.; Encinas, J. C.; Burruel-Ibarra, S.; Silvas-García, M. I.; García Alegría, A. M.; del Castillo-Castro, T. Thermosensitive Bioadhesive Hydrogels Based on Poly (N-isopropylacrilamide) and Poly (methyl vinyl ether-alt-maleic anhydride) for the Controlled Release of Metronidazole in the Vaginal Environment. *Pharmaceutics* **2021,** *13* (8), 1284.

(148) Larrañeta, E.; Barturen, L.; Ervine, M.; Donnelly, R. F. Hydrogels based on poly (methyl vinyl ether-co-maleic acid) and Tween 85 for sustained delivery of hydrophobic drugs. *International journal of pharmaceutics* **2018,** *538* (1-2), 147-158.

(149) Feng, X.; Hou, X.; Cui, C.; Sun, S.; Sadik, S.; Wu, S.; Zhou, F. Mechanical and antibacterial properties of tannic acid-encapsulated carboxymethyl chitosan/polyvinyl alcohol hydrogels. *Engineered Regeneration* **2021,** *2*, 57-62.

(150) Yang, J.; Li, M.; Wang, Y.; Wu, H.; Zhen, T.; Xiong, L.; Sun, Q. Double cross-linked chitosan composite films developed with oxidized tannic acid and ferric ions exhibit high strength and excellent water resistance. *Biomacromolecules* **2019,** *20* (2), 801-812.

(151) Wang, Z.; Zhang, S.; Zhao, S.; Kang, H.; Wang, Z.; Xia, C.; Yu, Y.; Li, J. Facile biomimetic self-coacervation of tannic acid and polycation: Tough and wide pH range of underwater adhesives. *Chemical Engineering Journal* **2021,** *404*, 127069.

(152) Kim, K.; Shin, M.; Koh, M. Y.; Ryu, J. H.; Lee, M. S.; Hong, S.; Lee, H. TAPE: A medical adhesive inspired by a ubiquitous compound in plants. *Advanced Functional Materials* **2015,** *25* (16), 2402-2410.

(153) Friedman, M.; Jürgens, H. S. Effect of pH on the stability of plant phenolic compounds. *Journal of agricultural food chemistry* **2000,** *48* (6), 2101-2110.

(154) Weber, F.; Sagstuen, E.; Zhong, Q.-Z.; Zheng, T.; Tiainen, H. Tannic acid radicals in the presence of alkali metal salts and their impact on the formation of silicate-phenolic networks. *ACS applied materials interfaces* **2020,** *12* (47), 52457-52466.

(155) Osawa, R.; Walsh, T. P. Effects of acidic and alkaline treatments on tannic acid and its binding property to protein. *Journal of Agricultural Food Chemistry* **1993,** *41* (5), 704-707.

(156) Sun, J.-Y.; Zhao, X.; Illeperuma, W. R.; Chaudhuri, O.; Oh, K. H.; Mooney, D. J.; Vlassak, J. J.; Suo, Z. Highly stretchable and tough hydrogels. *Nature communications* **2012,** *489* (7414), 133-136.

(157) Chen, Y.-N.; Jiao, C.; Zhao, Y.; Zhang, J.; Wang, H. Self-assembled polyvinyl alcohol–tannic acid hydrogels with diverse microstructures and good mechanical properties. *ACS omega* **2018,** *3* (9), 11788-11795.

(158) Wang, C.; Zhou, H.; Niu, H.; Ma, X.; Yuan, Y.; Hong, H.; Liu, C. Tannic acid-loaded mesoporous silica for rapid hemostasis and antibacterial activity. *Biomaterials science* **2018,** *6* (12), 3318-3331.

(159) Pandey, A.; Negi, P. S. Phytochemical composition, in vitro antioxidant activity and antibacterial mechanisms of Neolamarckia cadamba fruits extracts. *Natural product research* **2018,** *32* (10), 1189-1192.

(160) Kaczmarek, B. Tannic acid with antiviral and antibacterial activity as a promising component of biomaterials—A minireview. *Materials* **2020,** *13* (14), 3224.

(161) Iqbal, M. H.; Schroder, A.; Kerdjoudj, H.; Njel, C.; Senger, B.; Ball, V.; Meyer, F.; Boulmedais, F. Effect of the buffer on the buildup and stability of tannic acid/collagen multilayer films applied as antibacterial coatings. *ACS applied materials interfaces* **2020,** *12* (20), 22601-22612.

(162) Zhao, L.; Wang, K.; Wei, W.; Wang, L.; Han, W. High‐performance flexible sensing devices based on polyaniline/MXene nanocomposites. *InfoMat* **2019,** *1* (3), 407-416.

(163) Liu, Y.; Pharr, M.; Salvatore, G. A. Lab-on-skin: a review of flexible and stretchable electronics for wearable health monitoring. *ACS Nano* **2017,** *11* (10), 9614-9635.

(164) Kang, J.; Son, D.; Wang, G. J. N.; Liu, Y.; Lopez, J.; Kim, Y.; Oh, J. Y.; Katsumata, T.; Mun, J.; Lee, Y. Tough and water‐insensitive self‐healing elastomer for robust electronic skin. *Advanced Materials* **2018,** *30* (13), 1706846.

(165) Dahiya, R.; Yogeswaran, N.; Liu, F.; Manjakkal, L.; Burdet, E.; Hayward, V.; Jörntell, H. Large-area soft e-skin: The challenges beyond sensor designs. *Proceedings of the IEEE* **2019,** *107* (10), 2016-2033.

(166) Zhong, J.; Ma, Y.; Song, Y.; Zhong, Q.; Chu, Y.; Karakurt, I.; Bogy, D. B.; Lin, L. A flexible piezoelectret actuator/sensor patch for mechanical human–machine interfaces. *ACS Nano* **2019,** *13* (6), 7107-7116.

(167) Han, X.; Lv, Z.; Ran, F.; Dai, L.; Li, C.; Si, C. Green and stable piezoresistive pressure sensor based on lignin-silver hybrid nanoparticles/polyvinyl alcohol hydrogel. *International Journal of Biological Macromolecules* **2021,** *176*, 78-86.

(168) Wang, S.; Li, Q.; Wang, B.; Hou, Y.; Zhang, T. Recognition of different rough surface based highly sensitive silver nanowire-graphene flexible hydrogel skin. *Industrial Engineering Chemistry Research* **2019,** *58* (47), 21553-21561.

(169) Liao, M.; Liao, H.; Ye, J.; Wan, P.; Zhang, L. Polyvinyl alcohol-stabilized liquid metal hydrogel for wearable transient epidermal sensors. *ACS applied materials interfaces* **2019,** *11* (50), 47358-47364.

(170) Liu, Q.; Zhang, M.; Huang, L.; Li, Y.; Chen, J.; Li, C.; Shi, G. High-quality graphene ribbons prepared from graphene oxide hydrogels and their application for strain sensors. *ACS Nano* **2015,** *9* (12), 12320-12326.

(171) Zhang, Y.; Chen, K.; Li, Y.; Lan, J.; Yan, B.; Shi, L.; Ran, R. J. A. a. m.; interfaces. High-strength, self-healable, temperature-sensitive, MXene-containing composite hydrogel as a smart compression sensor. *ACS applied materials interfaces* **2019,** *11* (50), 47350-47357.

(172) Hsiao, L.-Y., Lin Jing, Kerui Li, Haitao Yang, Yang Li, and Po-Yen Chen. Carbon nanotube-integrated conductive hydrogels as multifunctional robotic skin. *Carbon* **2020,** *161*, 784-793.

(173) Liao, M.; Wan, P.; Wen, J.; Gong, M.; Wu, X.; Wang, Y.; Shi, R.; Zhang, L. Wearable, healable, and adhesive epidermal sensors assembled from mussel‐inspired conductive hybrid hydrogel framework. *Advanced Functional Materials* **2017,** *27* (48), 1703852.

(174) Liu, Z.; Wang, Y.; Ren, Y.; Jin, G.; Zhang, C.; Chen, W.; Yan, F. Poly (ionic liquid) hydrogel-based anti-freezing ionic skin for a soft robotic gripper. *Materials Horizons* **2020,** *7* (3), 919-927.

(175) Wei, D.; Wang, H.; Zhu, J.; Luo, L.; Huang, H.; Li, L.; Yu, X. Highly Stretchable, Fast Self‐Healing, Responsive Conductive Hydrogels for Supercapacitor Electrode and Motion Sensor. *Macromolecular Materials Engineering* **2020,** *305* (5), 2000018.

(176) Chen, J.; Peng, Q.; Thundat, T.; Zeng, H. Stretchable, Injectable and Self-Healing Conductive Hydrogel Enabled by Multiple Hydrogen Bonding toward Wearable Electronics. *Chemistry of Materials* **2019**.

(177) Li, Y.; Liu, C.; Lv, X.; Sun, S. A highly sensitive strain sensor based on a silica@ polyaniline core–shell particle reinforced hydrogel with excellent flexibility, stretchability, toughness and conductivity. *Soft Matter* **2021,** *17* (8), 2142-2150.

(178) Peng, Y.; Yan, B.; Li, Y.; Lan, J.; Shi, L.; Ran, R. Antifreeze and moisturizing high conductivity PEDOT/PVA hydrogels for wearable motion sensor. *Journal of Materials Science* **2020,** *55* (3), 1280-1291.

(179) Han, L.; Yan, L.; Wang, M.; Wang, K.; Fang, L.; Zhou, J.; Fang, J.; Ren, F.; Lu, X. Transparent, adhesive, and conductive hydrogel for soft bioelectronics based on light-transmitting polydopamine-doped polypyrrole nanofibrils. *Chemistry of Materials* **2018,** *30* (16), 5561-5572.

(180) Cheng, Y.; Ren, X.; Duan, L.; Gao, G. A transparent and adhesive carboxymethyl cellulose/polypyrrole hydrogel electrode for flexible supercapacitors. *Journal of Materials Chemistry C* **2020,** *8* (24), 8234-8242.

(181) Fang, Y.; Xu, J.; Gao, F.; Du, X.; Du, Z.; Cheng, X.; Wang, H. Self-healable and recyclable polyurethane-polyaniline hydrogel toward flexible strain sensor. *Composites Part B: Engineering* **2021,** *219*, 108965.

(182) Yang, Z.; Ma, J.; Bai, B.; Qiu, A.; Losic, D.; Shi, D.; Chen, M. Free-standing PEDOT/polyaniline conductive polymer hydrogel for flexible solid-state supercapacitors. *Electrochimica Acta* **2019,** *322*, 134769.

(183) Dou, P.; Liu, Z.; Cao, Z.; Zheng, J.; Wang, C.; Xu, X. Rapid synthesis of hierarchical nanostructured Polyaniline hydrogel for high power density energy storage application and three-dimensional multilayers printing. *Journal of Materials Science* **2016,** *51* (9), 4274-4282.

(184) Puiggalí-Jou, A.; Babeli, I.; Roa, J. J.; Zoppe, J. O.; Garcia-Amoros, J.; Ginebra, M.-P.; Aleman, C.; García-Torres. Remote Spatiotemporal Control of a Magnetic and Electroconductive Hydrogel Network via Magnetic Fields for Soft Electronic Applications. **2021,** *13* (36), 42486-42501.

(185) Wang, J.-J.; Zhang, Q.; Ji, X.-X.; Liu, L.-B. Highly stretchable, compressible, adhesive, conductive self-healing composite hydrogels with sensor capacity. *Chinese Journal of Polymer Science* **2020,** *38* (11), 1221-1229.

(186) Wu, J.; Han, S.; Yang, T.; Li, Z.; Wu, Z.; Gui, X.; Tao, K.; Miao, J.; Norford, L. K.; Liu, C. Highly stretchable and transparent thermistor based on self-healing double network hydrogel. *ACS applied materials & interfaces* **2018,** *10* (22), 19097-19105.

(187) Liu, S.; Li, L. Ultrastretchable and self-healing double-network hydrogel for 3D printing and strain sensor. *ACS applied materials interfaces* **2017,** *9* (31), 26429-26437.

(188) Yang, B.; Yuan, W. Highly stretchable and transparent double-network hydrogel ionic conductors as flexible thermal–mechanical dual sensors and electroluminescent devices. *ACS applied materials interfaces* **2019,** *11* (18), 16765-16775.

(189) Imato, K.; Nishihara, M.; Kanehara, T.; Amamoto, Y.; Takahara, A.; Otsuka, H. Self‐healing of chemical gels cross‐linked by diarylbibenzofuranone‐based trigger‐free dynamic covalent bonds at room temperature. *Angewandte Chemie* **2012,** *124* (5), 1164-1168.

(190) Wang, Q.; He, W.; Huang, J.; Liu, S.; Wu, G.; Teng, W.; Wang, Q.; Dong, Y. Synthesis of water soluble, biodegradable, and electroactive polysaccharide crosslinker with aldehyde and carboxylic groups for biomedical applications. *Macromolecular bioscience* **2011,** *11* (3), 362-372.

(191) Wu, M.; Chen, J.; Ma, Y.; Yan, B.; Pan, M.; Peng, Q.; Wang, W.; Han, L.; Liu, J.; Zeng, H. Ultra elastic, stretchable, self-healing conductive hydrogels with tunable optical properties for highly sensitive soft electronic sensors. *Journal of Materials Chemistry A* **2020,** *8* (46), 24718-24733.

(192) Phadke, A.; Zhang, C.; Arman, B.; Hsu, C.-C.; Mashelkar, R. A.; Lele, A. K.; Tauber, M. J.; Arya, G.; Varghese, S. Rapid self-healing hydrogels. *Proceedings of the National Academy of Sciences* **2012,** *109* (12), 4383-4388.

(193) Zhang, G.; Ngai, T.; Deng, Y.; Wang, C. An Injectable Hydrogel with Excellent Self‐Healing Property Based on Quadruple Hydrogen Bonding. *Macromolecular Chemistry Physics* **2016,** *217* (19), 2172-2181.

(194) Chen, J.; Wang, D.; Wang, L. H.; Liu, W.; Chiu, A.; Shariati, K.; Liu, Q.; Wang, X.; Zhong, Z.; Webb, J. An adhesive hydrogel with “Load‐Sharing” effect as tissue bandages for drug and cell delivery. *Advanced Materials* **2020,** *32* (43), 2001628.

(195) Li, Z.; Lu, W.; Ngai, T.; Le, X.; Zheng, J.; Zhao, N.; Huang, Y.; Wen, X.; Zhang, J.; Chen, T. Mussel-inspired multifunctional supramolecular hydrogels with self-healing, shape memory and adhesive properties. *Polymer Chemistry* **2016,** *7* (34), 5343-5346.

(196) Li, L.; Yan, B.; Yang, J.; Chen, L.; Zeng, H. Novel mussel‐inspired injectable self‐healing hydrogel with anti‐biofouling property. *Advanced Materials* **2015,** *27* (7), 1294-1299.

(197) Zhang, P.; Tang, A.; Zhu, B.; Zhu, L.; Zeng, H. Hierarchical Self‐Assembly of Dopamine into Patterned Structures. *Advanced Materials Interfaces* **2017,** *4* (11), 1601218.

(198) Shan, M.; Gong, C.; Li, B.; Wu, G. J. P. C. A pH, glucose, and dopamine triple-responsive, self-healable adhesive hydrogel formed by phenylborate–catechol complexation. *Polymer Chemistry* **2017,** *8* (19), 2997-3005.

(199) Wang, Y.; Yang, X.; Nian, G.; Suo, Z. Strength and toughness of adhesion of soft materials measured in lap shear. *Journal of the Mechanics Physics of Solids* **2020,** *143*, 103988.

(200) Liu, Y.-J.; Cao, W.-T.; Ma, M.-G.; Wan, P. J. A. a. m.; interfaces. Ultrasensitive wearable soft strain sensors of conductive, self-healing, and elastic hydrogels with synergistic "soft and hard" hybrid networks. *ACS applied materials interfaces* **2017,** *9* (30), 25559-25570.

(201) Lu, Y.; Qu, X.; Zhao, W.; Ren, Y.; Si, W.; Wang, W.; Wang, Q.; Huang, W.; Dong, X. Highly stretchable, elastic, and sensitive MXene-based hydrogel for flexible strain and pressure sensors. *Research* **2020,** *2020*.

(202) Holloway, J. L.; Lowman, A. M.; Palmese, G. R. The role of crystallization and phase separation in the formation of physically cross-linked PVA hydrogels. *Soft Matter* **2013,** *9* (3), 826-833.

(203) Shahi, S.; Roghani-Mamaqani, H.; Hoogenboom, R.; Talebi, S.; Mardani, H. Stimuli-Responsive Covalent Adaptable Hydrogels Based on Homolytic Bond Dissociation and Chain Transfer Reactions. *Chemistry of Materials* **2022**.

(204) Sun, M.; Qiu, J.; Jin, S.; Liu, W.; Sakai, E. J. C.; Physicochemical, S. A.; Aspects, E. Visible light induced synthesis of high toughness, self-healing ionic hydrogel and its application in strain sensing. *Colloids Surfaces A: Physicochemical Engineering Aspects* **2020,** *607*, 125438.

(205) Tseng, Y.; Lin, Y.; Shih, C.; Hsieh, H.; Lee, W.; Chiu, Y.; Chen, W. Morphology and properties of PEDOT: PSS/soft polymer blends through hydrogen bonding interaction and their pressure sensor application. *Journal of Materials Chemistry C* **2020,** *8* (18), 6013-6024.

(206) Zhang, L.; Zhao, J.; Zhu, J.; He, C.; Wang, H. Anisotropic tough poly (vinyl alcohol) hydrogels. *Soft Matter* **2012,** *8* (40), 10439-10447.

(207) Tie, J.; Rong, L.; Liu, H.; Wang, B.; Mao, Z.; Zhang, L.; Zhong, Y.; Feng, X.; Sui, X.; Xu, H. An autonomously healable, highly stretchable and cyclically compressible, wearable hydrogel as a multimodal sensor. *Polymer Chemistry* **2020,** *11* (7), 1327-1336.

(208) Wu, Y.; Ouyang, T.; Xiong, T.; Jiang, Z.; Hu, Y.; Deng, J.; Wang, Z.; Huang, Y.; Balogun, M. S. Boosted Storage Kinetics in Thick Hierarchical Micro–Nano Carbon Architectures for High Areal Capacity Li‐Ion Batteries. *Energy Environmental Materials* **2021**.

(209) Wang, M.; Chen, Y.; Khan, R.; Liu, H.; Chen, C.; Chen, T.; Zhang, R.; Li, H. A fast self-healing and conductive nanocomposite hydrogel as soft strain sensor. *Colloids Surfaces A: Physicochemical Engineering Aspects* **2019,** *567*, 139-149.

(210) Zhang, Q.; Liu, X.; Duan, L.; Gao, G. Ultra-stretchable wearable strain sensors based on skin-inspired adhesive, tough and conductive hydrogels. *Chemical Engineering Journal* **2019,** *365*, 10-19.

(211) Sun, X.; Qin, Z.; Ye, L.; Zhang, H.; Yu, Q.; Wu, X.; Li, J.; Yao, F. Carbon nanotubes reinforced hydrogel as flexible strain sensor with high stretchability and mechanically toughness. *Chemical Engineering Journal* **2020,** *382*, 122832.

(212) Frutiger, A.; Muth, J. T.; Vogt, D. M.; Mengüç, Y.; Campo, A.; Valentine, A. D.; Walsh, C. J.; Lewis, J. A. Capacitive soft strain sensors via multicore–shell fiber printing. *Advanced Materials* **2015,** *27* (15), 2440-2446.

(213) Lei, H.; Zhao, J.; Ma, X.; Li, H.; Fan, D. Antibacterial Dual Network Hydrogels for Sensing and Human Health Monitoring. *Advanced Healthcare Materials* **2021,** *10* (21), 2101089.

(214) Cheng, B.; Li, Y.; Li, H.; Li, H.; Yang, S.; Li, P.; Shang, Y. An adhesive and self-healable hydrogel with high stretchability and compressibility for human motion detection. *Composites Science and Technology* **2021,** *213*, 108948.

(215) Ling, Q.; Ke, T.; Liu, W.; Ren, Z.; Zhao, L.; Gu, H. Tough, Repeatedly Adhesive, Cyclic Compression-Stable, and Conductive Dual-Network Hydrogel Sensors for Human Health Monitoring. *Industrial and Engineering Chemistry Research* **2021**.

(216) Zhou, Z.; He, Z.; Yin, S.; Xie, X.; Yuan, W. Adhesive, stretchable and antibacterial hydrogel with external/self-power for flexible sensitive sensor used as human motion detection. *Composites Part B: Engineering* **2021,** *220*, 108984.

(217) Song, H.; Sun, Y.; Zhu, J.; Xu, J.; Zhang, C.; Liu, T. Hydrogen-bonded network enables polyelectrolyte complex hydrogels with high stretchability, excellent fatigue resistance and self-healability for human motion detection. *Composites Part B: Engineering* **2021,** *217*, 108901.

(218) Jin, R.; Xu, J.; Duan, L.; Gao, G. Chitosan-driven skin-attachable hydrogel sensors toward human motion and physiological signal monitoring. *Carbohydrate Polymers* **2021**, 118240.

(219) He, F.; You, X.; Gong, H.; Yang, Y.; Bai, T.; Wang, W.; Guo, W.; Liu, X.; Ye, M. Stretchable, biocompatible, and multifunctional silk fibroin-based hydrogels toward wearable strain/pressure sensors and triboelectric nanogenerators. *ACS applied materials & interfaces* **2020,** *12* (5), 6442-6450.

(220) Chortos, A.; Liu, J.; Bao, Z. Pursuing prosthetic electronic skin. *Nature materials* **2016,** *15* (9), 937-950.

(221) Shahi, S.; Roghani-Mamaqani, H.; Talebi, S.; Mardani, H. Chemical stimuli-induced reversible bond cleavage in covalently crosslinked hydrogels. *Coordination Chemistry Reviews* **2022,** *455*, 214368.

(222) Pu, X.; Liu, M.; Chen, X.; Sun, J.; Du, C.; Zhang, Y.; Zhai, J.; Hu, W.; Wang, Z. L. Ultrastretchable, transparent triboelectric nanogenerator as electronic skin for biomechanical energy harvesting and tactile sensing. *Science advances* **2017,** *3* (5), e1700015.

(223) Zhang, Y.; Jiang, M.; Zhang, Y.; Cao, Q.; Wang, X.; Han, Y.; Sun, G.; Li, Y.; Zhou, J. Novel lignin–chitosan–PVA composite hydrogel for wound dressing. *Materials Science Engineering: C* **2019,** *104*, 110002.

(224) Tottoli, E. M.; Dorati, R.; Genta, I.; Chiesa, E.; Pisani, S.; Conti, B. Skin wound healing process and new emerging technologies for skin wound care and regeneration. *Pharmaceutics* **2020,** *12* (8), 735.

(225) Liang, Y.; Zhao, X.; Hu, T.; Han, Y.; Guo, B. Mussel-inspired, antibacterial, conductive, antioxidant, injectable composite hydrogel wound dressing to promote the regeneration of infected skin. *Journal of colloid interface science* **2019,** *556*, 514-528.

(226) Dhivya, S.; Padma, V. V.; Santhini, E. Wound dressings–a review. *BioMedicine* **2015,** *5* (4), 1-5.

(227) Sood, A.; Granick, M. S.; Tomaselli, N. L. Wound dressings and comparative effectiveness data. *Advances in wound care* **2014,** *3* (8), 511-529.

(228) Stoica, A. E.; Chircov, C.; Grumezescu, A. M. Hydrogel dressings for the treatment of burn wounds: an up-to-date overview. *Materials* **2020,** *13* (12), 2853.

(229) Pan, Z.; Ye, H.; Wu, D. Recent advances on polymeric hydrogels as wound dressings. *APL bioengineering* **2021,** *5* (1), 011504.

(230) Li, L.; Yan, B.; Yang, J.; Huang, W.; Chen, L.; Zeng, H. Injectable self-healing hydrogel with antimicrobial and antifouling properties. *ACS applied materials interfaces* **2017,** *9* (11), 9221-9225.

(231) Chen, J.; Peng, Q.; Peng, X.; Zhang, H.; Zeng, H. Probing and Manipulating Noncovalent Interactions in Functional Polymeric Systems. *Chemical Reviews* **2022,** *122* (18), 14594-14678.

(232) Wang, W.; Xiang, L.; Gong, L.; Hu, W.; Huang, W.; Chen, Y.; Asha, A. B.; Srinivas, S.; Chen, L.; Narain, R. Injectable, self-healing hydrogel with tunable optical, mechanical, and antimicrobial properties. *Chemistry of Materials* **2019,** *31* (7), 2366-2376.

(233) Cheung, R. C. F.; Ng, T. B.; Wong, J. H.; Chan, W. Y. Chitosan: an update on potential biomedical and pharmaceutical applications. *Marine drugs* **2015,** *13* (8), 5156-5186.

(234) Yilmaz Atay, H. Antibacterial activity of chitosan-based systems. In *Functional chitosan*; Springer: 2019; pp 457-489.

(235) Sogias, I. A.; Williams, A. C.; Khutoryanskiy, V. V. Why is chitosan mucoadhesive? *Biomacromolecules* **2008,** *9* (7), 1837-1842.

(236) Xu, L.; Zhang, X.; Zhu, C.; Zhang, Y.; Fu, C.; Yang, B.; Tao, L.; Wei, Y. J. J. o. B. S., Polymer Edition. Nonionic polymer cross-linked chitosan hydrogel: preparation and bioevaluation. **2013,** *24* (13), 1564-1574.

(237) Rodrigues, S.; Dionísio, M.; López, C. R.; Grenha, A. Biocompatibility of chitosan carriers with application in drug delivery. *Journal of functional biomaterials* **2012,** *3* (3), 615-641.

(238) VandeVord, P. J.; Matthew, H. W.; DeSilva, S. P.; Mayton, L.; Wu, B.; Wooley, P. H. Evaluation of the biocompatibility of a chitosan scaffold in mice. *Journal of Biomedical Materials Research* **2002,** *59* (3), 585-590.

(239) Kean, T.; Thanou, M. Biodegradation, biodistribution and toxicity of chitosan. *Advanced drug delivery reviews* **2010,** *62* (1), 3-11.

(240) Mi, F.-L.; Tan, Y.-C.; Liang, H.-F.; Sung, H.-W. In vivo biocompatibility and degradability of a novel injectable-chitosan-based implant. *Biomaterials* **2002,** *23* (1), 181-191.

(241) Periayah, M. H.; Halim, A. S.; Saad, A. Z. M. Chitosan: A promising marine polysaccharide for biomedical research. *Pharmacognosy reviews* **2016,** *10* (19), 39.

(242) Goy, R. C.; Britto, D. d.; Assis, O. B. A review of the antimicrobial activity of chitosan. *Polímeros* **2009,** *19* (3), 241-247.

(243) Jeon, T. I.; Hwang, S. G.; Park, N. G.; Jung, Y. R.; Im Shin, S.; Choi, S. D.; Park, D. K. Antioxidative effect of chitosan on chronic carbon tetrachloride induced hepatic injury in rats. *Toxicology* **2003,** *187* (1), 67-73.

(244) Bernkop-Schnürch, A.; Dünnhaupt, S. Chitosan-based drug delivery systems. *European journal of pharmaceutics biopharmaceutics* **2012,** *81* (3), 463-469.

(245) Prabaharan, M.; Mano, J. Chitosan-based particles as controlled drug delivery systems. *Drug delivery* **2004,** *12* (1), 41-57.

(246) Jiménez-Gómez, C. P.; Cecilia, J. A. Chitosan: a natural biopolymer with a wide and varied range of applications. *Molecules* **2020,** *25* (17), 3981.

(247) Chen, C.; Liu, Y.; Wang, H.; Chen, G.; Wu, X.; Ren, J.; Zhang, H.; Zhao, Y. Multifunctional chitosan inverse opal particles for wound healing. *ACS Nano.* **2018,** *12* (10), 10493-10500.

(248) Myung, D.; Waters, D.; Wiseman, M.; Duhamel, P. E.; Noolandi, J.; Ta, C. N.; Frank, C. W. Progress in the development of interpenetrating polymer network hydrogels. *Polymers for advanced technologies* **2008,** *19* (6), 647-657.

(249) Sahiner, N.; Godbey, W.; McPherson, G. L.; John, V. T. Microgel, nanogel and hydrogel–hydrogel semi-IPN composites for biomedical applications: synthesis and characterization. *Colloid Polymer Science* **2006,** *284* (10), 1121-1129.

(250) Wang, M.; Fang, Y.; Hu, D. Preparation and properties of chitosan-poly (N-isopropylacrylamide) full-IPN hydrogels. *Reactive Functional polymers* **2001,** *48* (1-3), 215-221.

(251) Racine, L.; Texier, I.; Auzély‐Velty, R. Chitosan‐based hydrogels: recent design concepts to tailor properties and functions. *Polymer International* **2017,** *66* (7), 981-998.

(252) Jain, E.; Kumar, A. Designing supermacroporous cryogels based on polyacrylonitrile and a polyacrylamide–chitosan semi-interpenetrating network. *Journal of Biomaterials Science, Polymer Edition* **2009,** *20* (7-8), 877-902.

(253) Zhu, P.; Hu, M.; Deng, Y.; Wang, C. One‐pot fabrication of a novel agar‐polyacrylamide/graphene oxide nanocomposite double network hydrogel with high mechanical properties. *Advanced Engineering Materials* **2016,** *18* (10), 1799-1807.

(254) Wahid, F.; Hu, X.-H.; Chu, L.-Q.; Jia, S.-R.; Xie, Y.-Y.; Zhong, C. Development of bacterial cellulose/chitosan based semi-interpenetrating hydrogels with improved mechanical and antibacterial properties. *International journal of biological macromolecules* **2019,** *122*, 380-387.

(255) Chung, T.-W.; Lin, S.-Y.; Liu, D.-Z.; Tyan, Y.-C.; Yang, J.-S. Sustained release of 5-FU from Poloxamer gels interpenetrated by crosslinking chitosan network. *International journal of pharmaceutics* **2009,** *382* (1-2), 39-44.

(256) Zoratto, N.; Matricardi, P. Semi-IPNs and IPN-based hydrogels. *Polymeric Gels* **2018**, 91-124.

(257) Özbaş, Z.; Gürdağ, G. Swelling kinetics, mechanical properties, and release characteristics of chitosan‐based semi‐IPN hydrogels. *Journal of Applied Polymer Science* **2015,** *132* (16).

(258) Matricardi, P.; Di Meo, C.; Coviello, T.; Hennink, W. E.; Alhaique, F. Interpenetrating polymer networks polysaccharide hydrogels for drug delivery and tissue engineering. *Advanced drug delivery reviews* **2013,** *65* (9), 1172-1187.

(259) Wu, M.; Chen, J.; Huang, W.; Yan, B.; Peng, Q.; Liu, J.; Chen, L.; Zeng, H. Injectable and self-healing nanocomposite hydrogels with ultrasensitive pH-responsiveness and tunable mechanical properties: implications for controlled drug delivery. *Biomacromolecules* **2020,** *21* (6), 2409-2420.

(260) Wang, W.; Zeng, Z.; Xiang, L.; Liu, C.; Diaz-Dussan, D.; Du, Z.; Asha, A. B.; Yang, W.; Peng, Y.-Y.; Pan, M. Injectable self-healing hydrogel via biological environment-adaptive supramolecular assembly for gastric perforation healing. *ACS nano* **2021,** *15* (6), 9913-9923.

(261) Cutright, C.; Brotherton, Z.; Alexander, L.; Harris, J.; Shi, K.; Khan, S.; Genzer, J.; Menegatti, S. J. A. S. S. Packing density, homogeneity, and regularity: Quantitative correlations between topology and thermoresponsive morphology of PNIPAM-co-PAA microgel coatings. **2020,** *508*, 145129.

(262) Ngai, T.; Behrens, S. H.; Auweter, H. J. C. c. Novel emulsions stabilized by pH and temperature sensitive microgels. **2005,** (3), 331-333.

(263) Ahiabu, A.; Serpe, M. J. Rapidly responding pH-and temperature-responsive poly (N-isopropylacrylamide)-based microgels and assemblies. *ACS omega* **2017,** *2* (5), 1769-1777.

(264) Schmidt, S.; Motschmann, H.; Hellweg, T.; von Klitzing, R. Thermoresponsive surfaces by spin-coating of PNIPAM-co-PAA microgels: A combined AFM and ellipsometry study. *Polymer Chemistry* **2008,** *49* (3), 749-756.

(265) Guo, S.; Carvalho, W. S. n. P.; Wong, D.; Serpe, M. J. J. A. A. M.; Interfaces. Alkanethiol Molecular Barriers for Controlling Small Molecule Release Kinetics from a Microgel-Based Reservoir Device. **2019,** *11* (50), 47446-47455.

(266) Gao, Y.; Zago, G. P.; Jia, Z.; Serpe, M. J. J. A. a. m.; interfaces. Controlled and triggered small molecule release from a confined polymer film. **2013,** *5* (19), 9803-9808.

(267) Gao, Y.; Ahiabu, A.; Serpe, M. J. J. A. A. M.; Interfaces. Controlled drug release from the aggregation–disaggregation behavior of pH-responsive microgels. **2014,** *6* (16), 13749-13756.

(268) Smith, M. H.; Lyon, L. A. Tunable encapsulation of proteins within charged microgels. *Macromolecules* **2011,** *44* (20), 8154-8160.

(269) Vinogradov, S. V. J. C. p. d. Colloidal microgels in drug delivery applications. **2006,** *12* (36), 4703-4712.

(270) Hu, J.; Kurokawa, T.; Hiwatashi, K.; Nakajima, T.; Wu, Z. L.; Liang, S. M.; Gong, J. P. Structure optimization and mechanical model for microgel-reinforced hydrogels with high strength and toughness. *Macromolecules* **2012,** *45* (12), 5218-5228.

(271) Zhao, W.; Duan, L.; Zhang, B.; Ren, X.; Gao, G. H. Tough and ultrastretchable hydrogels reinforced by poly (butyl acrylate-co-acrylonitrile) latex microspheres as crosslinking centers for hydrophobic association. *Polymers* **2017,** *112*, 333-341.

(272) Gao, Y.; Zago, G. P.; Jia, Z.; Serpe, M. J. Controlled and triggered small molecule release from a confined polymer film. *ACS Appl. Mater. Interfaces.* **2013,** *5* (19), 9803-9808.

(273) Nakayama, A.; Kakugo, A.; Gong, J. P.; Osada, Y.; Takai, M.; Erata, T.; Kawano, S. J. A. f. m. High mechanical strength double‐network hydrogel with bacterial cellulose. **2004,** *14* (11), 1124-1128.

(274) Huo, D. X.; Li, Y.; Kobayashi, T. In *Temperature-pH controlled uptake and release of bovine serum albumin protein in environmental sensitive microgel based on crosslinked poly (N-isopropylacrylamide-co-acrylic acid)*, Advanced Materials Research, Trans Tech Publ: 2006; pp 299-302.

(275) Wei, X.; Ma, K.; Cheng, Y.; Sun, L.; Chen, D.; Zhao, X.; Lu, H.; Song, B.; Yang, K.; Jia, P. Adhesive, conductive, self-healing, and antibacterial hydrogel based on chitosan–polyoxometalate complexes for wearable strain sensor. *ACS Applied Polymer Materials* **2020,** *2* (7), 2541-2549.

(276) Gaabour, L. Spectroscopic and thermal analysis of polyacrylamide/chitosan (PAM/CS) blend loaded by gold nanoparticles. *Results in physics* **2017,** *7*, 2153-2158.

(277) Pawar, V.; Dhanka, M.; Srivastava, R. Cefuroxime conjugated chitosan hydrogel for treatment of wound infections. *Colloids Surfaces B: Biointerfaces* **2019,** *173*, 776-787.

(278) Wu, Z.; Zhang, X.; Zheng, C.; Li, C.; Zhang, S.; Dong, R.; Yu, D. Disulfide-crosslinked chitosan hydrogel for cell viability and controlled protein release. *European Journal of Pharmaceutical Sciences* **2009,** *37* (3-4), 198-206.

(279) Hu, X.; Wang, Q.; Liu, Q.; Li, Z.; Sun, G. Villus-like nanocomposite hydrogels with a super-high water absorption capacity. *Journal of Materials Chemistry A* **2020,** *8* (25), 12613-12622.

(280) Wu, J.; Wei, Y.; Lin, J.; Lin, S. Preparation of a starch‐graft‐acrylamide/kaolinite superabsorbent composite and the influence of the hydrophilic group on its water absorbency. *Polymer international* **2003,** *52* (12), 1909-1912.

(281) Schulze, K. D.; Hart, S. M.; Marshall, S. L.; O'Bryan, C. S.; Urueña, J. M.; Pitenis, A. A.; Sawyer, W. G.; Angelini, T. E. Polymer osmotic pressure in hydrogel contact mechanics. *Biotribology* **2017,** *11*, 3-7.

(282) Povea, M. B.; Monal, W. A.; Cauich-Rodríguez, J. V.; Pat, A. M.; Rivero, N. B.; Covas, C. P. J. M. S.; Applications. Interpenetrated chitosan-poly (acrylic acid-co-acrylamide) hydrogels. Synthesis, characterization and sustained protein release studies. **2011,** *2* (06), 509.

(283) Yang, Y.; Wang, X.; Yang, F.; Shen, H.; Wu, D. J. A. M. A universal soaking strategy to convert composite hydrogels into extremely tough and rapidly recoverable double‐network hydrogels. **2016,** *28* (33), 7178-7184.

(284) Dutta, A.; Maity, S.; Das, R. K. J. M. M.; Engineering. A Highly Stretchable, Tough, Self‐Healing, and Thermoprocessable Polyacrylamide–Chitosan Supramolecular Hydrogel. **2018,** *303* (12), 1800322.

(285) Gao, Y.; Ahiabu, A.; Serpe, M. Controlled drug release from the aggregation–disaggregation behavior of pH-responsive microgels. *ACS Applied Materials Interfaces* **2014,** *6* (16), 13749-13756.

(286) Shi, Q.; Zhou, Y.; Sun, Y. Influence of pH and ionic strength on the steric mass‐action model parameters around the isoelectric point of protein. *Biotechnology progress* **2005,** *21* (2), 516-523.

(287) Jett, B. D.; Hatter, K. L.; Huycke, M. M.; Gilmore, M. S. Simplified agar plate method for quantifying viable bacteria. *Biotechniques* **1997,** *23* (4), 648-650.

Appendices

Appendix A Supporting Information for Chapter

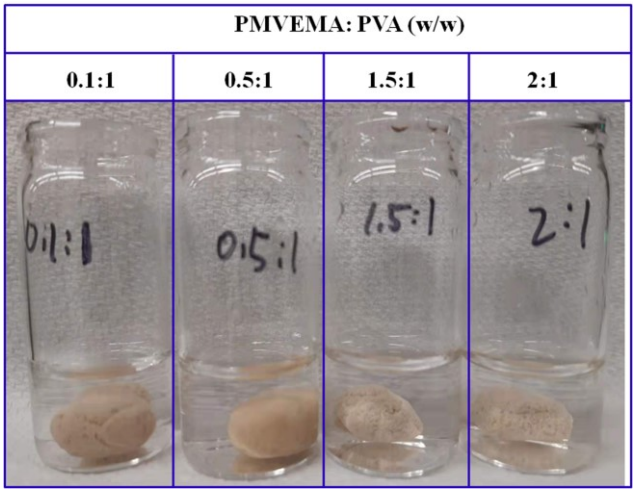

Figure S2.1. Pictures of PPTA coacervate gels formed with different PMVEMA/PVA mass ratios.

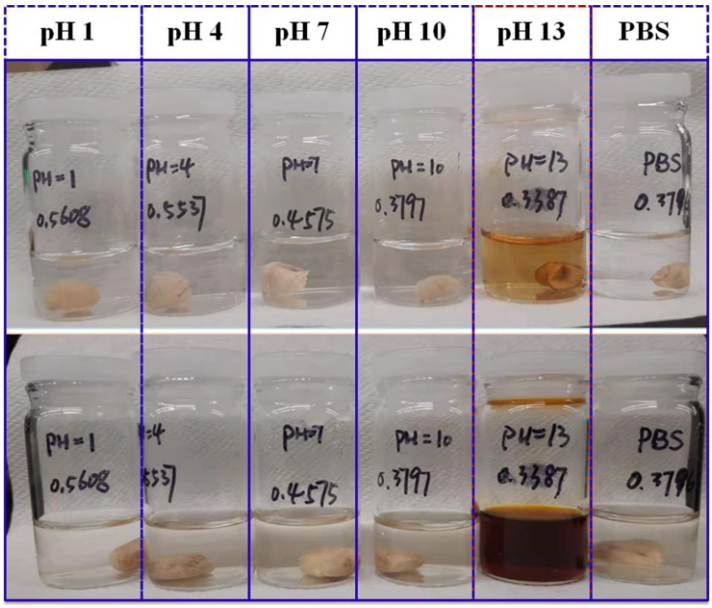

Figure S2.2. Photo images of PPTA coacervate gel soaked in aqueous solutions with different pH conditions for Day 0 (Up row) and Day 1 (Down row).

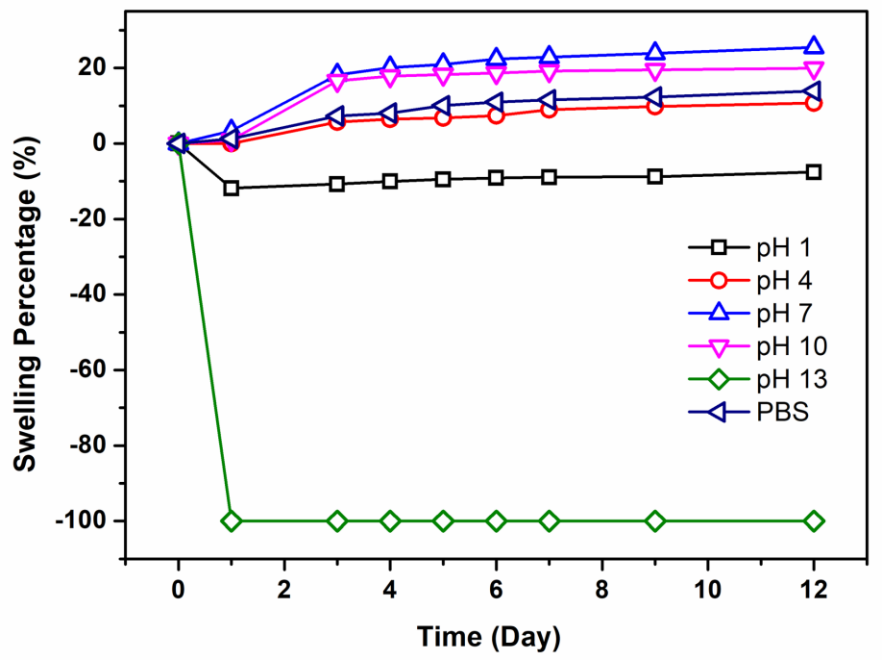

Figure S2.3. Swelling test results of PPTA coacervate gel under different pH conditions.

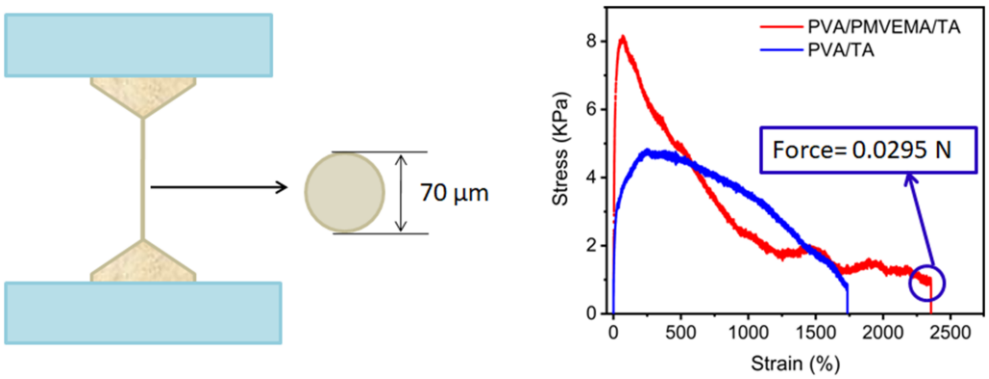

Figure S2.4. True stress calculation on the point of disruption as a demonstration of the discussion about the mechanical properties of the PPTA coacervate gel, which could be calculated using the force divided by the cross area of the fiber formed during the stretching process.

Appendix B Supporting Information for Chapter 3

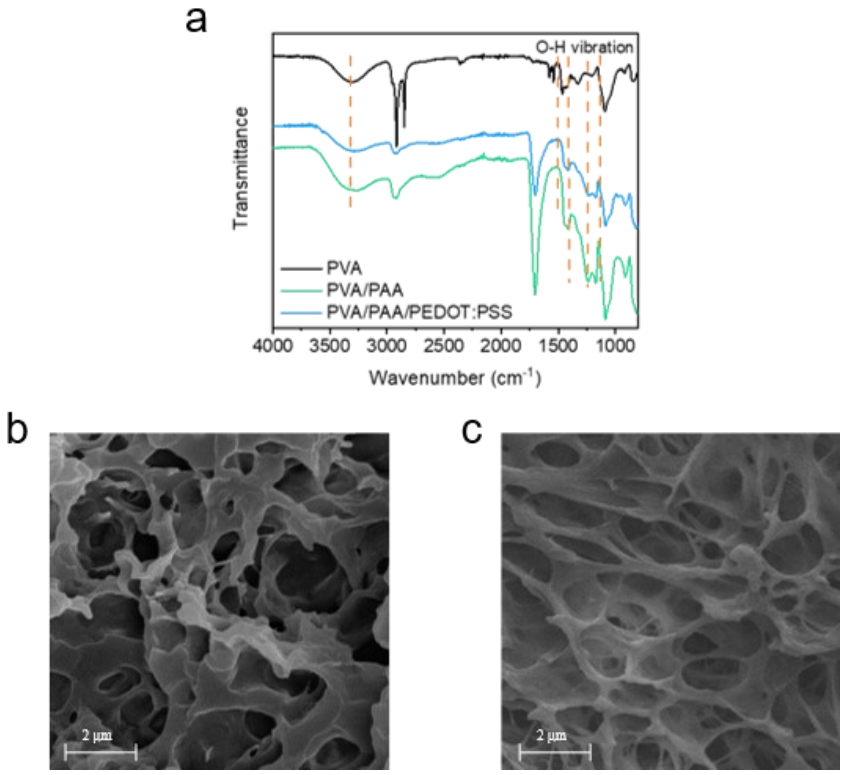

Figure S3.1. (a) FTIR spectra of PVA, PVA/PAA and PEDOT:PSS@PVA/PAA DN hydrogels. SEM images of (b) PVA/PAA and (c) PEDOT:PSS@PVA/PAA DN hydrogel.

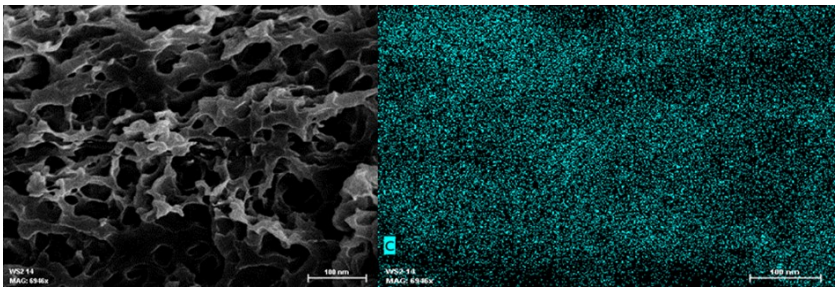

Figure S3.2. EDS of pure PVA/PAA hydrogel.

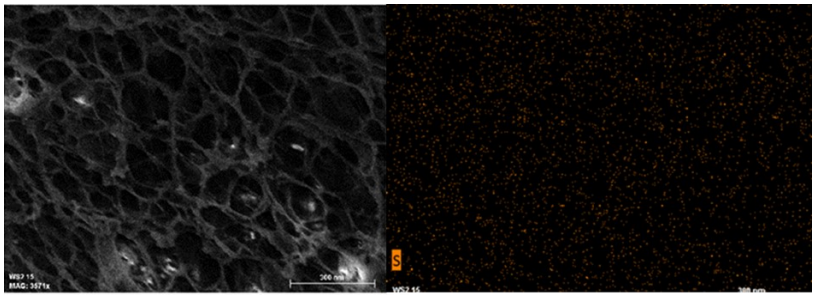

Figure S3.3. EDS of PEDOT:PSS@PVA/PAA hydrogel.

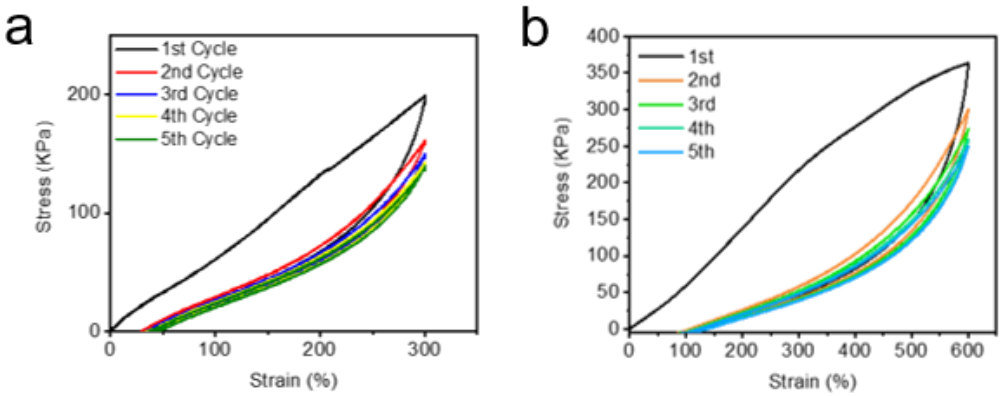

Figure S3.4. (a) Continuous 5 loading-unloading tensile cycles with 300% strain (b) with 600% strain of PEDOT:PSS@PVA/PAA hydrogel.

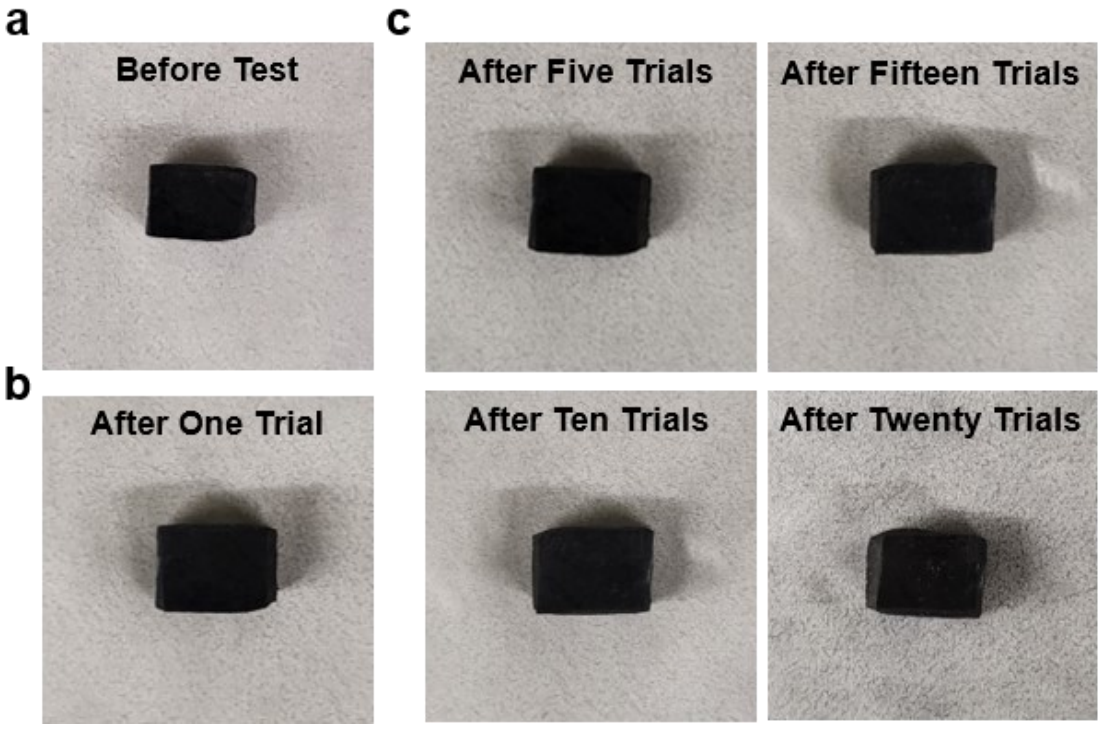

Figure S3.5. Image of specimen (a) Before hammering test, after (b) One trial (c) Five trials (d) Ten trials, (e) Fifteen trials and (f) Twenty trials.

Figure S3.6. Picture demonstration of one-piece PEDOT:PSS@PVA/PAA hydrogel sample glue and lift a 500-gram weight.

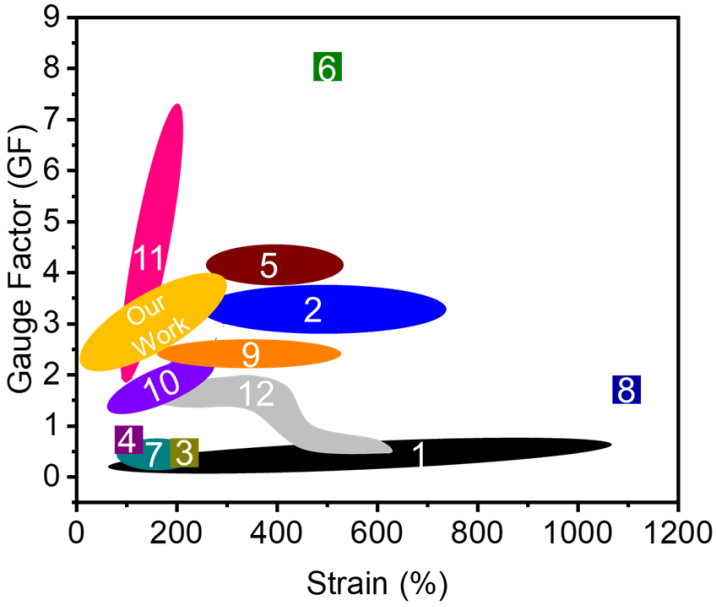

Figure S3.7. Comparison of Gauge Factor with other previously published hydrogel strain sensor systems.[1-12]

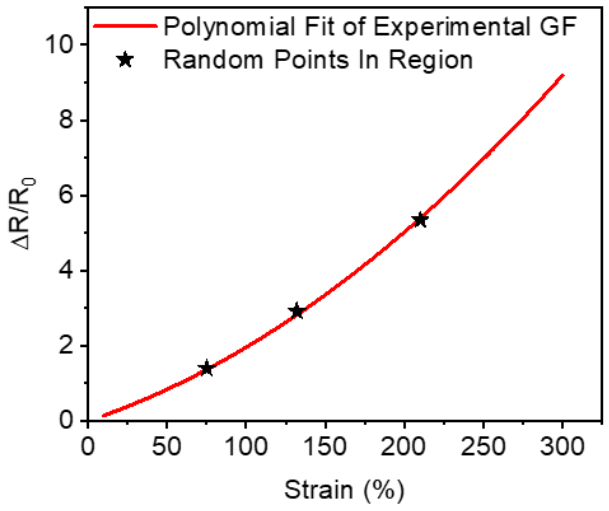

Figure S3.8. Strain sensing test results for random strain conditions (start points) agree well with the predicted signal curve (red curve) using the as-prepared PEDOT:PSS@PVA/PAA hydrogel sensor.

References

(1) Pu, X.; Liu, M.; Chen, X.; Sun, J.; Du, C.; Zhang, Y.; Zhai, J.; Hu, W.; Wang, Z. L. Ultrastretchable, transparent triboelectric nanogenerator as electronic skin for biomechanical energy harvesting and tactile sensing. *Science advances* **2017,** *3* (5), e1700015.

(2) Sun, X.; Qin, Z.; Ye, L.; Zhang, H.; Yu, Q.; Wu, X.; Li, J.; Yao, F. Carbon nanotubes reinforced hydrogel as flexible strain sensor with high stretchability and mechanically toughness. *Chemical Engineering Journal* **2020,** *382*, 122832.

(3) Frutiger, A.; Muth, J. T.; Vogt, D. M.; Mengüç, Y.; Campo, A.; Valentine, A. D.; Walsh, C. J.; Lewis, J. A. J. A. M. Capacitive soft strain sensors via multicore–shell fiber printing. **2015,** *27* (15), 2440-2446.

(4) Lei, H.; Zhao, J.; Ma, X.; Li, H.; Fan, D. Antibacterial Dual Network Hydrogels for Sensing and Human Health Monitoring. *Advanced Healthcare Materials* **2021,** *10* (21), 2101089.

(5) Cheng, B.; Li, Y.; Li, H.; Li, H.; Yang, S.; Li, P.; Shang, Y. An adhesive and self-healable hydrogel with high stretchability and compressibility for human motion detection. *Composites Science and Technology* **2021,** *213*, 108948.

(6) Ling, Q.; Ke, T.; Liu, W.; Ren, Z.; Zhao, L.; Gu, H. Tough, Repeatedly Adhesive, Cyclic Compression-Stable, and Conductive Dual-Network Hydrogel Sensors for Human Health Monitoring. *Industrial and Engineering Chemistry Research* **2021**.

(7) Zhang, J.; Wan, L.; Gao, Y.; Fang, X.; Lu, T.; Pan, L.; Xuan, F. Highly stretchable and self-healable MXene/polyvinyl alcohol hydrogel electrode for wearable capacitive electronic skin. *Adv. Electron. Mater.* **2019,** *5* (7), 1900285.

(8) Yang, B.; Yuan, W. Highly stretchable and transparent double-network hydrogel ionic conductors as flexible thermal–mechanical dual sensors and electroluminescent devices. *ACS applied materials interfaces* **2019,** *11* (18), 16765-16775.

(9) Zhou, Z.; He, Z.; Yin, S.; Xie, X.; Yuan, W. Adhesive, stretchable and antibacterial hydrogel with external/self-power for flexible sensitive sensor used as human motion detection. *Composites Part B: Engineering* **2021,** *220*, 108984.

(10) Song, H.; Sun, Y.; Zhu, J.; Xu, J.; Zhang, C.; Liu, T. Hydrogen-bonded network enables polyelectrolyte complex hydrogels with high stretchability, excellent fatigue resistance and self-healability for human motion detection. *Composites Part B: Engineering* **2021,** *217*, 108901.

(11) Jin, R.; Xu, J.; Duan, L.; Gao, G. Chitosan-driven skin-attachable hydrogel sensors toward human motion and physiological signal monitoring. *Carbohydrate Polymers* **2021**, 118240.

(12) He, F.; You, X.; Gong, H.; Yang, Y.; Bai, T.; Wang, W.; Guo, W.; Liu, X.; Ye, M. Stretchable, biocompatible, and multifunctional silk fibroin-based hydrogels toward wearable strain/pressure sensors and triboelectric nanogenerators. *ACS applied materials & interfaces* **2020,** *12* (5), 6442-6450.

Appendix C Supporting Information for Chapter 4

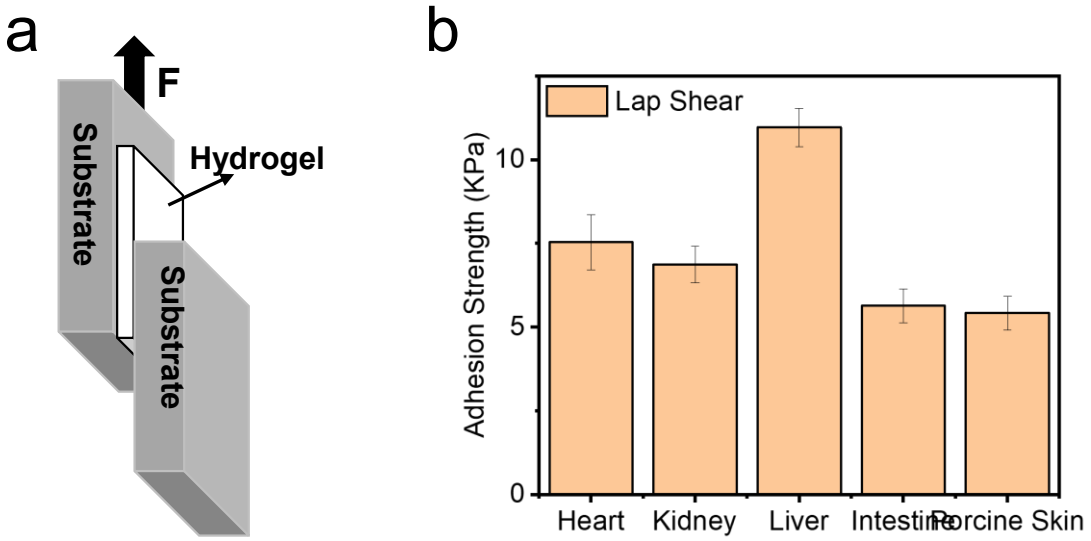

Figure S4.1. (a) Scheme of lap shear adhesion test. (b) Results of adhesion strength through lap shear method.